High Performance Polyetheretherketone Nanocomposites and Hierarchical Composites

Steven Lamorinière

November 2009

A dissertation submitted in partial fulfilment of the requirements for the degree of
Doctor of Philosophy of the University of London and
the Diploma of Imperial College London

Department of Chemical Engineering and Chemical Technology
Imperial College London
London, SW7 2AZ, UK

Declaration

This dissertation is a description of the work carried out by the author in the Department of Chemical Engineering and Chemical Technology, Imperial College London (and in the Federal Institute of Materials Research and Testing (BAM) Berlin in February/March 2006 and August 2006) between September 2004 and November 2009 under the supervision of Prof Alexander Bismarck, Prof Milo Shaffer and Dr Emile Greenhalgh. Except where acknowledged, the material presented is the original work of the author and no part of it has been submitted for a degree at this or any other university.

Signature 

Abstract

There is currently a timely opportunity to create dramatically improved structural materials. By combining conventional reinforcing fibres and carbon nanotubes (CNT) within thermoplastic matrices, a new class of materials with both superior mechanical, environmental, and chemical performance, as well as significantly reduced through-life costs should be possible. CNTs have generated huge interest in the composites community due to their remarkable physical and mechanical properties. Numerous studies have reported the production and characterisation of CNT reinforced polymers. Although promising results have been obtained, progress has been limited by several factors; CNT synthesis (quality), dispersion, alignment and interfacial adhesion. On the other hand, traditional carbon fibre reinforced polymers have found a wide range of applications. Although traditional composites have excellent in-plane properties, the relatively weak compression, transverse and interlaminar properties remain a major challenge.

The main aim of the research reported here was to develop CNT polyetheretherketone (PEEK) nanocomposites and fibre reinforced PEEK nanocomposites, which have been called "hierarchical composites". The combination of CNTs and conventional fibres as reinforcements to produce *unidirectional fibre reinforced nanocomposites* is extremely challenging. The focus is on PEEK as matrix because it is a high performance polymer with excellent mechanical and friction properties and a superb chemical resistance. PEEK is certified for aerospace use, and is covered by a wealth of background data. Since it is a high value polymer, any improvements will be welcomed, particularly because PEEK is more expensive than some commercial CNTs.

This research summarises the development and characterisation of a PEEK CNT nanocomposite, which was turned into a micrometre sized powder. This powder than was used for the production of hierarchical composites. In order to produce these hierarchical composites a laboratory scale continuous composite tape production line had to be designed and built. Prior to the fabrication of real hierarchical composite the interfacial characteristics of model, single fibre nanocomposites were characterised using single fibre pull out tests. The specific achievements of the work are:

- Thirteen different CNT materials have been thoroughly characterised and based on these results and the commercial larger volume availability Nanocyl CNTs were chosen.
- Laboratory-scale production of CNT/PEEK nanocomposites with various loading fractions of up to 15 wt% and with a high degree of CNT dispersion. These nanocomposites have been characterised with respect to their crystallisation behaviour and mechanical properties. Unfortunately, only minor improvements in mechanical properties have been achieved, which were reduced when the materials were annealed.
- Single fibre hierarchical PEEK composites were characterised using single fibre pull-out tests. The apparent interfacial shear strength increased significantly with increasing CNT loading fraction, while the frictional stress was independent of the CNT loading fraction.
- Successful development of a method to produce CNT/PEEK nanocomposite powders with a d50 of 50 μm using a temperature induced solution precipitation method.
- Design, construction and validation of a modular laboratory-scale powder impregnation line for the production of continuous fibre reinforced thermoplastic composite tapes. CF/PEEK composites produced had a slightly better mechanical performance than APC-2.
- Manufacturing of unidirectional carbon fibre reinforced CNT reinforced polymer composites using the home-built laboratory scale composite production line. Conventional mechanical testing was used to determine critical engineering properties. Unfortunately, the flexural and short beam shear properties decrease slightly with increasing loading fraction of CNTs.

As a result, a generic method to produce continuous unidirectional carbon fibre reinforced CNT reinforced thermoplastics (PEEK) was developed using a powder impregnation route. A patent protecting hierarchical thermoplastic composites and the method to produce such material has been filed and is currently in the Patent Cooperation Treaty (PCT) stage.

Acknowledgements

I would like to take this opportunity to thank all the people that have made this thesis possible. I would to start thanking EPSRC and Dstl for sponsoring this project (grant no.: GR/T24029/01 called "Nanotube wettability and modification: The key to hierarchical fibre-reinforced nanocomposites") and to Security Composites Ltd for extra financial support. I would like to thank Dr Gary Wells, Dr Doug Imeson, Prof Paul Curtis (Dstl) and Chris Price (Security Composites Ltd) for their technical know-how and input.

For constant guidance, supervision and advice throughout my years at Imperial, I would like to thank Prof Alexander Bismarck, Prof Milo Shaffer and Dr Emile Greenhalgh. Especially for taking the time to answer any questions and being so understanding. They provided me with the tools to learn and improve my knowledge and develop my thoughts, which made me appreciate research in general, especially since I never have dreamt of becoming a researcher before joining Imperial. A special thanks goes to Alexander (but also Katherina for her understanding) for all the discussions, thoughts and patience, it made my time at Imperial much more pleasant by having the opportunity and freedom to do some exciting but challenging work.

I would like to thank Dr John Hodgkinson, without him I would never have come to Imperial in the first place to study for my Master and have the chance of experiencing all that I did to this day.

I would like to continue by thanking all the people I met throughout my PhD, without them my time in London would not have been the same and who now became invaluable friends. Especially, I would like to thank Dr Kingsley Ho and Dr Michael Tran for all the hard work and fun times in the lab, getting on each other's nerves and for the help given and that I gave back. I would also like to thank all the other people at Imperial from the PaCE group and within Chem Eng, Chemistry and Aero departments with (in no particular order and without accents, sorry guys): Dr Shu San Manley, Ivan Zadrazil, Koon Yang Lee, Dr Juntaro Julasak, Dr Urosh Vukicevic, Charnwit Tridech, Dr James Griffin, Dr Katsumi Maeda, Dr Ryo Murakami, Dr Angelika Menner, Dr Jonny Blaker, Anthony Abbot, Dr Kiheung Kim, Dr Francesca Palombo, Kunal Masania, Matthew Laffan, Dr Boris Thomas, Dr Jerry Heng, Dr Ben Cottam, Achilleas Sesis, David Dowdell, Su Bai,... and so on, I probably forgot many, but it's not on purpose. And a big thank goes to the support staff in Chem Eng and Aero: Richard Wallington, Sarah Everall, Susi Underwood, Keith Walker, Patricia Carry, Anusha Sri-Pathmanathan, Pim Amrit, Tawanda Nyabango, Jo Meggyesi, Gary Senior and Anna Dowden... And also I would like to thank Mr Hugh MacGillivray from the Mechanical Engineering Department, without his help it would not have been possible to conduct any mechanical testing during my PhD. I would like to thank also Dr Adam Lee from the University of York for conducting the X-ray photoelectron spectroscopy (XPS) measurements and Dr Gerhard Kalinka from the Federal Institute of Materials Research and Testing (BAM) in Berlin for the help conducting single fibre pull-out measurements. I apologise if I missed anyone.

I would also like to thank all the people I met in Swansea before moving to London with whom I stayed in touch after all the fun years and who will always be there, thanks Marie Penkerc'h, Jonathan Guilloux and Vincent Le Duff.

Un grand remerciement aussi pour les personnes de France qui au fil des années sont restés des amis, cela n'aurais pas été la même chose sans vous et avec encore plein de beaux jours devant nous. Une petite liste non-exhaustive quand même comme: Arnaud Fouchet, Nicolas Marivin, Yoann Dubreuil, Veronique Cannieux, Thomas Le Guigner, Morwenna Le Floch, Sophie Boulogne...

Finally I would like to thank my family, without them I would not be where I am now, they always supported me any way possible and that's just fab. A big thanks to Mickaël, Gwen and Alexandra, my brother and my sisters without forgetting their better halves Mireille and Allan, and of course there are the kids Mathilde, Mathieu and Louis. Last but not least to my parents Guy and Yvonne Lamorinière who I hope will be proud of what I achieved taking so many years of studies. Thanks for everything!!!

List of Publications

Refereed Journal Papers

1. Michelle Lewis, **Steven Lamoriniere**, Joachim H. G. Steinke, Milo Shaffer, Anne E. Bishop and Alexander Bismarck. *Carbon nanomaterial – PMMA composites for tissue engineering applications.* To be submitted.

2. Seckin Erden, Kingsley K. C. Ho, **Steven Lamoriniere**, Adam F. Lee, Hasan Yildiz and Alexander Bismarck. *Continuous atmospheric plasma oxidation of carbon fibres: Influence on the surface and bulk properties and adhesion to polyamide 12.* Plasma Chemistry and Plasma Processing, in press.

3. Siti R. Shamsuddin, Kingsley K. C. Ho, **Steven Lamoriniere**, Adam F. Lee and Alexander Bismarck. *Impact of in-line atmospheric plasma fluorination of carbon fibres on the performance of unidirectional carbon fibre reinforced polyvinylidene fluoride.* Advances in Polymer Technology, accepted.

4. Kingsley K. C. Ho, Alexandros Kolliopoulos, **Steven Lamoriniere**, Emile Greenhalgh and Alexander Bismarck. *Atmospheric plasma fluorination as means to improve the mechanical properties of short carbon fibre reinforced poly(vinylidene fluoride).* Composites Part A: Applied Science and Manufacturing, in press.

5. Kingsley K. C. Ho, Adam F. Lee, **Steven Lamoriniere** and Alexander Bismarck. *Continuous atmospheric plasma fluorination of carbon fibres.* Composites Part A: Applied Science and Manufacturing, 39:364-373, 2008.

6. Kingsley K. C. Ho, **Steven Lamoriniere**, Gerhard Kalinka, Eckhard Schultz and Alexander Bismarck. *Interfacial behavior between atmospheric plasma fluorinated carbon fibers and poly(vinylidene fluoride).* Journal of Colloid and Interface Science, 313:476-484, 2007.

7. Raquel Verdejo, **Steven Lamoriniere**, Ben Cottam, Alexander Bismarck and Milo Shaffer. *Removal of oxidation debris from multi-walled carbon nanotubes.* Chemical Communications, 513-515, 2007.

Awards

International Union of Pure and Applied Chemistry (IUPAC) Poster Prize awarded at Polychar-14 World Forum on Advanced Materials 17-22. 04. 2006, Nara, Japan.

Conference Presentation

1. Shamsuddin, S., Ho, K.K.C., Laffan, M., **Lamoriniere, S.**, Bismarck, A. "Unidirectional Carbon Fibre Reinforced Polyvinylidene Fluoride: Impact of Atmospheric Plasma Fluorination on Composite Performance" ICCM 17 17th International Conference on Composite Materials, Edinburgh, UK, 26.-31.07.2009.

2. Ho, K.K.C., **Lamoriniere, S.**, Qian, H., Menner, A., Greenhalgh, E.S., Shaffer, M. and Bismarck, A. "Fibre Reinforced Nanocomposites: Creating hierarchical structures in composites" European Conference and Exhibition on Advanced Materials and Processes – EuroMat 2009, Glasgow, UK, 07.-10.09.2009 (**Highlight** (Key Note) **Lecture**).

3. Qian, H., **Lamoriniere, S.**, Tran, M.Q., Greenhalgh, E.S., Shaffer, M. and Bismarck, A. "Hierarchical Thermoplastic Composites", Sicomp Conference 2009, Pitea, Sweden, 08.-09.06. 2009.

4. Lewis M., **Lamoriniere, S.**, Steinke, J.H.G, Bishop, A., Shaffer, M. and Bismarck, A. "Polymer nanocomposites for lung cell culture applications" Symposium 5 Advances in Bio-related Polymeric Materials, Macro 2008, Taipei, Taiwan, 29.06. – 04.07.2008.

5. Lewis, M., **Lamoriniere, S.**, Steinke, J., Bishop, A., Shaffer, M. and Bismarck, A. "Polymer Nanocomposites for Lung Cell Culture Applications", Euromat 2007 European Congress on Advanced Materials and Processes, Nürnberg, Germany, 10.-13.09.2007. (**Highlight** (Key Note) **Lecture**)

6. **Lamoriniere, S.**, Greenhalgh, E., Shaffer, M. and Bismarck, A. "En Route to Hierarchical Composites", Polychar-14 World Forum of Advanced Materials, Nara, Japan, 17-22.04.2006.

7. **Lamoriniere, S.**, Greenhalgh, E., Shaffer M. and Bismarck, A. "En route to Hierarchical Composites", Composite Centre Industrial Affiliates Meeting, London, 04.05.2004.

Patents

Tran, M. Q., **Lamoriniere, S.**, Menner, A., Greenhalgh, E., Shaffer, M. S. P., Bismarck, A., A method for the production of thermoplastic composite materials reinforced with anisotropic nanomaterials, Filed, PCT Stage.

Table of Contents

List of Figures

List of Tables

Nomenclature

List of Symbols

A_e	embedded fibre area
A_f	fibre cross-sectional area
a_m	molecular cross-sectional area
A_s	specific surface area
at.%	atomic percent
B	width
C	BET parameter
C	optimum wet slurry concentration
C	coefficient related to the micro-extruder
d	diameter
d_f	diameter of fibre
d_{50}	average particle size
D	maximum central deflection at the centre of the beam
ΔL	change in length
E	Young's modulus
E_f	flexural modulus
ε_f	flexural strain
F_{max}	maximum force
F^{SBS}	short beam shear strength
G_{IC}	mode I interlaminar fracture toughness
G_{IIC}	mode II interlaminar fracture toughness
l	length

l	length of failed area
L	Avogadro constant
L	support span
L_e	embedded fibre length
L_0	original length
m	mass
m	slope of force-displacement curve
n_a	specific amount adsorbed
n_m	specific monolayer capacity of adsorbate
N	rotating speed
η	viscosity
η_r	relative viscosity
ρ	density
P	pressure
P_{max}	maximum force at failure
P_0	initial pressure
$P_{0.2}$	maximum shear load at offset 0.2 %
P/P_0	relative pressure
r	radius of fibre
R	radius of polymer particle
σ	strength
σ_f	flexural strength
σ_s	in-plane shear strength
σ_t	tensile strength
t	thickness

T	torque
T_c	composite torque
T_g	glass transition temperature
T_m	matrix torque
T_m	melting temperature
τ_{IFSS}	apparent interfacial shear strength
V_c	volume of unit cell
V_f	volume fraction
V_{fc}	fibre volume per unit cell
V_p	volume of polymer particle
V_s	volume of space occupied by water
wt%	weight percent
z	depth

List of Abbreviations

APC	Aromatic polymer composites
ASTM	American Society for Testing and Materials
BET	Brunauer-Emmett-Teller
CF(s)	Carbon fibre(s)
CNF	Carbon nanofibre
CNT(s)	Carbon nanotube(s)
CO_2	Carbon dioxide
CS_2	Carbon disulphide
CVD	Chemical vapour deposition
D band	Defect band

DPS	Diphenylsulfone
DSC	Differential scanning calorimetry
DWCNT	Double wall carbon nanotube
EPD	Electrophoretic deposition
EU	European Union
FEG	Field emission gun
FSS	Frictional shear stress
G band	Graphitic band
G/D	Graphitic over defective band ratio
HRTEM	High-resolution transmission electron microscopy
ICVD	Injection chemical vapour deposition
IFSS	Interfacial shear strength
ILSS	Interlaminar shear strength
IR	Infrared radiation
Inc	Incorporated (business)
ISO	International Standards Organisation
LRS	Laser Raman Spectroscopy
L/D	Length / diameter aspect ratio
MWCNT	Multi wall carbon nanotube
n/a	Not applicable
n/d	Not determined
nanoHAC	Nanostructured Hierarchical Assemblies and Composites Group
NaOH	Sodium hydroxide
NH_2	Amino functional group
PaCE	Polymer and Composites Engineering Group

PAN	Polyacrylonitrile
PC	Polycarbonate
PCT	Patent Cooperation Treaty
PE	Plasma enhanced
PE	Polyethylene
PEEK	Polyetheretherketone
PEI	Polyetherimide
PES	Polyethersulfone
PI	Polyimide
PID	Proportional integral differential
PLLA	Poly(L-lactic acid)
PP	Polypropylene
PSD	Particle size distribution
PSU	Polysulfone
RTM	Resin transfer moulding
R&D	Research and Development
SBS	Short beam shear
SEM	Scanning electron microscope
SWCNT	Single wall carbon nanotube
TCE	1,1,2,2-tetrachloroethane
TGA	Thermogravimetric Analysis
VARTM	Vacuum assisted resin transfer moulding
WAXS	Wide Angle X-ray Scattering
2-D	Two-Dimensional
3-D	Three-Dimensional

Chapter 1 - Introduction

Carbon nanotubes (CNTs) were first observed by Oberlin, Endo and Koyama in 1976 [1]. They possess a nano-metre scale graphitic structure (Figure 1). Three varieties of CNTs are known, namely single wall (SWCNT), double wall (DWCNT) or multi wall (MWCNT) CNTs. Theoretical simulations highlighted that single wall CNTs possess an axial elastic modulus of approximately 1 TPa [2]. In addition to this, CNTs were also found to be able to withstand a maximum tensile strain in the order of 40 % without any brittle behaviour, bond rupture or plastic deformation [2]. Single wall CNTs only bend or buckle when a compressive load is applied. CNTs kink under compressive stress and relax during unloading. They will not break or rupture. Due to their impressive properties, incorporation of CNTs into various matrices aiming to produce nanocomposites has attracted various research interest [2-4]. Some promising improvements in the tensile properties of 20 % to 40 % of CNT based polymer nanocomposites with CNT loading fractions of 15 wt% as compared to the pure polymers have been reported [5,6]. Unfortunately, further improvements of the tensile properties of CNT polymer nanocomposites are difficult to be achieved mainly because of processing issues, limiting the dispersion and alignment of CNTs but also because sufficient interfacial adhesion between CNTs and polymer matrices remains a challenge.

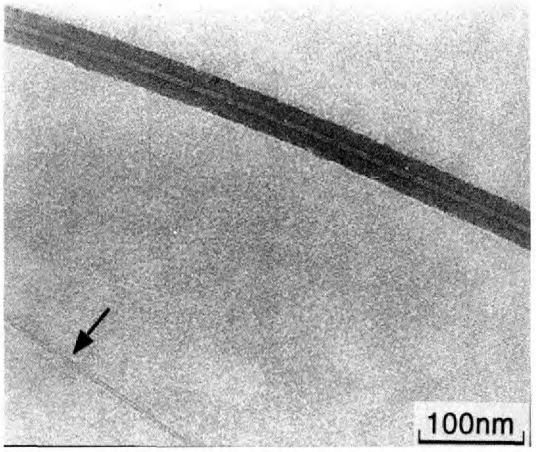

Figure 1: High-Resolution Transmission Electron Microscopy (HRTEM) micrograph showing a MWCNT (upper region) together with a SWCNT indicated by an arrow [1]

Most research focuses on the use of CNT solely as the reinforcement of polymer matrices to produce nanocomposites. However, because of the nanoscale dimensions of the CNTs, they could potentially be well suited to reinforce fine structures such as thin polymer fibres [7, 8], the walls in polymer foams [9 - 12] but also polymer matrices in advanced composites [13, 14]. Conventional continuous (glass and carbon) fibre reinforced polymer composites have come a long way over the past few years. Advanced fibre reinforced polymer composites can now be considered a well-accepted material; they have found many applications in the aerospace and defence, oil and gas but also sports industry mainly because of their excellent mechanical properties combined with their light weight and decent chemical resistance. However, the interlaminar shear, off-axis and compression properties of continuous fibre reinforced composites depend upon the interfacial fibre/matrix adhesion and matrix properties. By incorporating both CNTs and carbon fibres into the same matrix, a hierarchical reinforcing structure consisting of nano- and micrometre sized reinforcements within a composite can be created. Within Polymer and Composites Engineering (PaCE), nanostructured Hierarchical Assemblies and Composites

(nanoHAC) and the Composites Centre at Imperial College London, these composites are called "hierarchical composites". It is expected that the incorporation of CNTs into the matrix of conventional composites would lead to an improvement of interlaminar and compression properties as compared to the "unreinforced" polymer composites. The carbon fibres used to reinforce the (nanomaterial reinforced) matrix mainly determine the tensile and flexure properties of the (hierarchical) composites. By combining conventional fibres and CNTs within thermoplastic matrices, a new class of materials with superior mechanical, environmental, and chemical performance, as well as significantly reduced through-life costs should be possible. To date not much research has been dedicated towards the continuous production of CNT-reinforced thermoplastic-matrix fibre composites.

The primary aim of this research project is to develop a new high performance thermoplastic composite material in which the matrix is additionally reinforced with CNTs and to study their interactions with a high performance thermoplastic polymer to gain a better understanding of their behaviour. Firstly, the interaction and effect of CNT diameters on the mechanical properties of produced nanocomposite will be investigated. Secondly, the developed optimised nanocomposite will be used as a matrix for carbon fibre reinforced composites to create a hierarchical structure with nanophase and mesophase reinforcements combined within the polymer (Figure 2). This could improve the overall properties of the new composite materials in compression and shear, which have shown to be the two critical areas in a wide range of applications. The specific objectives of the research project are to:

1. produce novel nanomaterial reinforced micrometre sized polymer powders which could be used in a conventional powder impregnation process used for manufacturing of thermoplastic composites,
2. manufacture unidirectional nanomaterial-reinforced fibre-reinforced polymer composites on a laboratory scale and hence demonstrate hierarchical fibre-reinforced thermoplastic nanocomposites and
3. quantify the degree of improvement of the critical engineering composite properties as well as investigating secondary benefits such as improved thermal stability.

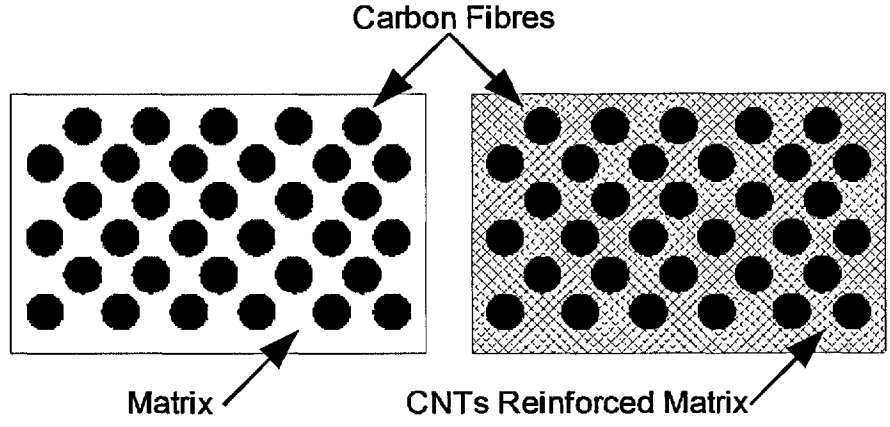

Figure 2: Standard composite material and hierarchically-reinforced composite material

Chapter 2 - Literature Review

Numerous composite materials exist in terms of reinforcements or matrices used. A review focusing on thermoplastic composites is described in this chapter. An overview on the advantages of using thermoplastic composites is presented, followed by their developments and the various manufacturing processes available to create continuous unidirectional carbon fibre-reinforced thermoplastic composites. A focus on PEEK as a matrix and the challenges associated with the processing and manufacture at high temperatures using a semi-crystalline polymer are examined. An overview on the work already published regarding CNT-reinforced PEEK is presented. PEEK being a semi-crystalline polymer, crystallinity is of importance and can affect mechanical properties, its control is necessary through monitored cooling or annealing. Finally an overview on hierarchical composites is examined with the various types of hierarchical composites, their manufacture and their mechanical properties.

2.1 Thermoplastic polymers as matrix for composite materials

Although thermoset systems such as epoxy resins have been at the forefront of composite development due to their exceptional specific strengths and stiffness, there are significant limitations to their performance [15]. For instance, thermosets exhibit undesired characteristics such as brittle failure, significant weakening on the exposure to polar solvents like water, and the loss of strength from barely visible impact damage [16]. Apart from thermosets, thermoplastics are also another type of polymers widely utilised in composite materials. Thermoplastics/thermosets typically consist of long-chain molecules that are entwined with each other. Below their glass transition temperature (T_g), they exist as a hard, glass-like materials and upon heating

above their T_g, the molecular chains start to move. Upon further heating, all the molecules lose their short-range order and the semi-crystalline thermoplastics are considered to be melted [17].

One of the major issues confronting the use of polymers and composites in the automotive industry is the European Union (EU) End of Life Vehicles legislation. This EU legalisation limits the incineration quota to just 5 % and this has forced car manufacturers to recycle their products [18]. Although cured thermosets can be re-used through pyrolysis, recycling thermoplastics is simpler and less energy is required in the process (melting and remoulding of the thermoplastics) [19]. In terms of composite materials such as continuous fibre composites, they can be recycled easily by grinding the composites into pellets. These pellets can then be used to make short fibre composite materials [20].

2.2 Development of thermoplastic composites

In recent years, the evolution of composite materials has had a major impact on a range of industries, especially those requiring high-performance for structural applications. By using composites, improved performance can be specified by the designer and can come in a variety of forms, whether it is an increase in strength, a decrease in weight or cost, or ease of manufacture [21]. Composites can offer many advantages over conventional materials.

The most extensively used composite materials are fibre-reinforced polymers. Currently, the market is dominated by composites based on thermosetting resins, with developments in the field of thermoplastic composite materials having distinctly

lagged behind. When viewing the entire market for plastic and composite materials, that is all products employing polymers, thermoplastic represents 80 % of the total. However, the market for reinforced materials, that is composite materials, thermoplastics represent 20 % of the entire plastic and composite market. Within this narrow composite market, thermosets represent 80 % of the total material used, just the reverse of the entire market[22]. The increasing demands of high performance applications in terms of toughness and chemical resistance are motivating the developments in the field of thermoplastic composites[23, 24]. Due to the inherent processing problems posed by thermoplastics, such as the high processing temperatures, melt-viscosities, consolidation temperatures and cost for high performance thermoplastics, thermosetting composites became established as excellent prototyping materials and were gradually translated into full scale production. Although a typical carbon-fibre epoxy composite will have excellent mechanical properties in terms of strength and stiffness, the implementation of this material in some fields of engineering is restricted as the ability of this material to cope with harsh environment is poor. For this reason, the development of high performance thermoplastic composites has taken place particularly for applications in the aerospace industry[25-27], where exposure to aviation fuels and hydraulic fluids as well as extreme temperature ranges is frequent. In addition to this, thermoplastic composites have the possibility of healing (by melting and re-moulding). Thermoset composites, on the other hand, do not have this ability. Thermoset components have to be removed and the whole structure has to be replaced by new thermosetting composites. All these features have resulted in the development of thermoplastics composites for a number of commercially available products.

From a manufacturing point of view, the development of thermoplastic composite processing has mirrored thermosets. However, the former can offer distinct advantages over the latter such as unlimited shelf life and the recyclability. A 2-D thermoplastic composite can be re-moulded into a 3-D component. Two different thermoplastic composite components can also be joined using welding to form a composite assembly. In addition to this, no chemical reaction takes place during these processes, as only heat and pressure are required for composite consolidations[28]. Therefore, thermoplastic composites are particularly attractive for automated high volume production.

2.3 An overview of thermoplastic composite manufacturing

The manufacturing of continuous fibre reinforced thermoplastic materials requires the production of a prepreg by impregnating the fibres with the thermoplastic resins. The prepreg consists of either unidirectional or woven fibres. In order to fabricate the actual structural components, the prepreg is then laid in a mould and subsequently consolidated under a specific temperature and pressure[29]. The two main difficulties in manufacturing encountered in the production of continuous fibre reinforced thermoplastic composites are[30]:

(a) Achieving full impregnation of the fibres (this problem arises from the inherent melt viscosity of the polymer).
(b) The lack of formability of thermoplastic prepreg (difficulty in laying up in the mould).

Unidirectional, continuous fibre reinforced thermoplastic composites can be manufactured mainly by pultrusion [31], the commingled yarn approach [32], film stacking [33] or powder impregnation [32]. The next section aims to give a brief outline on the manufacturing of continuous fibre thermoplastic composite.

2.3.1 Film stacking

The process of film stacking involves the impregnation of a woven fibre base with a reduced amount of resin, producing prepreg with a relatively high fibre volume fraction, V_f [33]. Due to the low resin content, the resulting prepreg is easily formable. To produce a part, the prepreg is stacked alternately in a mould with films of pure resin. The layers are then consolidated under a specific temperature and pressure, resulting in the desired thermoplastic composite structure. The disadvantage of this method lies in uneconomically high consolidation pressures (~10 MPa), which reduce the permeability of the fibre bed, and the long consolidation times (up to 2 h) [30]. Therefore, the film stacking method is not easily transferable to large-scale production and is best suited for small, lab-scale operations.

2.3.2 Commingling of hybrid yarns

The process of commingling hybrid yarns involves weaving the yarns of reinforcement and matrix polymer into a hybrid tow [34]. A model cross section is shown below (Figure 3) [35].

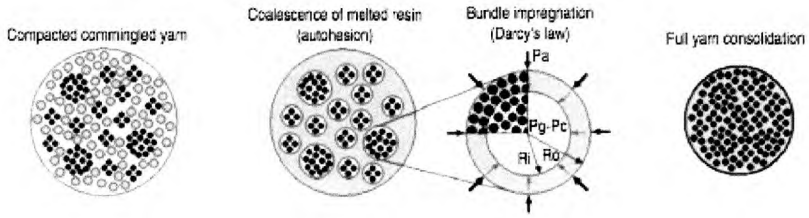

Figure 3: Commingling impregnation model [35]

The yarn can be braided to produce a two-dimensional textile or 3-D structure before consolidation [36 - 39]. The setup (Figure 4) shows an example of how this form of composite can be processed and formed before consolidation [40]. It has been showed that after consolidation, the homogeneity of the resulting composite is strongly dependent on diameters of the commingled fibres [41]. A commingled weave of matrix and reinforcement with diameters that are approximately equal produces a more uniform composite.

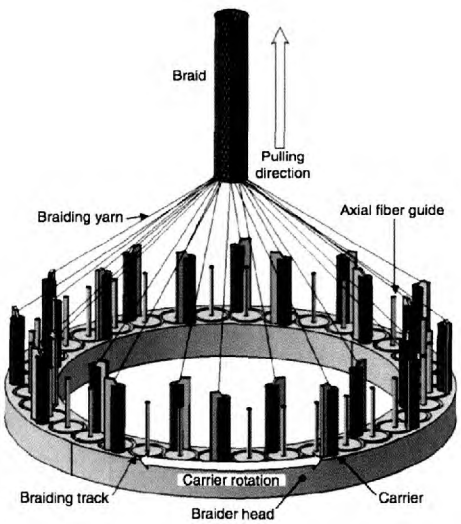

Figure 4: Weaving of commingled yarns [40]

Recent developments in processing have led to the production of three-dimensional woven parts from commingled yarns, these near net-shape parts exhibit good performance in terms of impact tolerance and interlaminar properties [42].

2.3.3 Solvent impregnated fabrics

Thermoplastic resins such as polyethersulfone (PES) and polyetherimide (PEI) can be dissolved in a suitable organic solvent and the resulting solution used to produce prepregs in a similar way to thermosets [43]. A commercial example of this is TenCate's Cetex®, which is currently finding application in interior and exterior structural elements in new Boeing aircraft, such as the latest 737-800, 777-300ER, and 787 Dreamliner models, as well as in Airbus's A380-800 [44]. One of the downfalls of this method lies in the manufacturing advantages: it has inherent difficulty in removing residual solvent creating plasticised regions within the polymer; these are weaker than crystalline regions in terms of mechanical properties and chemical resistance.

2.3.4 Tape production by aqueous polymer slurries

Vodermayer et al. [45, 46] described a powder impregnation method using an aqueous polymer suspension, which is versatile enough to produce a variety of carbon fibre-reinforced unidirectional thermoplastic prepreg tapes. Tang et al. [47] presented a model to correlate particle size, fibre diameter and fibre volume fraction with aqueous slurry concentration.

In this study, a powder impregnation method based on the process developed by Vodermayer et al. [48] was used. The powder suspension thermoplastic composite tape manufacturing process was based on a polymer suspension-based fibre impregnation step that was followed by a drying, melting and consolidation. The process allowed direct control over the fibre volume content of the composites and reproducible and continuous composite manufacturing. However, more generally a powder

impregnation system consists of an impregnation chamber containing a slurry or fluidized powder through which the fibres are pulled. In a polymer suspension based process the continuous phase is usually water. In order to produce a consolidated thermoplastic composite tape from a powder impregnated preform (which are either unidirectional fibres or a woven mat), the powder impregnated fibres exiting the impregnation chamber has to pass through a set of ovens which dry off the water and melt the powder. To impregnate the fibres, it is followed by either cooled dies, nip rolls or a belt press to squeeze the molten polymer into the fibres and to remove all voids, producing a fully consolidated continuous thin thermoplastic composite tape. The main advantage of such thin thermoplastic composite prepregs is that they are very flexible and much cheaper and more environmentally friendly than prepregs produced by solvent or melt impregnation. Moreover, the short distance that the polymer has to spread to wet out the fibres is beneficial if high viscosity polymer melts, including potentially nanocomposites melts, are to be used. However, the main drawback of this method is that the composites properties may be affected by the presence of residual surfactants used to suspend the polymer powder in the impregnation bath.

The consolidated thin thermoplastic composite tapes obtained from the powder impregnation process can be further processed into composite structures using a number of processes, such as compression moulding, filament winding or tape laying.

2.3.5 Full consolidation of unidirectional thermoplastic prepregs

A fully impregnated composite tape can be produced via a modified pultrusion process, whereby the presence of a suitable reagent on the fibre surfaces causes an increase in molecular weight of the polymer during processing[42]. The resulting composite comes in the form of tape of variable width. The fully impregnated prepreg is stiff and does not exhibit the drape properties commonly seen in its thermosetting cousins. This problem has been somewhat overcome by weaving narrow tapes into fabric form.

2.4 Carbon fibre reinforced PEEK composites

PEEK is a semi-crystalline thermoplastic. It is slowly replacing metals and other materials in high performance application such as in the aerospace industry such as leading edges of A350 Airbus wings. This is due to the fact that PEEK is a high strength thermoplastic with high thermal properties and good chemical resistivity[49, 50]. This polymer is ideal for highly aggressive environments. PEEK can withstand a continuous temperature of up to 260 °C and even higher temperatures for short duration. It also has outstanding wear resistance over wide ranges of pressure, velocity and temperature[51, 52]. More importantly, it has excellent chemical resistivity to jet fuels, salt spray and chemical/biological agents at elevated temperatures. As far as the mechanical properties of PEEK are concerned, it possesses tensile modulus and tensile strength of 3.6 GPa and 100 MPa[53], respectively. It also possesses flexural modulus and flexural strength of 4.1 GPa and 170 MPa[53], respectively.

When PEEK is reinforced with carbon fibres, its properties can be improved[54-58]. This is highly favourable as a combination of high stiffness and low density of the

carbon fibre reinforced PEEK composites makes the material ideal for innovative designs that require the combination of non-metallic and metallic materials. The resulting composites will also have high toughness (approximately 10 times higher than traditional carbon fibre reinforced thermosets composites). High performance PEEK composites can be produced. Table 1 shows the mechanical properties of carbon fibre reinforced PEEK composites.

Table 1: Mechanical properties of carbon fibre reinforced PEEK composites [54]

Fibre direction	0°		90°	
	Modulus / GPa	Strength / MPa	Modulus / GPa	Strength / MPa
Tensile	138	2070	10.5	99
Compression	124	1360	n/d	n/d
Flexural	124	2000	n/d	n/d

2.4.1 Processing and manufacturing of carbon fibre reinforced PEEK composites

When pressing laminates, it is crucial that the fibres in all plies are aligned accurately and that the surfaces are free of contaminants, such as oil, as this could potentially lead to poor adhesion in the polymer. Associated problems with pressing tend to be dry fibre regions, excess polymer regions, specimens that are not flat, fibre waviness in the sample and poor consolidation resulting in delamination. Different curing cycles have been examined and it was found that differences on specimen dimensions and consolidation pressures strongly affect the mechanical performance. Cogswell [59] suggests three clear stages of hot pressing laminates:

1. Heating with a 0.1 MPa surface pressure up to between 370 °C – 390 °C for 5 min + 1 min / ply up to 30 min
2. Consolidation at 6 MPa for 5 min
3. Cooling with consolidation pressure maintained for about 5 min at 40 °C/ min

When carbon fibres are added into PEEK, the crystallinity of the polymer matrix can be affected[57,60]. Kim et al.[61,62] also studied the optimisation of processing carbon fibre/PEEK composites for maximum mechanical properties. Figure 5 summarises the effect of cooling rates on crystallinity in PEEK composites. The authors also examined the effects of cooling rate on crystallinity on the interlaminar shear strength (ILSS) as measured by short beam shear tests and the results are shown in Figure 6.

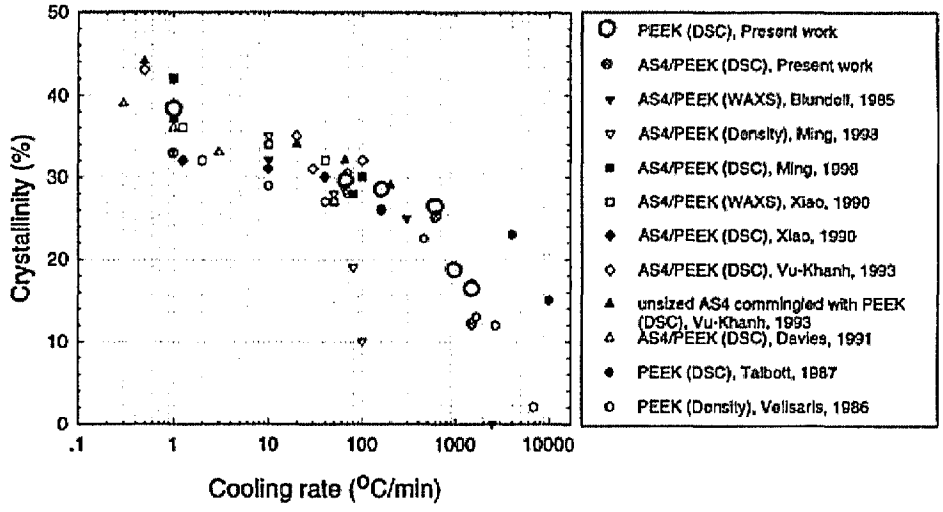

Figure 5: Effect of cooling rate on the crystallinity in CF/PEEK composites [62]

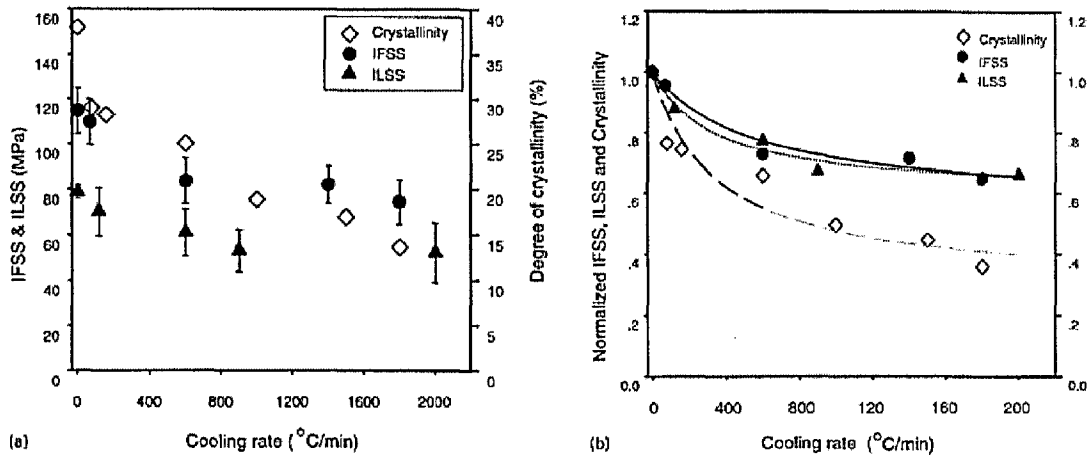

Figure 6: Interlaminar shear strength (ILSS) and interfacial shear strength (IFSS) of CF/PEEK with varying cooling rate [62]

In addition to various cooling rates, the crystallinity of PEEK can also be altered through the use of solvents. PEEK composites are resistant to solvents, but they can swell in dichloromethane (degreasing agent) and paint stripper (methyl ether ketone). Stober et al. [63] explored the effect of dichloromethane on PEEK films of varying crystallinity. This work aims at studying the thermo-mechanical properties for processing applications (possible applications include the use of methylene chloride for the reduction of annealing times to induce crystallinity). It was found that amorphous PEEK swells in 1,1,2,2-tetrachloroethane (TCE) [64] with up to 240 % mass uptake within 2 to 3 min upon immersion in solvent. This is a direct result of acid-base interaction with the C=O and O-O bonds in the PEEK, which acts as a weak base. TCE exhibits such good interaction with PEEK in comparison with other organic solvents such as chloroform because it has more acidic sites per molecule [64]. Wolf et al. [65] investigated the adsorption - desorption and resorption of toluene and carbon disulphide (CS_2) on amorphous and semi-crystalline PEEK. The authors reported that absorption in amorphous PEEK is much more apparent than in crystalline PEEK, where toluene is not absorbed and no swelling occurs. This could

be due to the reduction in the number of free basic sites since they are involved in the formation of lamella in a crystalline phase. The authors also found a higher rate of swelling with CS_2 when compared to toluene. In addition to this, the extent of swelling by CS_2 is uniform. Solvent induced crystallisation occurred when the PEEK is amorphous because swelling is predominantly through the thickness of the PEEK whilst in semi-crystalline PEEK it is near isotropic.

Dillon [66] reported problems with pressing flat laminates uniformly due to uneven pressure from the machine. This had led to PEEK melt flowing out from the edges of the mould. Patel [67] reported that the hot plates vibrated at higher consolidation pressures which results in reduced crystallisation rates. The authors also found delaminations around the sides of the samples that were subjected to re-pressing. Nevertheless, it was found that carbon fibre/PEEK can be re-pressed up to five times without any detrimental effects on the mechanical properties of the composites.

2.5 Carbon nanotubes reinforced PEEK nanocomposites

Individual CNTs have been predicted and observed to have remarkable properties. Axial stiffness and strength are of the order of 1 TPa and 50 GPa [2, 68], respectively, and densities of less than 2 g/cm^3. A high degree of flexibility is retained, with recorded reversible deflections of over 120°. On the other hand, multi-walled CNTs are generally electrical conductive and if sufficiently crystalline may be ballistic conductors [69].

Over recent years a number of attempts have been made to produce CNT-based nanocomposites stimulated by these constituent properties [70]. There has been

considerable success in generating useful levels of electrical conductivity in otherwise insulating thermoplastic matrices [71], and at remarkably low loading fractions (less than 0.01 wt%) in epoxies [72, 73]. Regarding mechanical properties, nanocomposites with improved properties have been made, but progress has so far been hindered by a number of issues, not least the difficulty of growing perfectly crystalline CNTs in large quantities. Nevertheless, useful composite properties may be obtained with existing bulk materials and given the enormous research efforts on CNT synthesis, further improvements may be anticipated as new materials become available.

Table 2: Mechanical properties of CNT reinforced PEEK nanocomposites containing various CNT loading fractions [79]

	Tensile Modulus (GPa)	Tensile Strength (MPa)
0 wt%	4.0	95
5 wt%	4.6	105
10 wt%	5.2	110
15 wt%	5.5	120

High performance PEEK nanocomposites can also be produced by the incorporation of carbon nanotubes into the matrix. This will create so-called nanocomposites [74 - 78]. Due to the high specific area and high strength of CNTs, the mechanical properties of CNTs reinforced PEEK nanocomposites can be improved [79, 80]. Sandler et al. [79] showed that the tensile strength and modulus of the nanocomposites improved by as much as 38 % and 26 %, respectively, at a loading fraction of 15 wt%. Table 2 shows the mechanical properties of PEEK nanocomposites at various CNT loading fractions.

2.6 Crystallinity of semi-crystalline polymers as a matrix for composite materials

An important factor that influences the mechanical properties of composite materials is the crystallinity of the polymer. As aforementioned, the crystallinity of a polymer is strongly governed by the cooling rates employed during manufacturing or post manufacturing annealing of the specimens [81, 82]. During these processes, the fracture toughness of the composite can be altered [83]. Furthermore, the addition of the CNT into polymer matrix is known to affect the degree of crystallinity of the composite. The trends observed are due to the acceleration of crystallisation, enhanced nucleation, reduced growth rate, changes in spherulitic morphology and formation of imperfect crystallites.

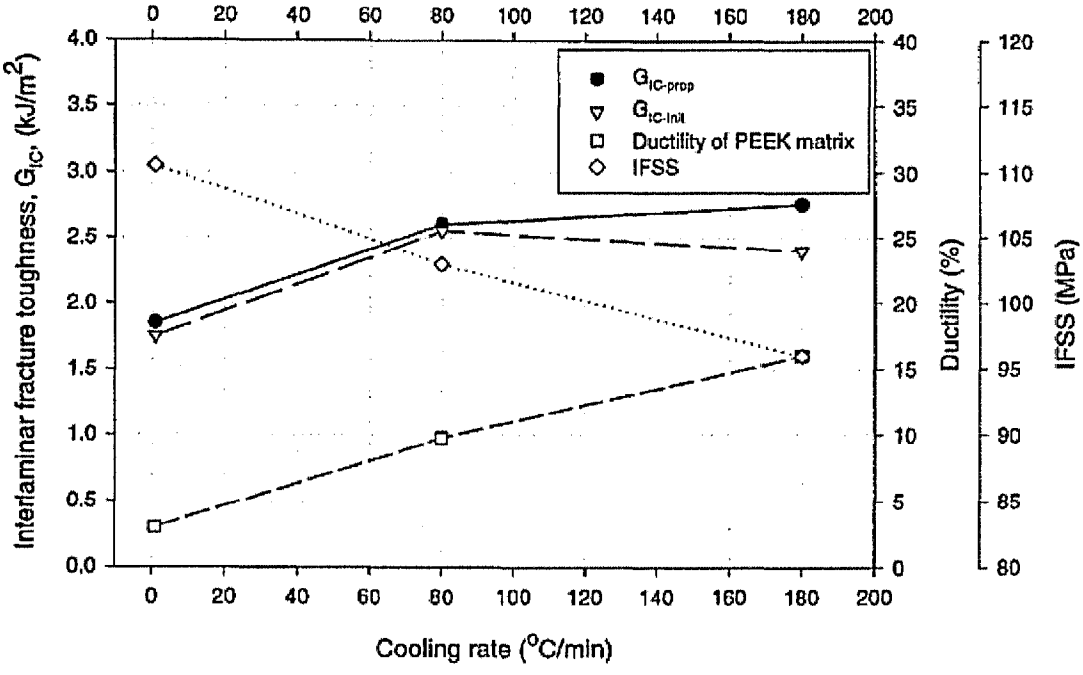

Figure 7: Variation of composite mode I interlaminar fracture toughness, matrix ductility, interfacial shear strength (IFSS) as a function of cooling rate [82]

However, experimental evidence for the crystalline coating around the CNT has not been conclusively demonstrated due to the lack of quantitative correlations [84]. Studies by Gao et al. [81, 82] have explored into Mode I and Mode II fracture toughness and found that the G_{IC} increased as cooling rates increase, starting from 1 °C/min to 180 °C/min (Figure 7). As expected, a low cooling rate resulted in an increase in the degree of crystallinity of the polymer matrix. It should be noted that the fracture toughness is strongly correlated with the interaction between two important properties: the matrix ductility and the interface interaction at the fibre-matrix interface. The ductility is proportional to the cooling rate while it is non-proportional for the fibre interface bond strength.

Extensive studies comparing the crystallinity and the crystal morphology of carbon fibre reinforced PEEK (such as the commercially available APC-2 composites) and neat PEEK have been done [85 - 93]. Jar et al. [94] investigated the effects of different thermal treatments on the crystal morphology and growth. The authors found that specimens which were subjected to heat treatment at 350 °C allowed more crystallite formation as compared to those treated at 370 °C and 390 °C. In addition to this, the crystallinity increases with slower cooling rate (Figure 5). These findings were also confirmed by Cebe [95], where the author carried out extensive research on the annealing of PEEK. It was showed that increased annealing time resulted in increased density and greater crystal perfection of PEEK. Furthermore, when carbon fibres were incorporated into the matrix, the fibres acted as nucleating sites, which allow the spherulites to grow [96]. However, this effect is highly dependent upon the diameter, the quality and the distance between the carbon fibres [97].

2.7 Hierarchical fibre-reinforced polymer nanocomposites

Over the past four decades, fibre-reinforced polymer composites have been intensively studied and have found wide ranging practical applications, from sporting equipment to aerospace and even in the oil and gas industry. Despite these developments, there is still a need to improve certain fundamental properties, particularly transverse, interlaminar and off-axis performance, as well as the resistance to environmental, chemical, and thermal damage. In addition, the through-life costs associated with composites are a significant factor during material selection.

On the basis of the remarkable properties predicted for and measured on individual, high-quality CNTs, a wide range of applications have been suggested, ranging from nanoelectronics to catalyst support materials. However, one of the most promising areas is the use of CNTs in polymer composite materials. Research efforts were mainly focussed on exploiting the remarkable mechanical properties of individual CNTs, particularly their uniquely high strength, for the development of polymer nanocomposites. However, there is an immediate opportunity of utilising the existing, less crystalline CNTs produced in large quantities by a variety of manufacturers (such as Nanocyl, Bayer Materials Science and Arkema) in applications where conventional reinforcements cannot be physically accommodated. One particularly exciting prospect, and one which has not yet been fully explored although the numbers of publication are now rapidly increasing, is the possibility of producing CNT reinforced matrices for conventional advanced fibre reinforced polymers.

As mentioned above, conventional composite laminated have very good in-plane mechanical properties but are relatively weak in the through thickness direction, because the polymer matrix holds the micrometre sized reinforcing fibres in place. High mechanical loads cannot be sustained by polymers alone which have low mechanical properties. It was, therefore, anticipated that the incorporation of nanofillers, such as CNTs or carbon nanofibres (CNFs), into the matrix of conventional composites to create a hierarchical structure would result in significant improvements of the through thickness matrix dominated properties.

Two entirely different concepts to create hierarchical composites were envisioned: namely to disperse the nanoreinforcement entirely throughout the composite matrix or to attach the nanoreinforcement directly onto the mircometre-sized reinforcing fibres (Figure 8). A real example of a hierarchical carbon fibre reinforced CNF reinforced polymer is shown in Figure 9. The literature contains quite a number of reports of CNT modification of thermosetting matrices [98 - 104]; however there is only very few reports on hierarchical thermoplastic composites which have yet to be published. The second approach has mainly focused on direct "grafting" CNTs or CNFs directly onto the reinforcing fibres and thereby creating "hairy fibres" (for a real example see Figure 10. The literature contains reports on CNT grafted inorganic (ceramic) [105 - 108] and glass fibres [109 , 110], carbon fibres [111 - 116] and even Kevlar fibres [117]. In addition to the direct growth of CNTs on fibres, with electrophoretic deposition (EPD) of CNTs on fibre surfaces [118] and the use of CNT containing epoxy sizings [119] have been explored to improve mainly interface dominated composite properties.

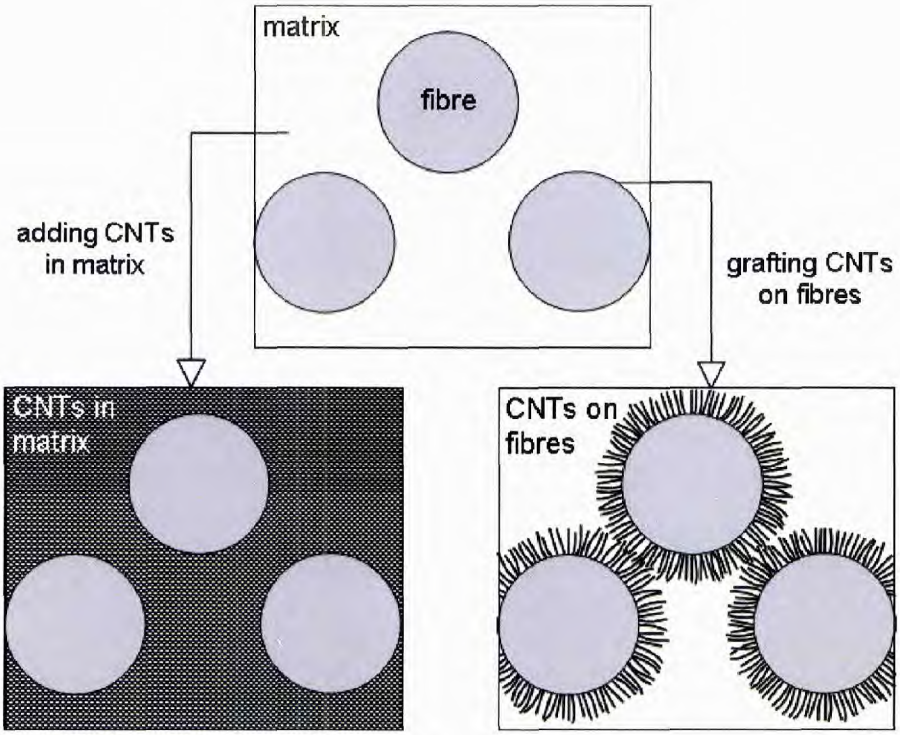

Figure 8: Schematic diagrams of conventional fibre-reinforced polymer composites and CNT-based hierarchical polymer composites [120]

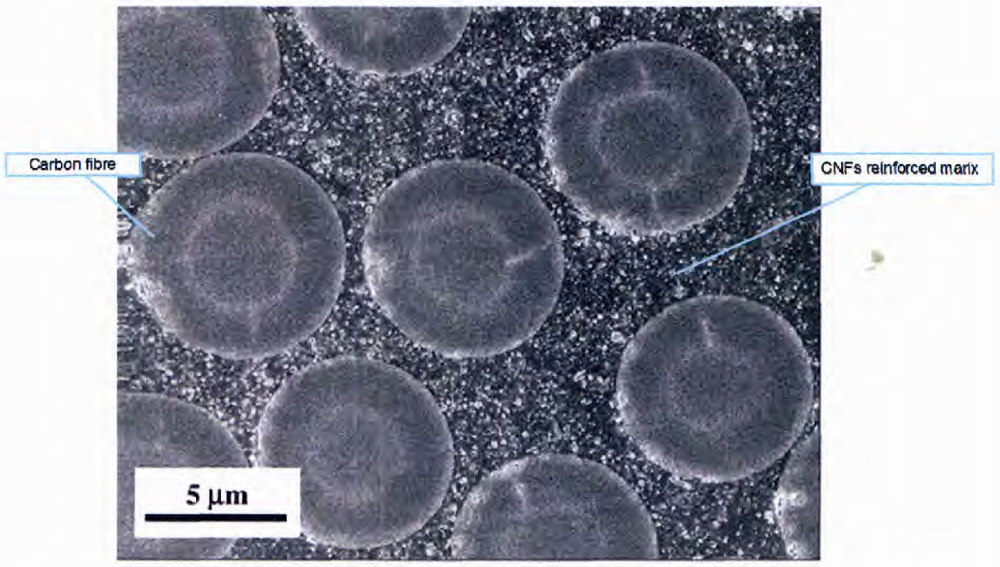

Figure 9: SEM micrograph of 5 wt% CNFs reinforced CF epoxy composites [121]

Because of the challenges associated with dispersing CNTs within a liquid matrix and the impregnation of a micrometre sized reinforcing fibres with such a CNT

modified resin, self-filtration effects occur. For example using resin transfer processes, self-filtration prevents resin-suspended CNTs from penetrating between the conventional fibres [122]. More research focused on directly "grafting" CNTs or CNFs onto the fibre surface using different catalyst systems and synthesis methods. A variety of morphologies and distributions of CNTs or CNFs grafted fibres has been reported (see Figure 10). Based on the early studies, the chemical vapour deposition (CVD) route is an effective and practical method for CNT grafting. However, plasma enhanced (PE) CVD is another effective way to graft CNTs or CNFs to fibres. This process [111] works at much lower temperature and allows for better control.

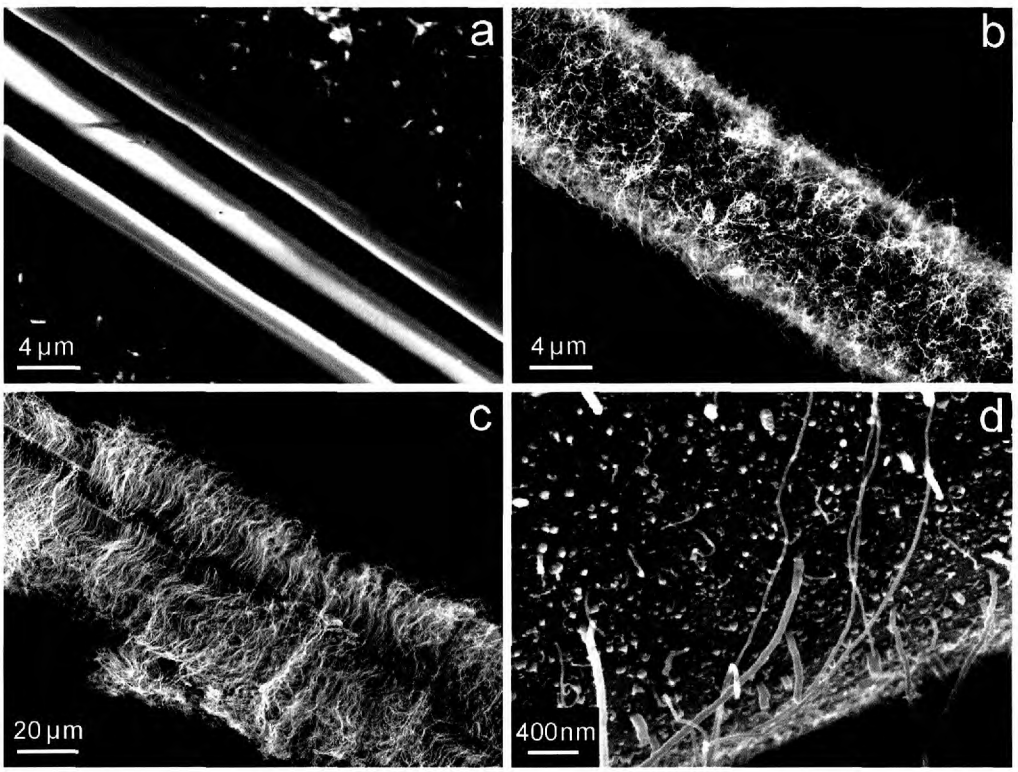

Figure 10: SEM micrographs of silica fibres before (a) and after CNT growth reaction (b), (c) using the ICVD method with increasing growth times and after the deliberate removal of the grafted CNTs (d) [110]

A green (biodegradable and renewable) analogue to the CNT grafted fibre system was produced by coating natural fibres with bacterial cellulose nanofibrils [123 - 125].

The mechanical properties of the primary sisal fibres were maintained. The IFSS between the bacterial cellulose coated sisal fibres and the bio-derived polymer poly(L-lactic acid) (PLLA), as determined using the single fibre pull out test, increased significantly. The modified sisal fibres were incorporated into PLLA, to obtain a new class of truly green hierarchical composites. The tensile strength and stiffness of unidirectional compression-moulded composites improved in both parallel and perpendicular loading direction to the primary fibres. The rate of water uptake, a critical problem for natural fibre composites, was also reduced. These results are both promising in their own right and encourage further development of the analogous CNT reinforced composite systems.

2.7.1 Fabrication of hierarchical composites

Three main processes for manufacturing hierarchical thermoset polymer composites are predominantly studied: resin transfer moulding (RTM), vacuum assisted resin transfer moulding (VARTM) and a manual resin impregnation-hot pressing technique [126]. In order to manufacture hierarchical composites with the desired properties, the CNTs or CNFs must be dispersed uniformly in the polymer matrix and self-filtration of the CNTs on micrometre sized fibre bed must be prevented. Furthermore, care must be taken to minimise the void content introduced during resin impregnation. It was shown that the agglomeration of CNFs or CNTs can reduce the effective bonding between the polymer and the reinforcement [127]. Moreover, large CNTs or CNFs agglomerates will be filtered more effectively by the reinforcing fibres bed during resin impregnation, especially if the agglomerate size is close to the pore dimensions (i.e. the spacing in between the reinforcing fibres) of the fibre assembly. Furthermore, with increasing the CNT (or CNF) concentration, the resin

viscosity increases massively, which will affect manufacturing processes, such as RTM and VARTM, which require the resin to flow easily. The high resin viscosity, local CNT filtration, air entrapment among CNTs can all result in voids, which significantly affect the mechanical properties of hierarchical composites. Hence, there are still many manufacturing issues that need to be addressed to achieve uniform CNT dispersion and better CNT alignment, higher loading fraction of CNTs and low void content. To circumvent these problems we proposed the use of thermoplastic matrices which will enable the successful manufacturing of unidirectional fibre reinforced nanocomposites. The use of thermoplastic systems may offer significant advantages in enabling suitable processing strategies. The difficulty in producing thermoplastic composites is the impregnation of the reinforcing fibres by very viscous polymer melts; however, new powder impregnation processes (described above) have proved to be very effective and versatile for the manufacture of unidirectional thermoplastic composites [46]. However, this process requires fine nanocomposite powders for fibre impregnation that can either be created by solution precipitation [128], spray-drying from solutions or micro-extrusion and cryogenic grinding. Such a process is expected to yield an approximately random arrangement of CNTs around the primary carbon fibre reinforcement, since the flow paths during composite consolidation are short in this technique.

2.7.2 Mechanical and physical properties of hierarchical composites

Nanocomposites with improved mechanical properties have been produced and given the enormous research efforts on CNT synthesis further improvements may be anticipated as new materials become available.

Iwahori et al. [129] measured the in-plane tensile properties of carbon fibre CNF reinforced epoxy composites. They found that the tensile strength of the CNF modified epoxy composites improved up to CNF loadings of 5 wt%. Moreover, longer CNFs at the same loading fractions resulted in larger property improvements. The authors reasoned that this improvement was because longer well dispersed CNF resulted in better interfacial adhesion between the CNFs and matrix. However, for increased CNF loadings (10 wt%) the longer CNFs resulted in a weakening of the composites as it became more difficult to disperse the longer CNFs in the matrix of the composites uniformly without creating voids and agglomerates. However, they also reported that the addition of CNFs resulted in a significant reduction of the tensile modulus, which may be due to the presence of defects such as voids and agglomerates. On the contrary, Yokozeki et al. [121] reported that the tensile stiffness of carbon fibre reinforced CNTs reinforced epoxy composites increase slightly with increasing CNTs content while the tensile strength was independent of CNT loading fraction. Based on these experimental results, it can be concluded that the in-plane tensile properties of fibre reinforced CNT (or CNF) reinforced thermoset polymer composites are not significantly improved in comparison to conventional fibre reinforced thermoset composites, which is not unexpected since tensile properties of composites are fibre dominated. Moreover, the introduction of defects during manufacturing of hierarchical composites, such as nanomaterial agglomerates and voids, can reduce the tensile strength of hierarchical composites.

Iwahori et al. [129] measured the compressive properties of carbon fibre reinforced CNF reinforced epoxy composites. They found that the incorporation of CNFs into the matrix resulted in 15% higher compressive strength as compared to the neat

carbon fibre epoxy resin composites. However, longer CNFs at higher loading caused a dramatic decrease of the compressive modulus of the hierarchical composites, which they attribute to the presence of defects, such as voids and CNFs agglomerates, induced during manufacturing. Based on these experimental results, it can be concluded that CNF reinforcement of carbon fibre epoxy composites can yield a considerable improvement in the compressive properties over conventional carbon fibre epoxy composites. The main reason for the improvement of the compressive properties is the increased modulus of resin matrix which restricts fibre buckling under compression load.

Since interlaminar properties are matrix dominated it is reasonable to expect a significant improvement of the interlaminar properties by modifying the matrix of conventional composites by incorporation of CNTs or CNFs. Gojny et al. [130] conducted short beam tests to determine the interlaminar shear strength (ILSS) of glass fibre reinforced carbon black and DWCNT-NH_2 reinforced epoxy composites. A significant improvement of the ILSS by 20 % with the addition of 0.3 wt% DWCNT-NH_2 into the composite was found. The increased epoxy matrix strength caused by the incorporation of the nanoreinforcements is the most important reason for the increased ILSS. Moreover, the increased interfacial bonding between the glass fibres and the nanoreinforcement could be another possible mechanism which enhances the ILSS.

As discussed above, the incorporation of carbon nanomaterials does not affect the tensile properties of thermoset composites but leads to, if processed into defect free composites, significant improvements of matrix dominated interlaminar and

compression properties of these composites. However, the presence of CNTs in fibre-reinforced composites can be beneficial for other physical properties, such as electrical [130, 131] and thermal conductivity, thermal stability [132] and flame retardancy [133].

2.8 Summary

Published results indicate the importance of thermoplastic composites but also the difficulty associated to their manufacturing and processing, particularly in the case of PEEK which has a high processing temperature and hence demands specific equipments. Annealing seems to be of importance and carbon fibre can sometimes act as a nucleating agent promoting spherulite growth. CNTs have excellent theoretical mechanical properties. Reinforcing a matrix with CNTs could lead to improved mechanical properties but these improvements have so far not been seen, specifically in thermoplastic matrices. CNTs could also act as nucleating agents, hence care must be taken to differentiate the reinforcing effect of CNTs from that of CNTs being a nucleating agent. Hierarchical composites show promising results to enhance matrix dominated properties, such as mechanical but also, electrical, thermal and chemical properties.

Chapter 3 - Experimental

This chapter describes the experimental work on carbon nanomaterial characterisation, composite manufacturing and composite mechanical testing performed during the course of this research using various materials, characterisation techniques and testing methods. Materials used are described and their properties as published by suppliers provided. Characterisation techniques used, such as scanning electron microscopy (SEM), surface area measurement (BET), thermal gravimetric analysis (TGA), laser raman spectroscopy (LRS), differential scanning calorimetry (DSC), laser diffraction particle sizing and single fibre pull-out test, are explained including the parameters used. Furthermore, the manufacturing of PEEK composites using various equipments including a micro-extruder, twin-screw laboratory extruder, injection moulder are described. This chapter also describes the production of CNT-reinforced PEEK powder as well as the thermoplastic continuous composite line process and the compression moulding of laminates. Finally mechanical testing is explained including tensile testing of extruded monofilament and injection moulded specimens, compression, in-plane shear and flexural testing of injection moulded materials and lastly flexural and short beam shear testing of thermoplastic and hierarchical composites."

3.1 Materials

Carbon nanotubes (CNTs) were chosen for their (theoretical) high strength and modulus compared to any other available reinforcements (such as carbon fibres). The main advantage of using CNTs is their small diameter, which results in high specific surface area [134]. Since their discovery, much work has been done to synthesise CNTs on an industrial scale at lower cost. Several companies now produce CNTs with

different qualities and diameters mainly by using the Chemical Vapour Deposition (CVD) technique. The choice of CNTs for this specific project was chosen based on past experience, as is detailed below. The CNTs used were from NanoAmor [135], Nanocyl [136], Heji Inc [137], Baytubes [138] and Toray R&D [139] (Table 3).

Table 3: The different types of CNTs used in this study [135] - [139]

Supplier	Type of carbon nanotube	Diameter (nm)
Heji Inc	Multi wall CNT	<8
	Multi wall CNT	8 – 15
	Multi wall CNT	10 – 20
	Multi wall CNT	20 – 30
	Multi wall CNT	30 – 50
	Multi wall CNT	20 – 40
	Single wall CNT	1 – 2
Toray R&D	Double wall CNT	~3
NanoAmor	Multi wall CNT	10 – 30
	Multi wall CNT	60 – 100
	Carbon Nanofibres	100 – 200
Nanocyl	Multi wall CNT	~10
Baytubes	Multi wall CNT	5 – 20

The first supplier was NanoAmor (Los Alamos, USA) and the second was Heji Inc (Beijing, P.R. China). These two suppliers offered a range of different diameters of CNTs, which had been produced in a similar manner. Heji Inc was chosen because of the lower cost of their materials. This was necessary within this investigation for making hierarchical nanocomposites where an increase in the quantity of the materials is required. Nanocyl (Sambreville, Belgium) has been improving its

processes and now produces different grades of CNTs, as well as different surface modified CNTs. They also have an industrial grade of CNTs (NC7000), which was selected for the current project, as it was available in large quantities at a relatively low cost (€ 500 for 2 kg). In addition to this, double wall CNTs from Toray Research & Development (Nagoya, Japan) was used to further complete the type of materials reviewed, as these CNTs have a very narrow diameter range. These are not commercially available yet but their quality could be of interest. The length of CNTs is not known as it is technically difficult to measure their length due to their small diameters and relatively high aspect ratio, it is assumed that in most cases, their length is around 1 μm.

Two different types of commercially available continuous, high strength and high strain, industrially oxidised, polyacrylonitrile (PAN) based carbon fibres were used for this research namely AS4 [140] and T700 [141]. The properties of these fibres, as well as epoxy matrix composites are summarised in Table 4.

The T700 carbon fibres were kindly supplied by Torayca® (Toray Industries, Tokyo, Japan) and the AS4 fibres by Hexcel Corporation (Duxford, Cambridge, UK). Although both carbon fibres were industrially oxidised, the Hexcel AS4 fibres were available in an unsized form whereas the Torayca T700 fibres were only available with an applied sizing.

Table 4: Properties of CF used in this study [140] , [141]

Fibre type	Torayca® T700SC	HexTow™ AS4
Typical fibre properties		
Tow count	12000	12000
Tensile strength / MPa	4900	4480
Tensile modulus / GPa	230	231
Elongation / %	2.1	1.8
Density / g/cm^3	1.8	1.79
Typical epoxy composite properties (matrix details unknown)		
Volume Fraction / %	60	62
Tensile strength / MPa	2550	2211
Tensile modulus / GPa	135	141
Short Beam Shear Strength / MPa	90	124

The thermoplastic used in this research is polyetheretherketone (PEEK). PEEK is widely regarded as the highest performance thermoplastic material available in the market [54]. It is a semi-crystalline thermoplastic with the chemical structure shown in Figure 11.

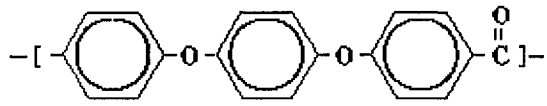

Figure 11: Molecular structure of PEEK (drawn using ChemDraw)

PEEK exhibits excellent thermal characteristics; a glass transition temperature of 143 °C, melting temperature of 343 °C, a process temperature of 360 °C [54] and a density of 1.30 g/cm^3. This polymer has found uses in sectors, which in the past would have been limited to thermoset polymers. The other benefits of PEEK are its

excellent resistance to chemical environments and superior toughness properties. In addition to this, it has also been shown that the toughness of this polymer is not compromised by the addition of reinforcement [142]. Unfortunately, this polymer is relatively expensive and therefore, limited to the defence and aerospace industry. In terms of the mechanical properties of PEEK, there are strongly dependent on the degree of crystallinity of the polymer. Regular sequencing of the repeat units allows elements of the neighbouring polymer chains to pack together in a preferred, lower energy, spherulitic crystalline configuration [59]. The degree of crystallisation and the distribution of spherulitic regions are governed by the thermal history of the polymer, also a suitable degree of crystallinity can be obtained by annealing of PEEK and subjecting it to regulated cooling conditions. The benefits of crystallinity can be found in the high temperature performance of the polymer and its resistance to creep phenomena. The increasing use of PEEK in the industries such as aerospace, offshore oil and gas industry stands as evidence to this. The grades of PEEK used in this study were 150, which is a low melt viscosity grade and available as a powder, and Vicote 804 dispersion (Victrex, Lancashire, UK).

The surfactant used in this study was Aerosol OT-75% E (Cytec, Wrexham, UK). Laminate consolidation was achieved using Upilex polyimide film and adhesive tape (UBE Europe GmbH, Düsseldorf, Germany) in combination with McLube 1862 mould release (McLube, Aston, PA, USA). Other chemicals used in this study were diphenylsulfone (DPS), acetone and ethanol (VWR, UK), tetrachloroethane (TCE) (Sigma Aldrich, UK), dry ice (BOC, UK) and polypropylene membrane support (Novaltex 3471, UK).

3.2 Characterisation techniques

3.2.1 Scanning electron microscopy (SEM)

SEM was performed using a LEO Gemini field emission gun electron microscope (Oberkochen, Germany) with an accelerating voltage of 5-10 kV. Carbon nanomaterials were placed on a stub using a carbon adhesive tab, no coating was applied prior to the SEM characterisation. It was used to measure the diameter of individual CNTs. A high number of CNTs were counted and measured to generate a statistically significant and hence an accurate image of their diameters (see Appendix for details of the procedure). All composites were coated using chromium with the following parameters, the coating current and coating time used were 50 mA and 30 s, respectively.

3.2.2 Surface area measurement (BET)

Brunauer-Emmett-Teller (BET) surface area measurement was performed on Micromeritics ASAP 2010 equipment. It uses the adsorption isotherm of nitrogen at 77 K under vacuum and calculates the volume of nitrogen adsorbed on the material surface for different relative pressures. Two types of surface area measurement can be calculated; a multipoint or a single-point determination, both are described in the International Standard 9277 [143]. The first one takes into account the portion of relative pressure from 0.05 to 0.3 and the second takes only one point at a relative pressure of 0.3. The BET equation is as follows:

$$\frac{\frac{P}{P_0}}{n_a\left[1-\left(\frac{P}{P_0}\right)\right]}=\frac{1}{n_m C}+\frac{C-1}{n_m C}\times\frac{P}{P_0} \qquad (1)$$

where n_a = specific amount adsorbed

P/P_0 = relative pressure

n_m = specific monolayer capacity of adsorbate

C = BET parameter

By plotting $\frac{P}{P_0}$ as the x-axis and $\frac{\frac{P}{P_0}}{n_a\left[1-\left(\frac{P}{P_0}\right)\right]}$ as the y-axis, a straight line $y = a + bx$ is obtained from relative pressure values of 0.05 to 0.3. Its slope b and intercept a correspond to $\frac{C-1}{n_m C}$ and $\frac{1}{n_m C}$, respectively and hence, it is possible to derived the monolayer capacity $n_m = \frac{1}{a+b}$ and BET parameter $C = \frac{b}{a} + 1$. The specific surface area A_s is calculated by assessing the average area occupied by each molecule in the whole monolayer $A_s = n_m \cdot a_m \cdot L$ where a_m is the molecular cross-sectional area (for nitrogen at 77 K, its value is 0.162 nm^2) and L is the Avogadro constant (6.022 x 10^{23} mol^{-1}). Finally, the specific surface area expressed in m^2/g is $A_s = 9.76 \times 10^4 n_m$.

Approximately 100 mg of dried CNT powder was added to a glass tube, sealed and weighed to the 4th decimal place (the scale was in mg). The tube was then subjected to a degassing step within the equipment to dry and condition the sample further under vacuum at a temperature of 120 °C for approximately 6 h. After the conditioning procedure, the sample was weighed again and positioned onto the adsorption part of the equipment, firmly sealed above a liquid nitrogen tank.

3.2.3 Thermal gravimetric analysis (TGA)

TGA measures the weight loss during an increase in temperature with variables that are both controlled and monitored. It provides information as to the purity of the sample by determining the amount of residue left at the end of the experiment. The level of graphitic structure of the sample is evaluated by measuring the onset decomposition temperature. The higher the latter is, the more graphitic the material should be and the lesser amorphous carbon is present. TGA data were recorded on a PerkinElmer Pyris 1 in a compressed air atmosphere. In all of the experiments, the ramp rates were 10 °C/min and air flow rates were 20 mL/min, using around 10 mg of material each time.

3.2.4 Laser Raman Spectroscopy (LRS)

Laser Raman spectroscopy is a vibrational spectroscopic technique [144], which is based on the non-zero change in polarisation during vibration. When an incident beam is shone on a molecule, the energy associated with the incident beam can be absorbed or scattered. The process of absorption requires that the energy of the incident beam is equal to the energy difference between the two states of the molecule. The two states are accompanied by a change in the dipole moment of the molecule. This virtual state system is very short lived and it relaxes by the emission of photons. This is the basic principle behind infrared spectroscopy. In addition to absorption, the incident beam can also be scattered. This scattering effect (Raman effect) is the exchange in energy between the incident and emitted radiation caused by the inelastic scattering of photons.

The two Raman active modes of carbon fibres can be observed at the Raman bands of 1580 cm^{-1} and 1355 cm^{-1}. The 1580 cm^{-1} Raman band corresponds to the deformation mode of the hexagonal carbon ring structure, which is usually associated with the graphite crystal layers. The 1355 cm^{-1} Raman band, on the other hand, corresponds to the polycrystalline graphitic mode [145]. Another important parameter is the ratio between the 1580 cm^{-1} and 1355 cm^{-1} Raman band. This parameter is directly related to the amount of defective and crystalline modes in carbon fibre samples. This parameter measures the edge dislocations, vacancies and crystal edges.

LRS was performed using a LabRam Infinity Analytical Raman Spectrometer (Jobin Yvon Horiba, Middlesex, UK) in order to examine the bulk properties of the carbon fibres. A red laser operating at a wavelength of 633 nm was used. The laser was focused on the sample using a 100x objective at a power of 100 % through a 200 μm aperture. A grating of 600 mm^{-1} with an acquisition time of 20 s was applied while the measurements were carried out in the wavenumber range from 100 to 3000 cm^{-1}. The room was temperature controlled (20 °C). Six individual spectra were taken at various locations along the sample. The spectra were analysed with a mixed Gaussian-Lorentzian curve fit with a linear baseline to determine the peak areas and shifts.

3.2.5 Differential scanning calorimetry (DSC)

DSC (Q2000, TA Instruments, UK) was used to evaluate the crystallinity of PEEK in a nitrogen environment. Two types of specimens were examined; PEEK and PEEK/CNT, both of which underwent the same thermal treatment prior to and during DSC characterisation. The weight of each specimen was approximately 10 mg,

which were cut from injection moulded specimens. A single heating at 10 °C/min was used for all specimens to evaluate crystallinity.

3.2.6 Laser diffraction particle sizing

Laser diffraction particle sizing was used to determine the powders particle size distribution (PSD) using a Mastersizer 2000 (Malvern, Malvern, UK). The principle of this technique is based on the scattering of a laser beam when particles passes through, the angle the light is scattered is directly related to the particle. The diffraction angle increases logarithmically with decreasing particle size. The average particle size (d_{50}) defines the diameter where 50 mass % of the particles will be larger and smaller than this average equivalent diameter. Solutions (5 ml) were prepared using a concentration of 60 mg/ml with 2 wt% of surfactant.

3.2.7 Single fibre pull-out test

Single fibre pull-out tests were performed to determine the apparent interfacial shear strength (τ_{IFSS}) between carbon fibres and the matrix. This is used as a measure of the practical adhesion at the fibre/matrix interface. A single fibre was partially embedded into the polymer melt at a pre-determined length of between 50-150 μm using a homemade apparatus [146]. The solid polymer pellets were placed on an aluminium sample carrier, heated and held at a temperature above T_m of the polymer while the fibre was penetrated into the melt. Once the embedding of the fibre has been performed the sample was cooled to room temperature using an air stream. A laser diffraction method [147] was used to determine the fibre diameter. The fibre pull-out test was performed using a piezo-motor fixed on a high stiff frame to avoid energy storage in the free fibre length between the matrix surface and the clamping device.

The fibre was drawn at a speed of 0.2 μm s^{-1} from the matrix while the force was recorded throughout the experiment by the load cell and logged using a computer. The maximum load is correlated to the full debonding of the fibre-matrix interface along the embedded length from the matrix. The shape of the curve itself reflects on the failure event at the interface [148]. The apparent shear strength τ_{IFSS} was calculated from the maximum pull-out force F_{max} required to trigger the debonding of the embedded carbon fibre from the matrix using the following equation:

$$\tau_{IFSS} = \frac{F_{max}}{\pi d_f L_e} \quad (2)$$

where d_f is the diameter of the fibre and L_e is the embedded fibre length. The embedded fibre length is measured by the intersection of the friction slope after debonding occurred and the displacement axis when the force is 0 N (Figure 59).

3.3 Manufacturing of PEEK composites

3.3.1 Micro-Extruder

Melt blending of PEEK/CNT was used to create nanocomposite blends using a micro-compounder (DSM Research 5 cm^3 micro-compounder, Geleen, The Netherlands). This is a counter-rotating twin-screw extruder (Figure 12) with a maximum capacity of 5 cm^3. A recirculation channel could be used to adjust the residence time. Prior to processing, materials were dried in an air circulating oven overnight at a temperature of 50 °C. Nitrogen purge gas was used during the whole processing through an inlet at the top of the micro-extruder to create an inert atmosphere during processing, to reduce the polymer degradation and remove any trapped air from within the melt.

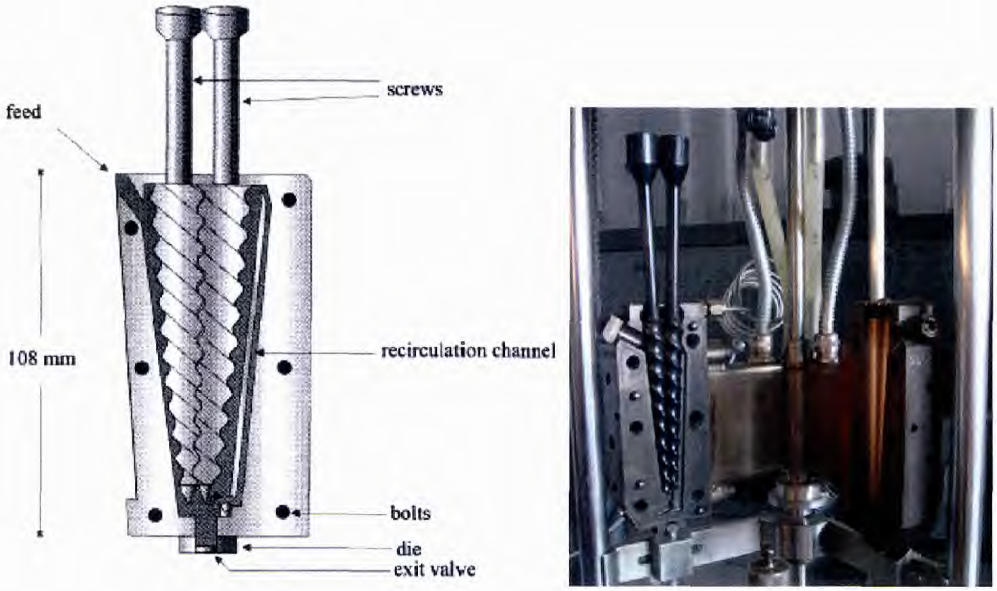

Figure 12: Cross-sectional view of the micro-extruder

5.5 g of nanocomposites were prepared in a two stage process, the parameters for which were optimised through parametric preliminary trials. The first step was to feed materials at a temperature of 400 °C and a speed of 20 rpm, these parameters were selected to ensure a low viscosity of the polymer upon melting (400 °C is the maximum processing temperature recommended before excessive degradation and oxidation of the polymer occur over time) and a low rotational speed to facilitate the feeding of the granules within the micro-compounder throat and feeding section. The speed was then increased to 80 rpm and the temperature was decreased to 360 °C and mixed for 5 min to increase the amount of shear mixing and therefore improve the level of CNT dispersion. The blends were extruded through a 1 mm diameter circular shape die as monofilaments.

Films were also manufactured from the micro-compounder by compression moulding 2 g of material was placed under a 2 MPa pressure at 390 °C. The produced films have a typical thickness of 100 μm. Dog-bone shaped specimens

were cut out using a die cutter (Zwick GmbH, Ulm, Germany) in accordance with ISO 527-2 (Specimen type 5B) [149], with an overall length of 35 mm, a gauge length of 10 mm and a width within the gauge length of 2 mm.

3.3.2 Twin-Screw laboratory extruder

Scale-up of nanocomposites were performed using a continuous twin-screw co-rotating extruder (PRISM TSE-16 TC laboratory extruder, Thermo Scientific Haake, UK) (Figure 14) equipped with a length to diameter ratio of 15 and a screw diameter of 16 mm. Force feeding was employed to ensure a constant supply of polymer powder/pellet to the screws. A custom screw design (Figure 13) was used to increase shear mixing of CNT and PEEK within the twin-screw extruder and to maximise the dispersion of carbon nanotubes within the polymer.

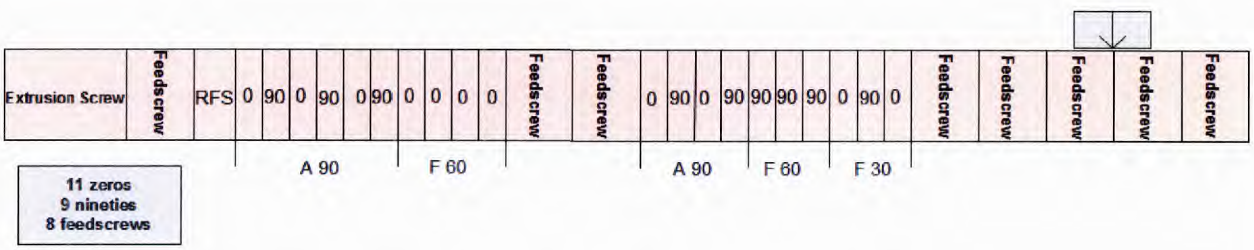

Figure 13: The screw design of the twin-screw extruder

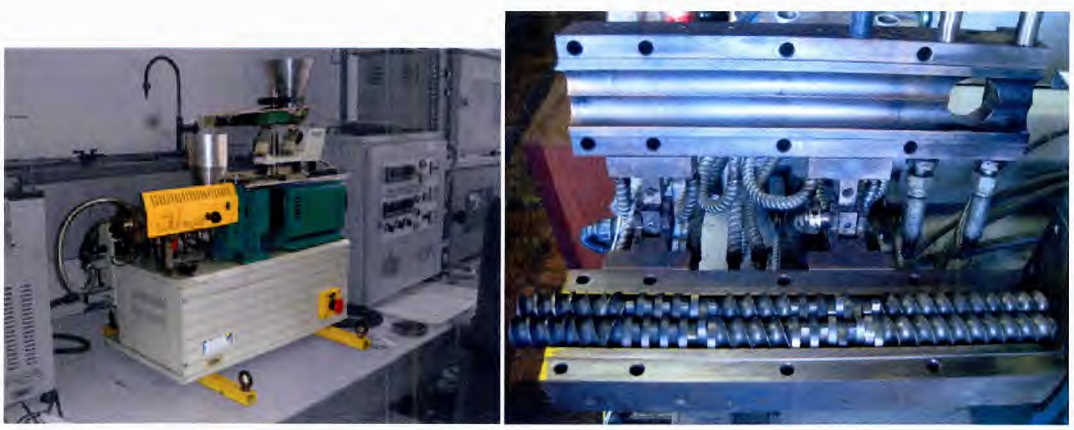

Figure 14: PRISM laboratory twin-screw co-rotating extruder. The screw length is 240 mm

Dispersion of CNTs in PEEK melt was achieved using a batch size of 500 g. All materials were dried overnight in an air circulated oven at 50 °C. As received CNTs were blended for 1 min using a 1 l stainless steel laboratory blender (Waring laboratory blender, UK), which allowed any large agglomerates of CNTs to be broken up. 50 g of PEEK powder were added at 30 s intervals in order to obtain a pre-mix CNT/PEEK, The blended CNT/PEEK pre-mix was then transferred to a dry powder-rotating mixer (tumble blender) and mixed at 50 rpm for 1 h to ensure a homogeneous blend. The CNT/PEEK mixed blend was force fed into the twin-screw extruder (80 rpm) at a rate of 1 kg/h. Both the feeding and the mixing zones temperatures were set at 360 °C while the die zone temperature was set at 370 °C. The corresponding residence time within the extruder was approximately 40 s. Continuous strands of extruded CNT/PEEK nanocomposites were pelletised using a PRISM pelletiser unit. The pelletised nanocomposites were re-extruded twice under the same conditions as described above to ensure consistency of CNTs dispersion within CNT/PEEK nanocomposites.

3.3.3 Preparation of nanocomposite specimens using injection moulding

Specimens for the mechanical testing of nanocomposites were prepared using a laboratory injection moulder (Thermo Scientific Haake MiniJet, UK). Figure 15 shows a picture of the equipment. Two different moulds were used in this study. The first mould was a dog-bone shape with dimensions in accordance of ASTM standard D638-type-V [150] and the second mould was a rectangular bar with dimensions 80 x 12.7 x 3.2 mm.

Figure 15: Haake miniJet injection moulder

In order to perform the injection moulding of nanocomposites, the same parameters were used throughout this study, hence ensuring the same thermal history is seen by all specimens. All materials were dried in an air circulated oven overnight at a temperature of 50 °C. Pellets were fed into the heated barrel at a temperature of 400 °C and were allowed to melt for 10 min before injection took place. The injection was conducted with a mould temperature of 250 °C and an injection pressure of 800 bar held for 10 s before being reduced to 400 bar and held for 30 s. This is to ensure a rapid filling of the mould cavity in the first step and the solidification of the melted polymer into the mould shape in the second step. The injection moulded nanocomposite specimens were removed immediately from the mould after.

3.3.4 Carbon nanotubes reinforced PEEK powder

To manufacture hierarchical composites on the in-house built thermoplastic prepreg composite line developed as part of this project, previously compounded CNT/PEEK nanocomposites that were extruded and pelletised must be turned into powders so

that the material could be utilised in the powder impregnation process. The limitation for such process is that for the CNT/PEEK nanocomposite powder to be picked up by the carbon fibres (see later discussion), typical powder particle sizes must be between 10-20 μm. Experimental trials were conducted using laboratory scale cryogenic grinder mills to achieve the required particle sizes. However, due to the inherent properties of PEEK, i.e. its excellent toughness property, it was not possible to achieve particle size that is below 200 μm. Other techniques that can be used to produce powders involve solution precipitation through the dissolution of PEEK using a non-solvent. The choice of suitable solvents is, nevertheless, highly restricted because PEEK is chemically resistant to most solvents. The use of hazardous chemicals such as strong and highly concentrated acid was not deemed appropriate for a large scale process in a laboratory environment due to health and safety issues. Another possible technique is temperature induced precipitation using diphenylsulfone (DPS) as a solvent, this is already widely used in industries, such as Cytec Engineered Materials. Dissolution of PEEK in DPS is complete at 300 °C. DPS itself is a solid at room temperature and has a melting temperature of 140 °C.

In order to make nanocomposite powders, 100 g of the nanocomposite blends of extruded CNT/PEEK pellets were dissolved in 900 g of DPS inside a 1 l cylindrical glass reaction vessel. The temperature was held at 300 °C using a heated mantle (Glas-Col 100B TM573, Wilmad Lab Glass, USA) equipped with a digital temperature controller. This procedure was repeated twice to give a total of 2 kg of dissolved nanocomposite/DPS batch. The reaction chamber was covered with a stainless steel lid while low shear stirring (200 rpm) was applied using a homemade stainless steel double anchor stirrer to ensure even mixing of the dissolved PEEK in

DPS as well as an even heat distribution. High shear/vigorous agitation of the PEEK/DPS solution would create a temperature gradient inside the reactor. A lower temperature at the upper portion of the reactor would result in the formation of a resin surface layer and hence inhibit the homogeneous precipitation of PEEK/CNTs powder. The crystallization of PEEK in DPS takes place at 265 °C, which was observed visually during initial trials. Once all the CNT/PEEK pellets had dissolved completely, the temperature was reduced to 240 °C at a rate of 10 °C/h. This ensures that PEEK would re-crystallise as particles while DPS remains in a liquid form. The precipitated nanocomposites in DPS were further cooled to 200 °C before the highly viscous solution was poured into a wide ceramic dish. The contents were then hand mixed (for approximately 5 min) using a standard laboratory spatula in order to prevent any agglomeration of DPS during crystallization, As a result a 'toffee' like solid was formed.

The 'toffee' was allowed to cool to room temperature before a hammer was used to fracture the toffee into smaller sizes. Granules of the 'toffee' were then passed through a 2 mm sieve to narrow down the particle size distribution. This 'toffee' powder was then ground down to a finer powder form which included several steps. 200 g of the 'toffee' powder was weighed out and added to a blender (1 l stainless steel laboratory blender, Waring Laboratory Science, UK) with 0.5 l of cooled ethanol solution and blended for 5 min. The ethanol was kept cool at -70 °C throughout using dry ice and the temperature was monitored using a digital thermometer (RS Components, UK). Additional dry ice was added at intervals directly to the toffee powder/ethanol mixture to ensure the temperature was kept low. This would ensure that the property of the 'toffee' is as brittle as possible while

blending took place. Afterwards the 'toffee' powder/ethanol mixture was poured into a 5 l beaker, kept at -70 °C using dry ice, and further ground down using a high speed homogenizer (SL2T, Silverson, Chesham, Bucks, UK) at a speed of 7000 rpm for 1 h.

Large quantities of DPS remaining within the precipitated nanocomposite powder would degrade the mechanical properties of the composite by acting as a plasticizer, defect sites or voids, hence lowering the strength of the material. Therefore, best attempts on removing DPS from the nanocomposite powders were done so by filtering the ethanol/powder solution using a polypropylene (PP) membrane support. The latter was chosen as compared to a standard filter paper, because it has an open mesh structure which promotes the passing of DPS. This is because clogging of the filter can occur easily when the DPS crystallize. The resulting filtered powder was re-dispersed in 5 l of acetone at 80 °C. Constant stirring together with the applied heat allowed DPS to be dissolved in acetone quickly before the purified CNT/PEEK nanopowder was filtered off using once again the PP membrane support. The whole acetone purification step was performed three times to ensure maximum removal of DPS from the nanocomposite powder.

3.3.5 Manufacturing of unidirectional carbon fibre reinforced PEEK composite tapes

Unidirectional carbon fibre reinforced PEEK tape (12.5 mm wide and 0.1 mm thick) was manufactured using a home-built modular laboratory scale composite production line (Figure 16). This production line is based on the powder impregnation technique used for thermoplastic composite manufacturing [151, 152]. The author was the main

person for the design of this production line. The author identified the main components and drew up the blueprints of this design. The author was also in charge of the negotiation for the construction of this production line with the workshop. Dr Kingsley Ho and Dr Michael Tran provided invaluable assistance to the construction of this production line as well.

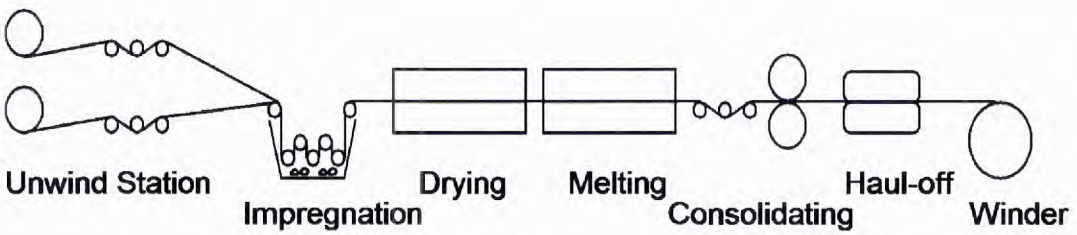

Figure 16: Schematic of the laboratory scale line for the production of unidirectional fibre reinforced thermoplastic polymers

3.3.5.1 Unwind station and tension control

A pair of creels was mounted on braked spindles. The 12k carbon fibre roving was subjected to 500 g of tension from a tension controlled let-off unit (Izumi International, USA) and passed through guiding rollers and over a roller mounted on a load cell that measures the tension, as can be seen in Figure 17.

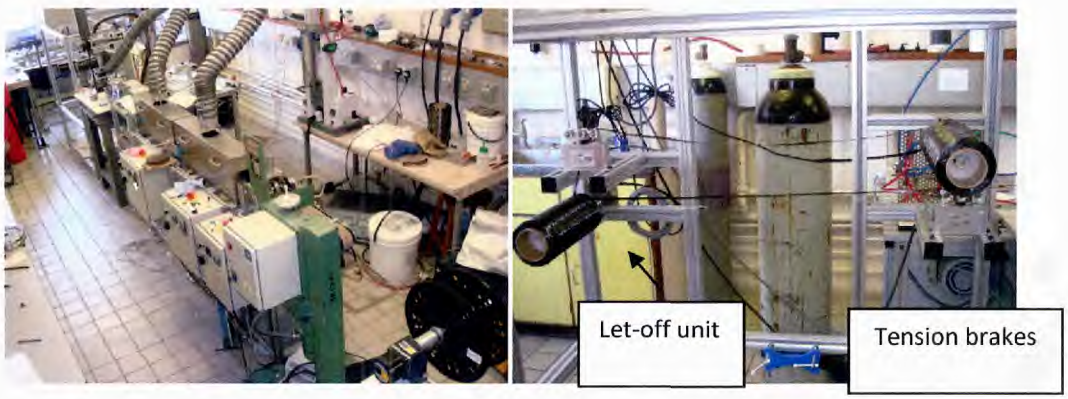

Figure 17: Overview of the home-build modular laboratory scale composites production line (left) and the fibre pre-tension unit (right)

There are several controllable variables that are associated with this production line. They are the processing speed, fibre-tow tension, spreading pin angles, bath concentration, drying-oven temperature, consolidation-oven temperature and the final spreading pin temperature.

3.3.5.2 Impregnation stage

The fibre tows were guided into the impregnation bath, which consists of a series of fixed pins that spread the fibres mounted in a frame that drops into a metal bath containing the slurry (Figure 18). A schematic diagram of the cross-section of the impregnation bath is shown in Figure 19. The impregnation bath contained x wt% amount of PEEK depending on processing conditions and particle size, and 1 wt% surfactant with respect to the polymer in 2 l of deionised water. This tank was agitated with two 60 mm magnetic stirring bars. The final pin is above the level of the dispersion, and as the tow passes over it, the excess liquid is squeezed out.

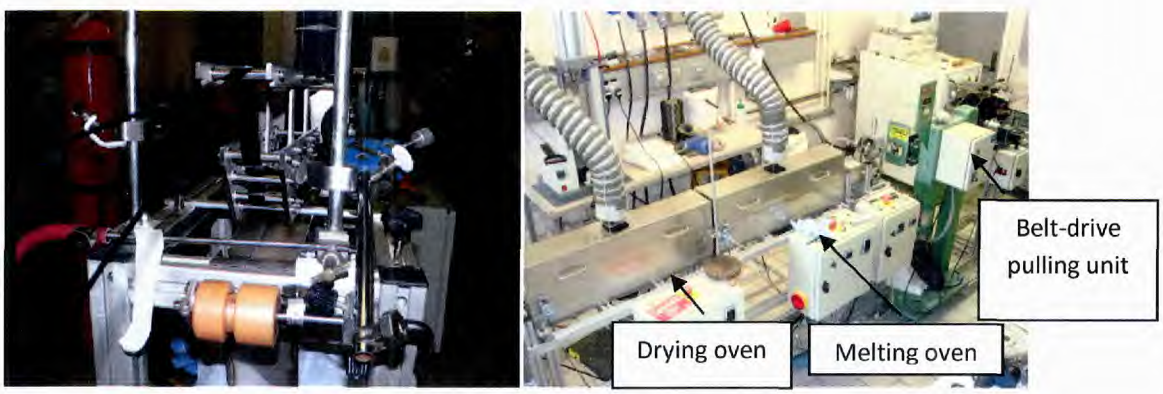

Figure 18: Images showing a tow of CFs in the impregnation setup (left) and infra-red ovens (right)

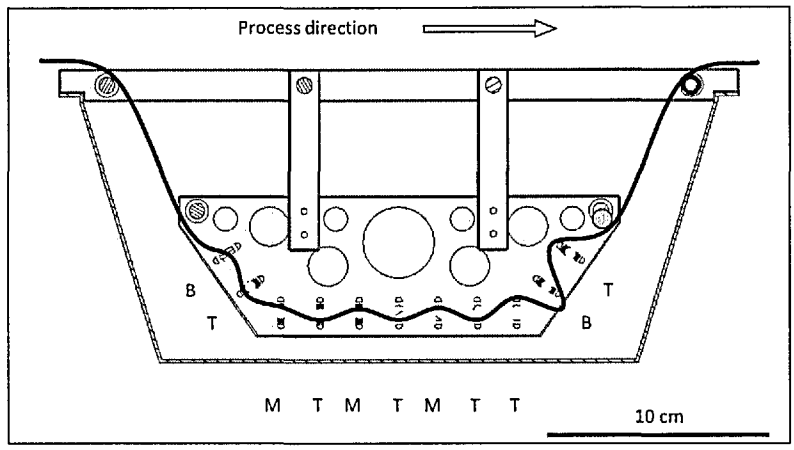

Figure 19: Schematic diagram showing the cross-section of the impregnation bath with pins placed either at the bottom (B), middle (M) or top (T) position within each slot of the frame (pins were removed to improve the clarity of the diagram)

3.3.5.3 Drying stage

The wet polymer impregnated fibre tow was then passed into a heating tunnel, and dried under infra-red heaters controlled by a thermocouple kept at 180 °C. The fibres were dried completely before melting to ensure no water is entrapped within the composite, which could cause blisters on the tape when it is consolidated at later stages.

3.3.5.4 Melting stage

Once the water has been evaporated, the tow entered an infra-red heated melting oven. This oven is identical to the infra-red heating oven in the drying stage but it is operated at 390 °C in order to melt the polymer. When 2 tows were used, as the polymer melts, surface tension pulls the fibres together. The edges of the tape melted first, causing the tow to separate or split into two or more parts. This causes a weakness down the centre of the tape, which was still apparent even after consolidation.

3.3.5.5 Control of IR heaters

The heaters in the drying and melt oven as well as in the consolidation unit were controlled by Eurotherm 3500 series PID controllers. These are very sophisticated units that are commonly used in a wide range of laboratory equipments such as ovens, tube furnaces, pumps etc. because of their extensive programmable functions. When deployed to controlling the heaters on the composite production line, it was found that the system heats up too quickly. After extensive rewiring and reprogramming, the units eventually responded and the temperature within the heating ovens could be controlled to within 0.5 °C.

3.3.5.6 Consolidation stage

The impregnated tape melts coming out from the melting infra-red ovens were passed over and under a series of three heated pins operated at 390 °C (Figure 20 and Figure 21). This smoothed the surfaces of the tape and spread the fibres further, driving the polymer into the tow. Loose fibres could accumulate here, requiring the build-up to be removed periodically. The hot, smooth tow was then pressed through a water-cooled rolling die to consolidate the tape and eliminate voids in the tape. The pressure exerted onto the tapes in this consolidation step can be varied by adding additional weights onto the upper roller.

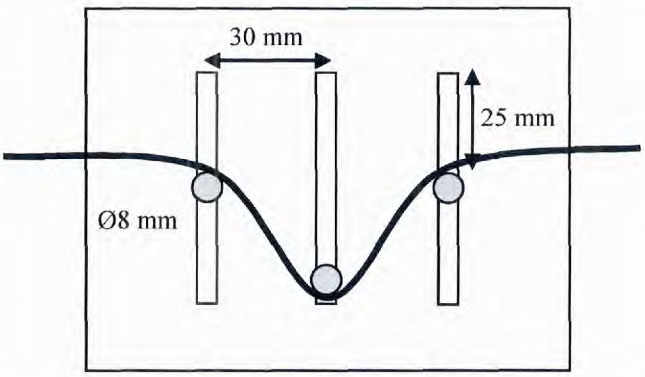

Figure 20: Schematic diagram showing the cross-sectional area of the shear pins in the composites production line. The dimensions are given in mm

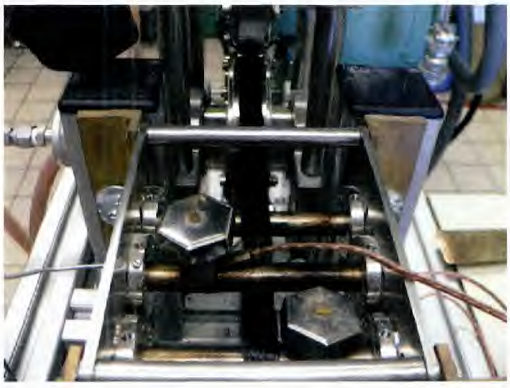

Figure 21: Image showing the heated consolidating shear pins and rolling die

3.3.5.7 Haul-off and winding station.

The tow was pulled through the line by the haul-off. This consists of a pair of drive belts that are pressed together to grip the tape. The speed of the line was controlled by adjusting the speed of the belt drive motor (Model 110-3, RDN manufacturing Co., USA), which was fixed to 1.0 m min^{-1} throughout this study. The tape was wound up onto a spool.

3.3.6 Determination of fibre volume fraction

The ratio of fibre to matrix in any composite is a major factor in determining its mechanical performance. Each method of impregnating the fibres has its strength and weaknesses, and one of the significant challenges of using an aqueous slurry is to control the amount of polymer picked up from the impregnation tank.

3.3.6.1 Control Factor Analysis

An attempt was made to identify and rank the key factors involved in the control of fibre volume fraction. The analysis is presented in a control factor tree diagram (Figure 22). The primary intent of this approach was twofold; to identify the optimum levers for controlling the volume fraction, and to find any manipulated variables that may have been overlooked.

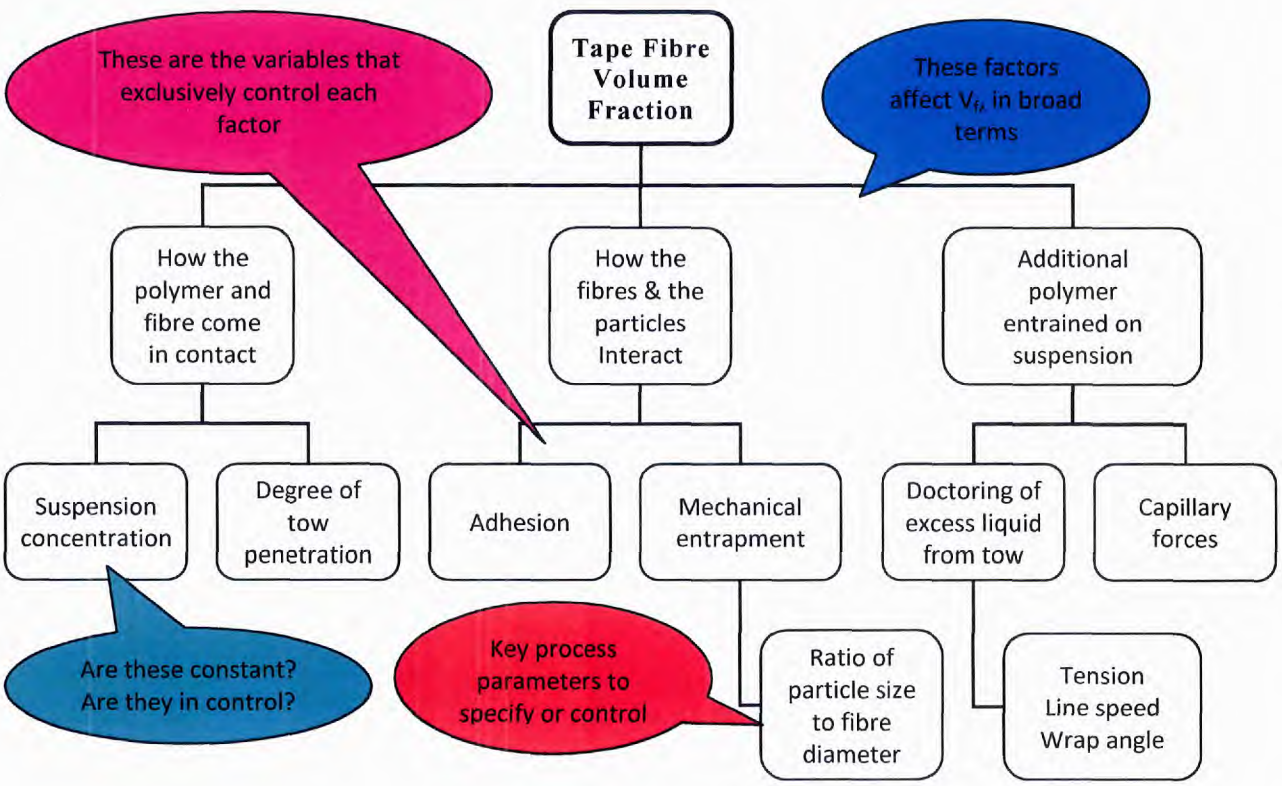

Figure 22: Control factor chart

3.3.6.2 Tank depletion

A mass balance was carried out on the slurry (polymer dispersion), and on subsequent runs such that an attempt was made to maintain the volume and concentration by topping up the tank with a make-up dispersion of a higher concentration.

3.3.6.3 Particle size distribution

During the operation of the line, samples were taken from the impregnation tank at regular intervals. An analysis of the particle size in the slurry was performed and the importance of particle size to the final product has been mentioned previously in section 3.3.4.

3.3.6.4 Polymer loading models

Tang et al. [47] developed a geometric model relating particle size, fibre diameter, fibre volume fraction with the ideal slurry concentration as described below:

$$C = \frac{\pi \rho (1 - V_f)}{2\left[V_f\left(\frac{R}{r}\right) + 1\right]^2 + \pi} \qquad (3)$$

where C is the optimum wet slurry concentration, V_f is the fibre volume fraction, r is the radius of fibre and R is the radius of polymer particle.

The model assumes homogeneous distribution of polymer powders throughout the system (in the spaces between the fibres and in the bulk). However, the rates of water and polymer removal are not the same. This may suggest that the geometry of the

model holds true while the fibres are immersed in the tank, but adopt a tighter packed structure, expelling the excess water when the tow is drawn from the tank under tension. A more compact packing arrangement would be hexagonal (Figure 23 to Figure 25), where each polymer particle touches six fibres. This could be modelled as series of hexagonal cells, of depth z.

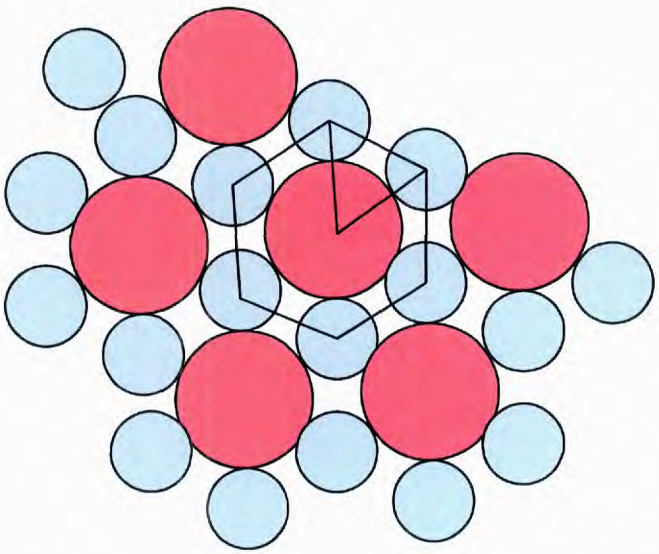

Figure 23: Hexagonal packing of fibres and polymer particles in water, with outline of unit cell

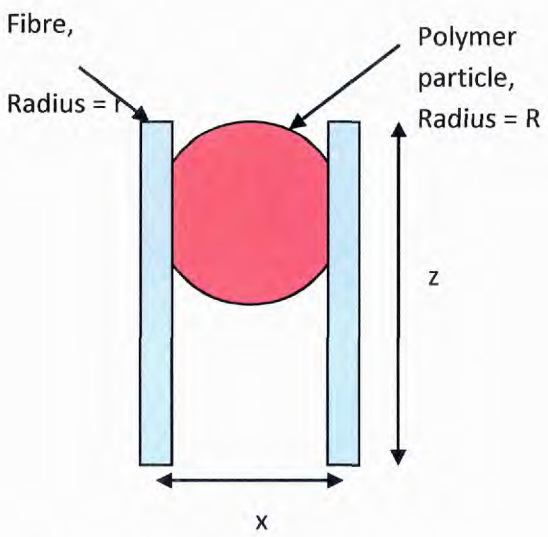

Figure 24: Side view of unit cell before consolidation

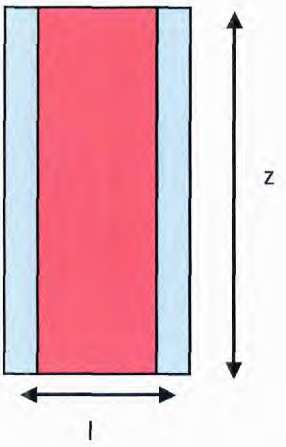

Figure 25: Unit cell after consolidation

Once the composite has been consolidated, the voids (where the water used to be) are removed, and the fibre volume fraction is a function of the fibre size, particle size and distance between particles. For each unit cell, the fibre volume, V_{fc} is given by:

$$V_{fc} = 2\pi r^2 z \tag{4}$$

The volume of the unit cell, V_c is:

$$V_c = \frac{3\sqrt{3}}{2}(R-r)^2 z \tag{5}$$

And the volume of the polymer particle, V_p is

$$V_p = \frac{4}{3}\pi R^3 \tag{6}$$

From this it can be deduced that the volume of space, V_s, occupied by water is

$$V_s = V_c - V_{fc} - V_p \tag{7}$$

Therefore,

$$V_s = \frac{3\sqrt{3}}{2}(R+r)^2 z - 2\pi r^2 z - \frac{4}{3}\pi R^3 \tag{8}$$

The consolidated fibre volume fraction is:

$$V_f = \frac{V_{fc}}{V_{fc} + V_p} \tag{9}$$

$$V_f = \frac{2\pi r^2 z}{2\pi r^2 z + \frac{4}{3}\pi R^3} \tag{10}$$

Rearranging the equation,

$$z = \frac{4V_f R^3}{6r^2(1-V_f)} \tag{11}$$

It can be noted that z < 2R for the model to be valid. Substituting equation (11) to (8),

$$V_s = \frac{3\sqrt{3}}{2}(R+r)^2 \frac{4V_f R^3}{6r^2(1-V_f)} - 2\pi r^2 \frac{4V_f R^3}{6r^2(1-V_f)} - \frac{4}{3}\pi R^3 \tag{12}$$

The desired concentration of dispersion, C is

$$C = \frac{V_p \rho}{V_s} \tag{13}$$

From equation (12),

$$C = \frac{\frac{4}{3}\pi R^3 \rho}{\frac{3\sqrt{3}}{2}(R+r)^2 \frac{4V_f R^3}{6r^2(1-V_f)} - 2\pi r^2 \frac{4V_f R^3}{6r^2(1-V_f)} - \frac{4}{3}\pi R^3} \tag{14}$$

Rearranging,

$$C = \frac{\pi \rho (1-V_f)}{\frac{3\sqrt{3V_f}}{4}\frac{(R+r)^2}{r^2} - \pi} \tag{15}$$

3.3.7 Carbon fibre handling during the manufacturing processes

3.3.7.1 Tension

The fibre tows were under considerable tension at the haul-off stage. The haul-off belts had to be periodically cleaned to maintain grip. Alternative belt materials were investigated to maximise the available pull, and new belts ordered with a covering of NR50 natural rubber. The initial tow tension is set by the Izumi unwind station, using a load cell and braked spindle, however most of the line tension is generated overcoming the friction in the impregnation tank. Here the tows pass over and under 15 non-turning pins. The angle of wrap around each pin can be adjusted by sliding the pins up and down in their mounting slots. The degree of wrap angle is a key factor in controlling the degree of spread of the fibres, which in turn is a parameter of

the quality of the impregnation. Friction is often encountered in the consolidation stage where the tape passes over the heated pins and through the roll die. However, the polymer used in this study (PEEK) has a very high melt viscosity and the frictional effect was kept to a minimum.

3.3.7.2 Fuzzing of carbon fibre tows

When handling fibre tows, broken fibres can accumulate and disrupt the process. The primary reason why sizing was applied onto carbon fibres was to minimise this effect. The heated pins had to be cleaned regularly with a pair of tweezers to prevent the debris becoming incorporated with the tape.

3.3.7.3 Splitting of tape

One of the issues encountered was the existence of a line of weakness, which runs down the middle of the tape and sometimes manifested itself as a complete separation of the tapes into two pieces. After careful inspection, this effect was found to occur when the tape passes through the melting stage.

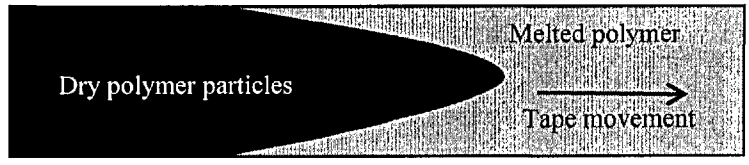

Figure 26: Profile of the polymer melt during tape production

The outer edges of the tape heat up faster than the centre, resulting in a visible line between the dry polymer particles and the melted polymer (Figure 26 and Figure 27).

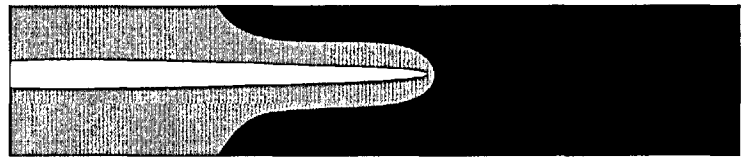

Figure 27: Action of surface tension on partially melted polymer

The surface tension of the freshly melted polymer tends to pull the fibre tow together cohesively. When this starts to occur in the edge band, the matrix will start to pull into two tows, separating due to surface tension effect (Figure 28).

Figure 28: Completely divided tape

Once the polymer has completely melted, the two halves typically stay separated until the tape passes through the consolidating pins, where the two halves are brought into contact and fused together under the rolling die.

3.3.8 Compression moulding of test specimen

Unidirectional carbon fibre reinforced PEEK composite laminates test specimens were consolidated in a stainless steel frame mould, coated with release agent (McLube 1862, Aston, PA, USA). Composite tapes that measure 200 mm long were cut using a paper guillotine, their width was 12 mm. A total of 34 layers of cut composite tapes were stacked and tightly wrapped using Upilex polyimide film (UBE Europe GmbH, Düsseldorf, Germany) before placing them into the steel mould (cavity dimensions: 200 mm × 12 mm × 5 mm) (Figure 30).

Figure 29: Images of the hot presses used for compression moulding

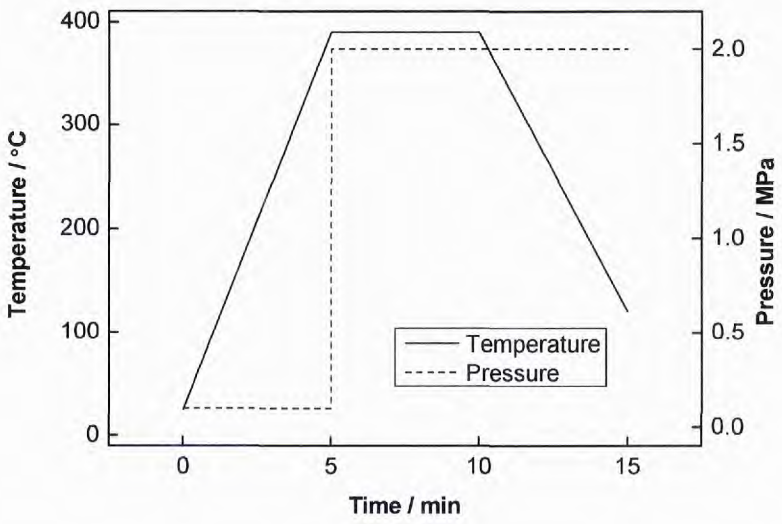

Figure 30: Image of the steel mould used for compression moulding (top) and the applied temperature and pressure profile during the compression moulding cycle (bottom)

In order to reduce the consolidation time, two hot presses (EDBRO, Bolton, UK and George E. Moore & Son, Birmingham, UK) were used (Figure 29). The mould containing the stacked carbon fibre tapes was placed into the first hot press at 390 °C and pre-heated for 5 min. After which the pressure was increased to 2 MPa and held for 5 min before transferring the mould to another hot press operated at 120 °C and where it was held for 5 min at a pressure of 2 MPa. The mould was then allowed to cool to ambient temperature before the specimen was removed from the mould.

3.3.9 Preparation of the samples for mechanical testing

Moulded test specimens were cut into the required dimensions for mechanical testing using a diamond blade cutter (Diadisc 4200, Mutronic GmbH & Co, Rieden am Forggensee, Germany). The quality of the edges of both compression and injection moulded specimens was improved by grinding using P320 grit silicon carbide paper. After all test specimens were trimmed and polished, the composite specimens were annealed at 240°C for 4 h and cooled to 140°C at a rate of 10°C h^{-1} prior to mechanical testing.

Optical microscopy specimens were prepared to evaluate the resin rich area and morphology of moulded plies. Specimens were embedded into an epoxy resin (Epoxicure, Buehler, UK) and cured at room temperature for 8 h. Embedded specimens were then grinded using a 7 stage process on a grinder/polisher (MetaServ / MetaPol, Buehler, UK) using silicon carbide papers with increasing grit designation (P120, P320, P800 and P2500) and final polishing using diamond based dispersions (6 μm, 3 μm and 1 μm) for 5 min at each stage under an individual specimen

pressure of 5 lb. Polished specimens were examined using optical microscopy (Olympus BX51M/DP70) investigation.

3.4 Mechanical testing

3.4.1 Tensile testing of extruded nanocomposites

The effect of CNT loading on the tensile strength and the Young's modulus of CNT reinforced nanocomposites was determined using a screw-driven test frame equipped with a 1 kN load cell (Model 4466, Instron, High Wycombe, UK) in accordance with ASTM D3822-01 standard [153]. CNT reinforced nanocomposites with a gauge length of 25 mm were glued onto a cardboard paper frame (Figure 31) using a cyanoacrylate adhesive and cured for 24 h.

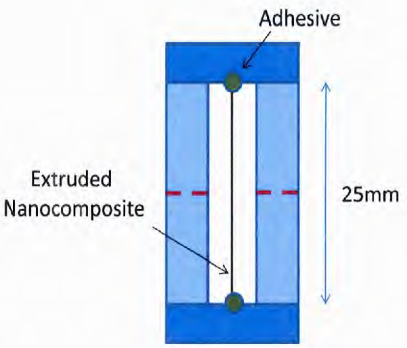

Figure 31: Schematic illustration of tensile test specimen of CNT reinforced PEEK

Each extruded strand was loaded at a rate of 2.5 mm min^{-1} until the nanocomposite failed whilst the loading force versus cross-head displacement was logged using a computer. For each fibre tested the tensile strength and Young's modulus were calculated using equations (16) and (17), respectively:

$$\sigma_t = \frac{F_{max}}{A_f} \tag{16}$$

$$E = \frac{F / A_f}{\Delta L / L_0} \tag{17}$$

where σ_t is the tensile strength (MPa), F_{max} is the tensile force (N) at break and A_f is the fibre cross-sectional area (mm^2) determined using a digital vernier (Mitutuyo, Tokyo, Japan); E is the Young's modulus (MPa), L_0 is the original length of the fibre and ΔL is the change in length of the fibre when subjected to an applied stress. Young's modulus was calculated in the interval 0.05-0.25 % strain. All measurements were repeated on 6 different samples of the extruded fibres to obtain a statistical mean. The effective specimen length was determined according to ASTM D3822-07 Annex 2 [153]. The errors are presented as standard errors.

3.4.2 Tensile testing of injection moulded nanocomposites

The tensile properties of CNT reinforced PEEK were determined using a screw-driven test frame equipped with a 10 kN load cell (model 4466, Instron, High Wycombe, UK) in accordance to ASTM D638-V [150]. Nanocomposites (dog-bone specimens, Figure 32) were loaded at a rate of 1 mm min^{-1} until failure whilst the loading force versus deformation was recorded. An instron extensometer with a gauge length of 12.5 mm was used to measure the strain. All measurements were repeated on six nominally identical samples to obtain a statistical mean. The values presented were averaged and errors are presented as standard errors.

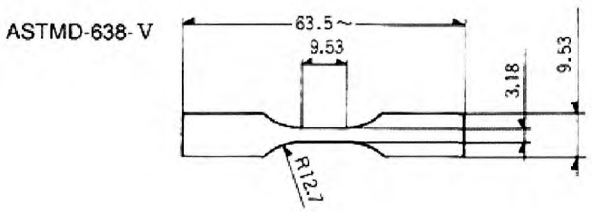

Figure 32: Schematic illustration of the ASTM D638-V dog bone tensile test specimen of CNT reinforced PEEK. The dimensions are given in mm [150].

3.4.3 Compression Testing

The compressive properties of injection moulded composites were determined using a screw-driven test frame equipped with a 10 kN load cell (model 4466, Instron, High Wycombe, UK) in accordance to ASTM D695-02a [154]. Specimens were loaded at a rate of 1 mm min^{-1} in an anti-buckling jig (Figure 33). All measurements were repeated on six nominally identical samples to obtain a statistical average and the compliance of the machine was subtracted from the data. The values presented were averaged and errors are presented as standard errors.

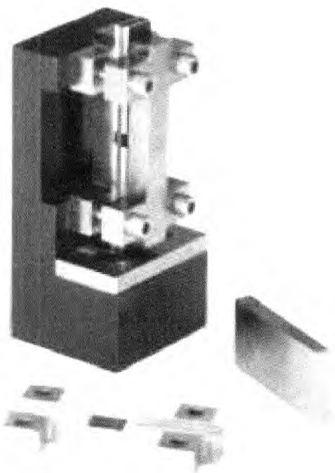

Figure 33: Support jig for thin compression test specimen [155]

Yield stress (offset strain of 0.2 %) was used to evaluate the compressive strength of the nanocomposites. Young's modulus was calculated using equation (17).

3.4.4 In-Plane shear testing

The shear properties of injection moulded composite were determined using a tensile screw-driven test frame equipped with a 10 kN load cell (model 4466, Instron, High Wycombe, UK) in accordance to ASTM D3846-02 [156] . Double-notched nanocomposites (Figure 34) were loaded at a rate of 1 mm min^{-1}. All measurements were repeated on six nominally identical samples to obtain a statistical average and the compliance of the machine was subtracted from the data. The values presented were averaged and errors are presented as standard errors. Nominal specimen size was 80 x 12.7 x 3.2 mm.

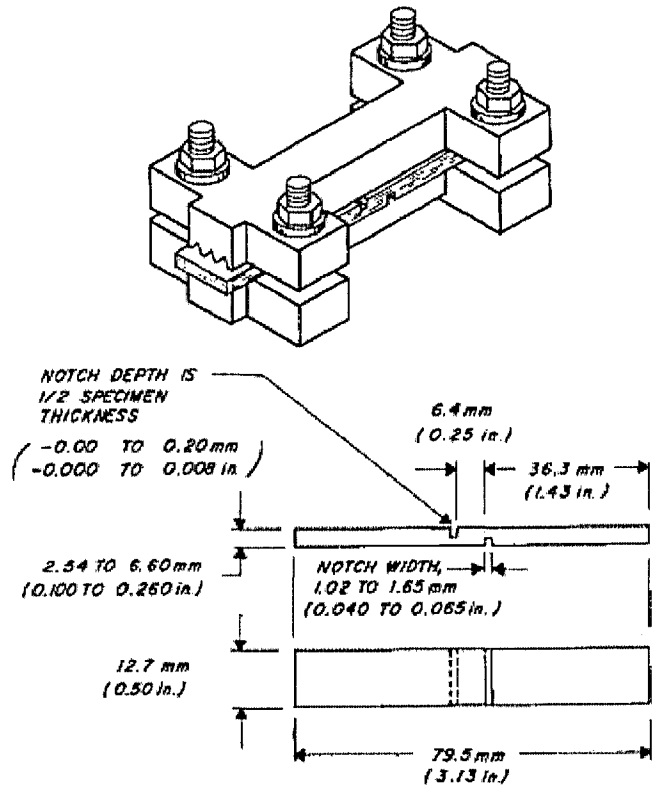

Figure 34: Specimen and loading jig for in-plane shear test [156]

The loading force versus displacement was logged throughout the experiment using a computer and the in-plane shear strength (offset strain of 0.2 %) σ_s was then calculated using:

$$\sigma_s = \frac{P_{0.2}}{b\,l} \tag{18}$$

where $P_{0.2}$ is the maximum shear load at offset 0.2 %, b is the specimen width and l is the length of the failed area.

3.4.5 Flexural testing

Flexural properties are important in engineering practice to determine the flexural modulus and flexural strength. Injection moulded / laminated composite bars with dimensions of 95 mm × 10 mm × 2 mm were prepared for the three-point bending test. Each composite specimen was loaded into a three-point bending rig at 16:1 (injection moulded nanocomposites) and 32:1 (laminated composite bars) span-to-thickness ratio, equipped with a 10 kN load cell (Model 4466, Instron, High Wycombe, UK) and secured with the support span set to 50 (injection moulded nanocomposites) and 64 mm (laminated composite bars). The crosshead speed was set to 1.34 mm min^{-1} (nanocomposites) and 1 mm min^{-1} (composites) and each specimen was tested until failure in accordance to ASTM D790-03 [157] (nanocomposites) and D7264-07 (composite) [158].

The loading force versus displacement was logged throughout the experiment using a computer and the specimen flexural strength σ_f and flexural strain ε_f were calculated using equations (19) and (20), respectively:

$$\sigma_f = \frac{3P_{max}L}{2bt^2} \tag{19}$$

$$\varepsilon_f = \frac{6Dt}{L^2} \tag{20}$$

where P_{max} is the force at composite failure load, L is the support span, b is the specimen width and t is the specimen thickness; D is the maximum deflection at the centre of the beam.

The flexural modulus E_f was then calculated using:

$$E_f = \frac{L^3 m}{4bt^3} \tag{21}$$

where m is the gradient of the initial part (0.05-0.25 % strain) of the force-displacement curve. The flexural strength and modulus of the CNT reinforced PEEK and unidirectional carbon fibre reinforced PEEK composites were each determined from six measurements in order to obtain a statistically significant average and the compliance of the machine was subtracted from the data. The values presented are mean values and errors are standard errors.

3.4.6 Short beam shear test

The ASTM Standard D2344 [159] states that during conventional short beam shear (SBS) testing of unidirectional fibre reinforced thermoplastics, the stress that is induced in the specimen is neither a pure shear stress nor a pure flexural stress but is a mixture of both stresses. Therefore, the test is called apparent short beam shear test.

The short beam shear strength method, which is based on classical beam theory is the simplest and the most commonly used test. It was used to characterise the interlaminar shear behaviour of carbon fibre reinforced PEEK. Short beam shear testing is very similar to flexural testing. This test allows maximum shear stresses to be introduced throughout the thickness of the test specimen whilst reducing the tensile and compressive flexural stresses to a minimum by reducing the length of the test specimens, i.e. lowering the span-to-thickness ratio.

Unidirectional carbon fibre reinforced PEEK laminates of 20 mm × 10 mm × 2.2 mm were prepared and secured again into the same test rig used for flexural test with a span-to-thickness ratio of 4:1, equipped with a 10 kN load cell (Model 4466, Instron, High Wycombe, UK). Specimens were then loaded at a rate of 1 mm min^{-1} until failure following the ASTM standard D2344 [159]. The short beam strength F^{SBS} was calculated using equation:

$$F^{SBS} = 0.75 \frac{P_{\max}}{bt} \tag{22}$$

where P_{max} is the force at composite failure load, b is the specimen width and t is the specimen thickness. All measurements were repeated on 6 different samples to obtain a mean and the compliance of the machine was subtracted from the data. The errors presented are standard errors.

3.5 Summary

Materials used throughout the research have been described. Characterisation techniques have been examined in details with the parameters used described. Manufacturing of PEEK composites has been reviewed using two types of extrusion,

a batch micro scale extrusion and a continuous type extrusion for scale-up purposes. Specimens were made using a monofilament die or by injection moulding. A continuous thermoplastic composite line was thoroughly discussed. Composite materials made using this line were compression moulded into laminates. Finally mechanical testing was performed on all specimens created using various methods such as tension, compression, in-plane shear, flexure and short beam shear tests.

Chapter 4 – Results and Discussion

In this section, the results obtained will be presented and discussed. Carbon nanomaterials were characterised using various techniques to examine their quality and potential as reinforcement for high performance composite materials combined with PEEK. Their dispersability in water was investigated, followed by the measurements of their diameters using SEM micrographs. Their bulk and surface properties were analysed using BET, TGA, LRS and XPS. A single carbon nanomaterial was selected for use in composite processing and characterisation. Single fibre model composites were tested using single fibre pull-out with different carbon fibres and CNT-reinforced matrices with varying loading content. Nanocomposites were analysed using tensile testing on monofilaments and films as a small scale study. Crystallisation is of importance when working with semi-crystalline polymers and a study on the crystallisation behaviour of CNT containing PEEK was conducted by annealing the specimens. Bulk properties and scale-up permitted the use of mechanical testing using tensile, compressive, flexural and in-plane shear tests. The design, commissioning and validation of the continuous thermoplastic composite production line was necessary through the assessment of PEEK/CF composite that were compared to a commercially available material. Finally hierarchical thermoplastic composites mechanical properties were also measured using flexural and short beam shear tests.

4.1 Carbon nanomaterials

Carbon nanotubes are supplied commercially from a wide variety of sources; most of the materials, certainly those available in bulk quantities, are produced by the CVD processes. Most manufacturers provide only very limited information about their

products; in addition, batch to batch variation is still very significant. It was, therefore, necessary to characterise the as-received carbon nanomaterials, in detail, before using them for further experiments. As well as providing valuable information about specific samples, a wider survey of materials provides insight into the suitability of various means of characterisation and the current status of world nanotube production. In this study, different techniques were applied, each giving specific information. Scanning electron microscopy was used to validate the diameter ranges stated by the various suppliers and to assess the overall character of the samples, providing a qualitative assessment of important factors such as entanglement, waviness and purity. BET adsorption measurements were used to quantify the surface area of the CNTs which should, in principle, relate directly to their diameters, although surface roughness may have an effect. Thermogravimetric analysis (TGA) was used to establish the presence of residues/contaminants associated with the growth catalyst; the degradation temperature under air (i.e. combustion) is often claimed to indicate, qualitatively, the degree of crystallinity. This hypothesis was explored by comparing the degradation data to another common indicator of graphitic quality, the G/D ratio, observed using laser Raman spectroscopy.

4.1.1 Carbon Nanotube / Carbon Nanofibre

A range of commercial CVD-grown multi-walled CNTs were sourced from commercial suppliers, as summarised in Table 5, below. In particular, two ranges of samples were obtained from NanoAmor (Los Alamos, USA) and Heji (Beijing, P.R. China) respectively, as they claimed to cover a series of diameters systematically using similar production conditions (note that there was one SWCNT sample within

the Heji set, presumably synthesised under different conditions). If confirmed, such samples would provide an excellent opportunity to study scaling issues systematically. Heji Inc was also selected for the low cost of their materials which makes them especially relevant for large volume applications, such as composites. Additional samples were obtained from well-known, large scale suppliers of MWCNTs, including Nanocyl, and Bayer. Finally, some double wall CNTs from Toray Research & Development (Nagoya, Japan) were added to complete the range of materials reviewed; note that some commentators have suggested that DWCNTs may be the ideal structure for composite applications [160].

Table 5: Diameters of CNT supplied by different manufacturers

Supplier	*Nanomaterial type*	*Diameter*
Heji Inc	Multi Wall CNT	<8 nm
	Multi Wall CNT	8-15 nm
	Multi Wall CNT	10-20 nm
	Multi Wall CNT	20-30 nm
	Multi Wall CNT	30-50 nm
	Multi Wall CNT	20-40 nm
	Single Wall CNT	1-2 nm
Toray R&D	Double Wall CNT	~3 nm
NanoAmor	Multi Wall CNT	10-30 nm
	Multi Wall CNT	60-100 nm
	Carbon Nanofibres	100-200 nm
Nanocyl	Multi Wall CNT	~10 nm
Baytubes	Multi Wall CNT	5-20 nm

4.1.2 Macroscopic observations

As a preliminary indication of processibility, in particular the compatibility with polar solvents or matrices, an attempt was made to disperse the as-received materials in water. 25 mg of CNT were added to 2.5 ml of distilled water in a vial that was shaken vigorously by hand for a few minutes and allowed to settle for 2 min. By visual observation (photographs shown in Figure 35), it can be seen that many of the CNT samples were hydrophobic in nature, as expected, floating above the water.

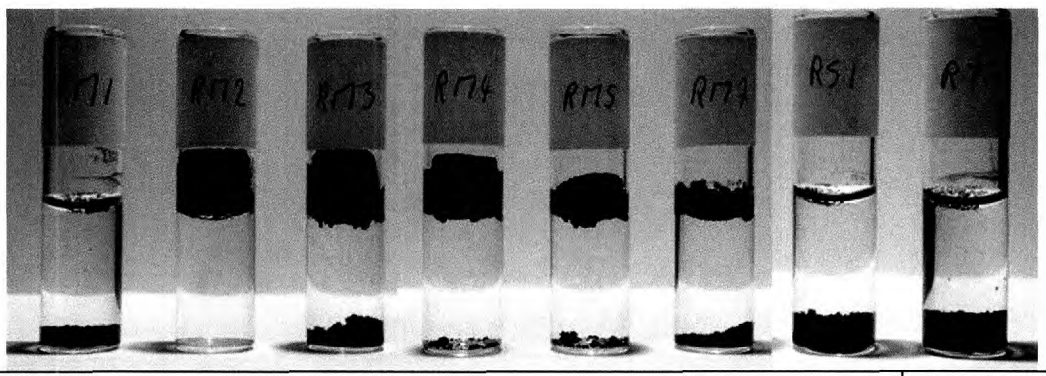

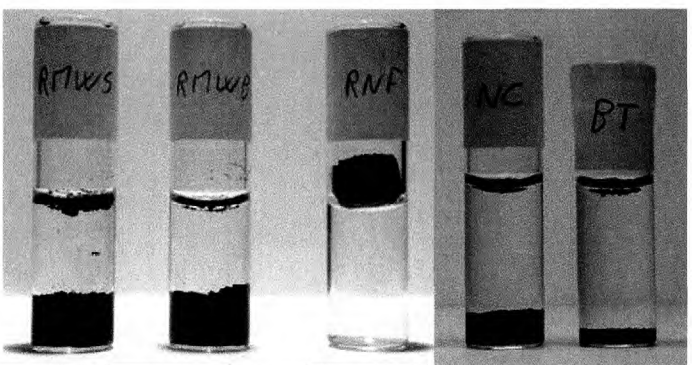

Figure 35: 25 mg CNT samples shaken in 2.5 ml of distilled water

However, the MWCNT 10-20 nm, 60-100 nm, SWCNT 1-2 nm, DWCNT 3 nm and MWCNT <8 nm were entirely immersed in water, suggesting a more hydrophilic

character; although the graphitic surface of ideal nanotubes should be hydrophobic, the presence of oxygen at some stage during the synthesis can, and frequently does, introduce polar, oxygen-containing surface groups [161]. The dispersibility test correlates with the concentration of oxygen observed in the Heji samples, as measured by XPS and discussed later.

The volume occupied by a known mass of a material relates directly to the bulk density. Comparing the height of MWCNT <8 nm with MWCNT 10-20 nm within the vial, it is clear that the apparent density varies enormously, by up to a factor of five. In general, the bulk density of raw CVD MWCNTs can be very low [162], down to as little as 0.1 g cm^{-3}. This low density can affect the processing of polymer CNT composites; in melt processed systems particularly, it can be difficult to wet out a large volume of dry powder with matrix which is the first step to successful blending.

4.1.3 SEM microscopy

The SEM micrographs were analysed digitally, in order to verify that the diameter stated by the supplier was correct (see Appendix for details). A large number of CNTs were measured to ensure statistical significance. It was not possible to establish the diameters of the SWCNT 1-2 nm, DWCNT ~3 nm and MWCNT <8 nm samples, as they fall below the maximum resolution of the FEG SEM used. Qualitative comments about the character of each sample, along with diameter distributions, and an overall summary table are included on the following pages.

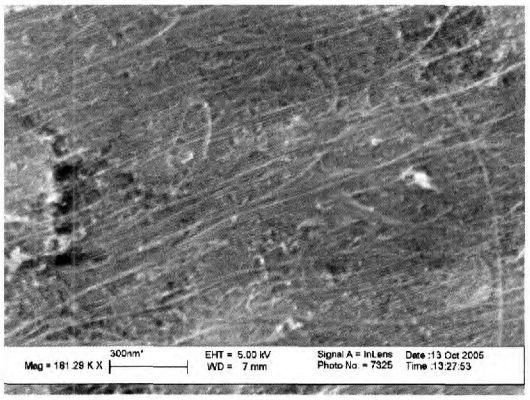

Figure 36: SWCNT 1-2 nm

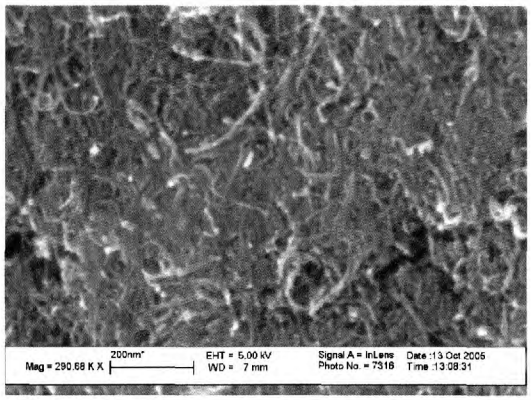

Figure 37: MWCNT < 8 nm

SWCNTs 1-2 nm are straight and MWCNTs <8 nm are wavy and entangled; although the structures appear bigger than stated, the effect may be due to bundle formation, or the resolution limit of the SEM probe.

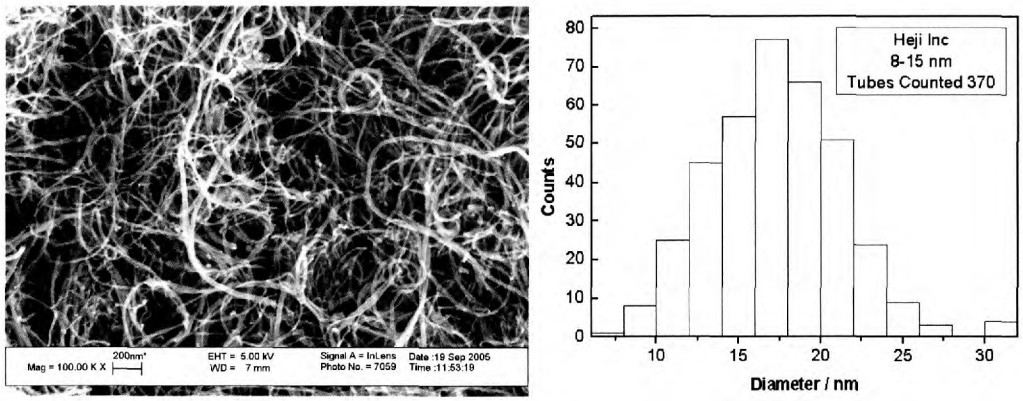

Figure 38: MWCNT 8-15 nm, mean diameter 17.40 ± 4.0 nm

MWCNTs 8-15 nm are wavy, entangled and form bundles; they have a larger diameter than stated.

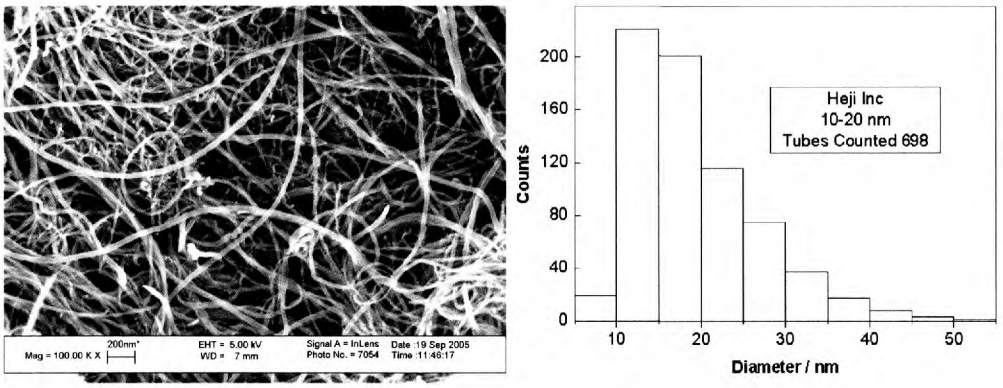

Figure 39: MWCNT 10-20 nm, mean diameter 19.15 ± 7.3 nm

MWCNTs 10-20 nm are entangled and form bundles; their diameters are within the range stated.

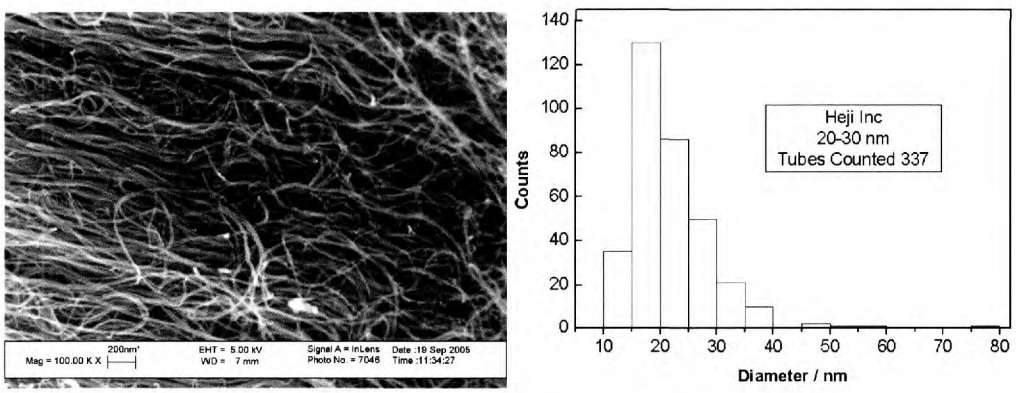

Figure 40: MWCNT 20-30 nm, mean diameter 21.80 ± 7.4 nm

MWCNTs 20-30 nm are straight and form bundles; their diameters are within the range stated.

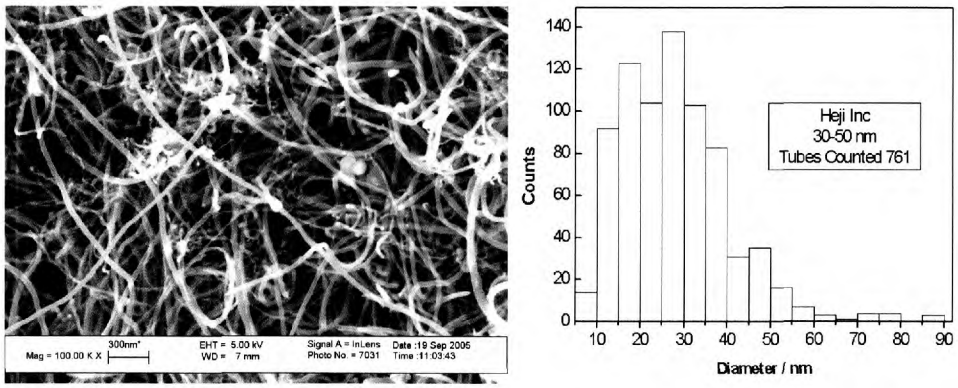

Figure 41: MWCNT 30-50 nm, mean diameter 27.80 ± 12.6 nm

MWCNTs 30-50 nm are wavy and entangled; they have a smaller diameter than stated.

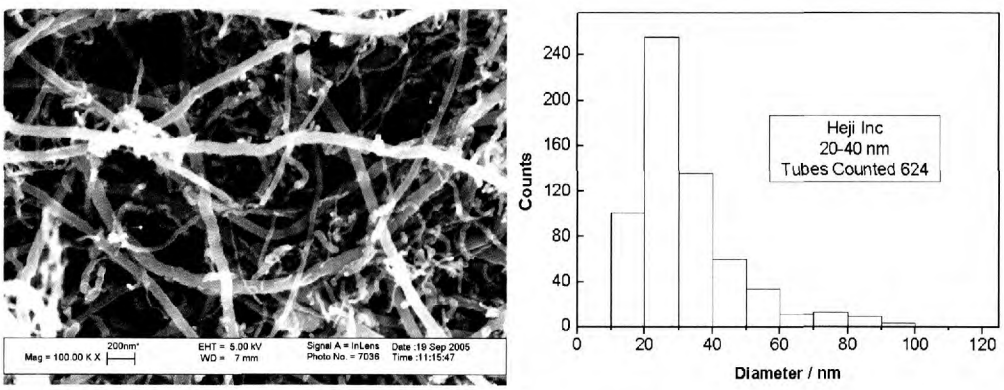

Figure 42: MWCNT 20-40 nm, mean diameter 32.20 + 15.5 nm

MWCNTs 20-40 nm are wavy, entangled and form bundles, some impurities can be seen and their diameters are within the range stated.

Toray R&D

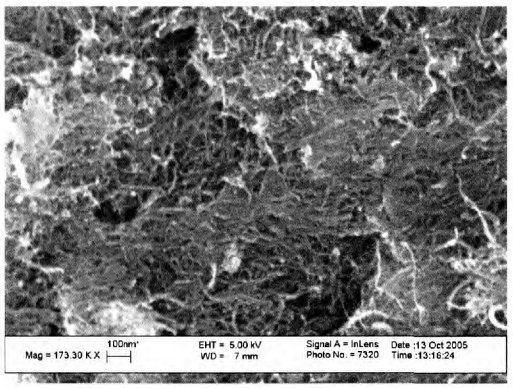

Figure 43: DWCNT ~3 nm

DWCNTs ~3 nm are wavy, entangled and form bundles; although the structures appear bigger than stated, the effect may be due to bundle formation, or the resolution limit of the SEM probe.

NanoAmor

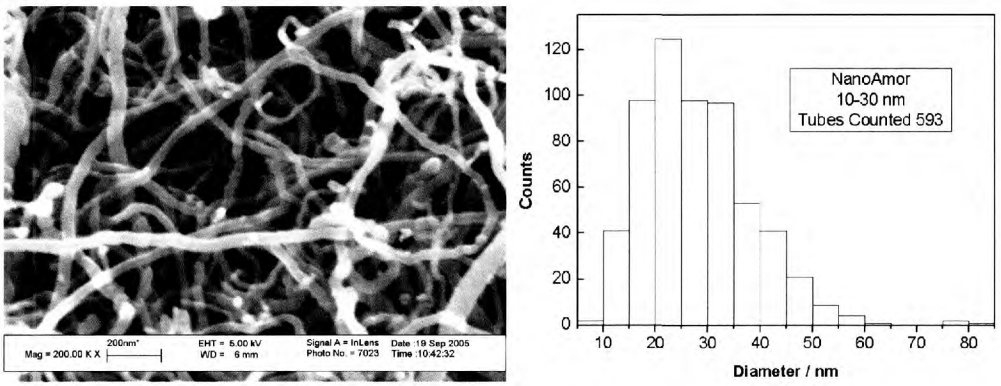

Figure 44: MWCNT 10-30 nm, mean diameter 28.15 ± 10.5 nm

MWCNTs 10-30 nm are wavy and entangled, they have a larger diameter than stated.

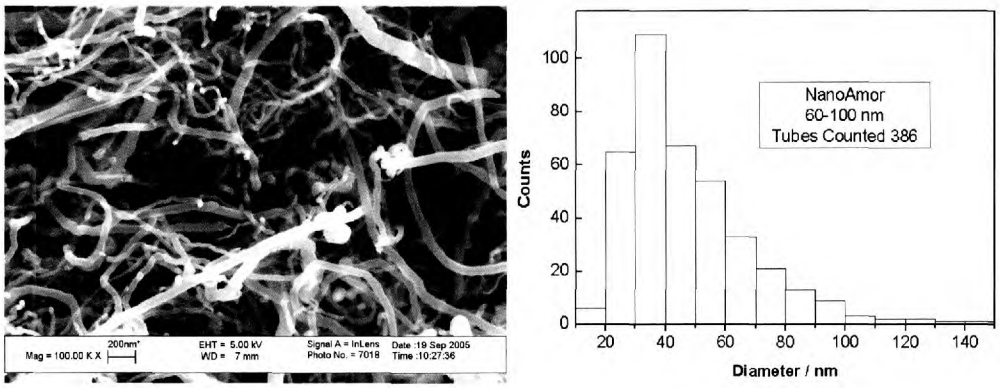

Figure 45: MWCNT 60-100 nm, mean diameter 47.80 ± 21.0 nm

MWCNTs 60-100 nm are wavy and entangled; they have a smaller diameter than stated.

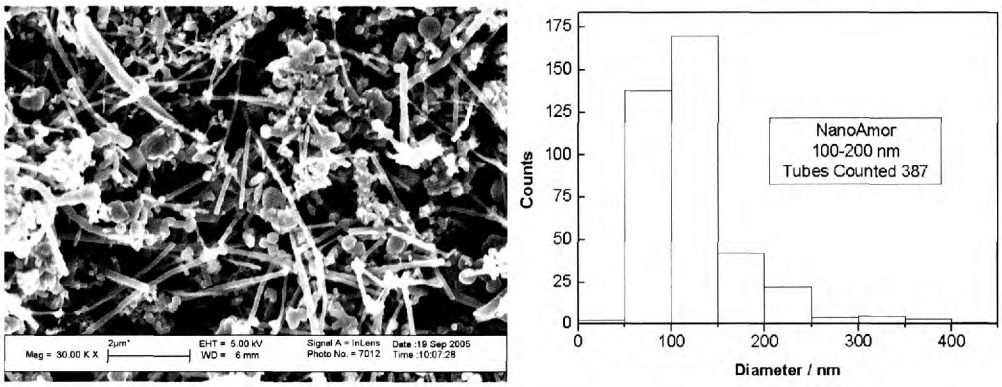

Figure 46: CNF 100-200 nm, mean diameter 123.90 ± 55.0 nm

CNFs 100-200 nm are straight but they show a large amount of impurities, their diameters are within the range stated.

Nanocyl

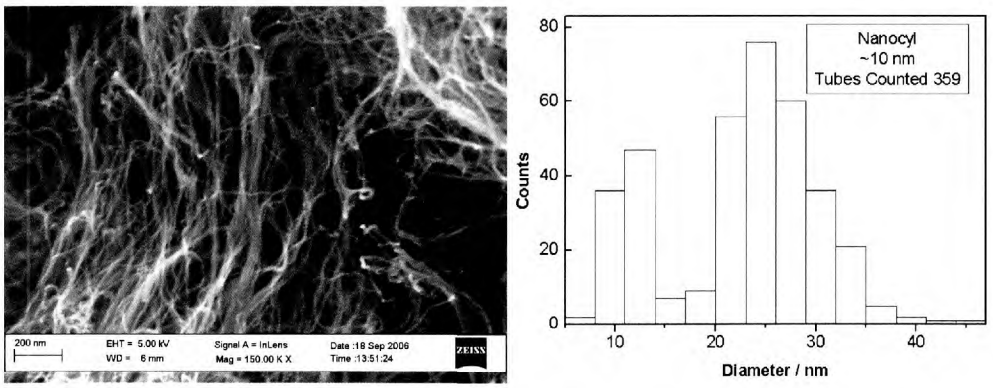

Figure 47: MWCNT ~10 nm, mean diameter 22.50 ± 7.6 nm

Nanocyl MWCNTs are wavy, entangled and form bundles; two diameter distributions can be seen, one being around 10 nm and the other one around 25 nm.

Baytubes

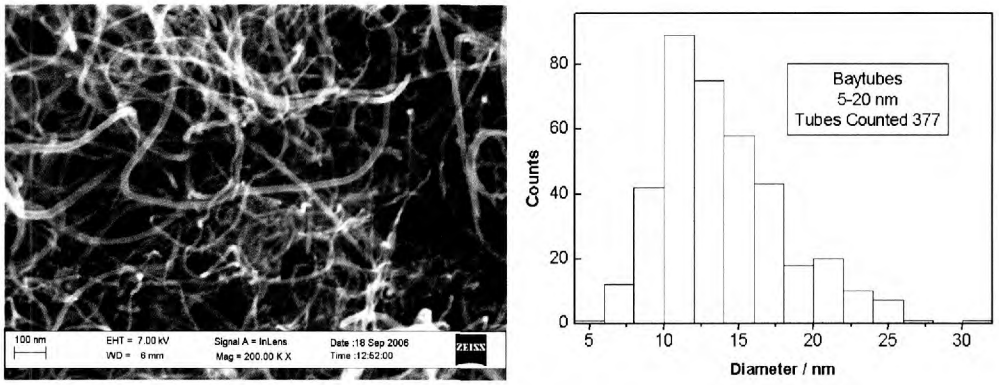

Figure 48: MWCNT 5-20 nm, mean diameter 13.90 ± 4.2 nm

Baytubes MWCNTs 5-20 nm are wavy, entangled and form bundles; their diameters are within the range stated.

Table 6: Summary of carbon nanomaterial diameters

Supplier	Supplier's Diameter / nm	Mean Measured Diameter / nm	Mean ± 1 Standard Deviation / nm
Heji Inc.	< 8	n/a	n/a
	8-15	17.40 ± 4.0	13.4 – 21.4
	10-20	19.15 ± 7.3	11.85 – 26.4
	20-30	21.80 ± 7.4	14.4 – 29.2
	30-50	27.80 ± 12.6	15.2 – 40.4
	20-40	32.20 ± 15.5	16.7 – 47.7
	1-2 (SWCNT)	n/a	n/a
Toray R&D	~3 (DWCNT)	n/a	n/a
NanoAmor	10-30	28.15 ± 10.5	17.65 – 38.6
	60-100	47.80 ± 21.0	26.8 – 68.8
	100-200 (CNF)	123.90 ± 55.0	68.9 – 178.9
Nanocyl	~10	22.50 ± 7.6	14.9 – 30.1
Baytubes	5-20	13.90 ± 4.2	9.7 – 18.1

There are significant inconsistencies in the values (Table 6) given by the supplier and the actual measured diameters. Disappointingly, many of the samples are not as different as claimed, limiting the potential for systematic scaling studies. Note also, that in the further characterisation and discussion of these nanomaterials, the mean measured diameter ± 1 standard deviation will be used along with the range provided by the manufacturers.

4.1.4 BET surface area

The theoretical surface area with respect to the carbon nanomaterials diameter has been calculated assuming that the CNTs are closed, and hence that only the external surface can absorb N_2 and has a contribution to the surface area.

$$\text{BET Surface Area:} \quad A_s = \frac{\pi d l}{m} \tag{23}$$

$$\text{Density:} \quad \rho = \frac{m}{V} = \frac{m}{\pi \frac{d^2}{4} l} \tag{24}$$

where d is the diameter, m is the mass, l is the length and V is the volume. By re-arranging both equations, we obtain:

$$\text{BET Surface Area} \left(\frac{m^2}{g} \right) = \frac{4}{d\rho} 1000 \tag{25}$$

where d is the diameter in nanometre and ρ is the estimated density of CNT (~ 1.8 g/cm^3).

Figure 49 and Figure 50 show the BET surface area of carbon nanomaterials as a function of their diameter. Single point and multipoint calculation methods[143] are presented and compared, however the difference is insignificant. Both data sets fit the theoretical values ranging from 20 up to 620 m^2/g, showing that the simple geometric model can be reasonably applied.

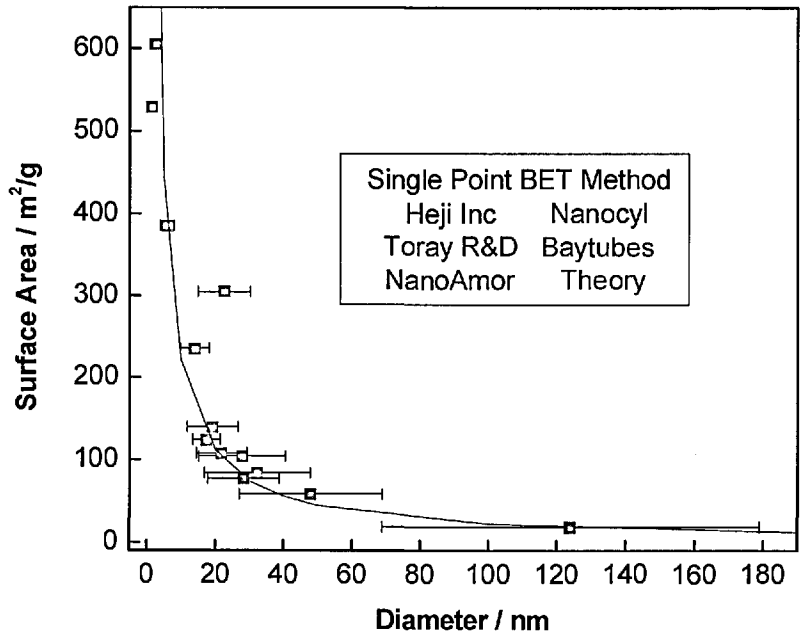

Figure 49: Single Point BET Surface Area calculation methods

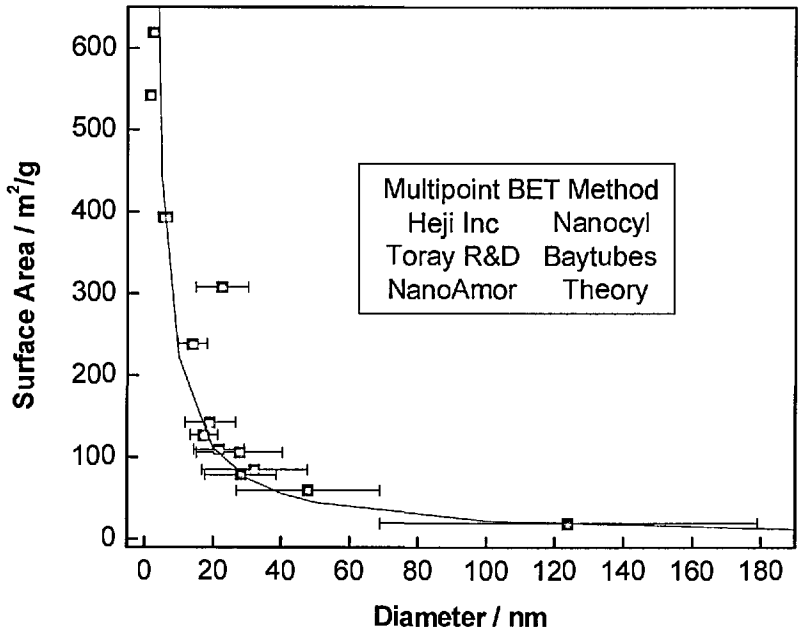

Figure 50: Multipoint BET Surface Area calculation methods

The two materials that differ most from the theoretical value are the SWCNTs which have a lower surface area than expected geometrically, as expected, due to bundling, and the Nanocyl MWCNTs. The reason for the higher surface area of the Nanocyl material is unclear, but may relate either to the distribution in diameters seen or its high surface roughness, or to the presence of opened nanotubes. The multipoint method will be used for the further comparisons in this study. A summary of the carbon nanomaterials surface area results is presented in Table 7.

Table 7: Summary of the multipoint measured surface area

Supplier	Given Diameter / nm	Mean Measured Diameter / nm	Surface Area / m^2/g
Heji Inc.	< 8	n/a	393
	8 - 15	13.4 - 21.4	127
	10 - 20	11.85 - 26.4	143
	20 - 30	14.4 - 29.2	110
	30 - 50	15.2 - 40.4	106
	20 - 40	16.7 - 47.7	85
	1 - 2 (SWCNT)	n/a	543
Toray R&D	~ 3 (DWCNT)	n/a	619
NanoAmor	10 – 30	17.65 - 39.6	79
	60 – 100	26.8 - 68.8	59
	100 - 200 (CNF)	68.9 - 178.9	19
Nanocyl	~ 10	14.9 - 30.1	308
Baytubes	5 - 20	9.7 - 18.1	239

4.1.5 Thermogravimetric analysis

Thermogravimetric analysis (TGA) gives several indications of the bulk carbon nanomaterial properties. The non-combustible residue content after the complete oxidation of carbon can be measured, as exemplified in Figure 51. Results for all the samples are summarised in Table 8, Figure 52 and Figure 53.

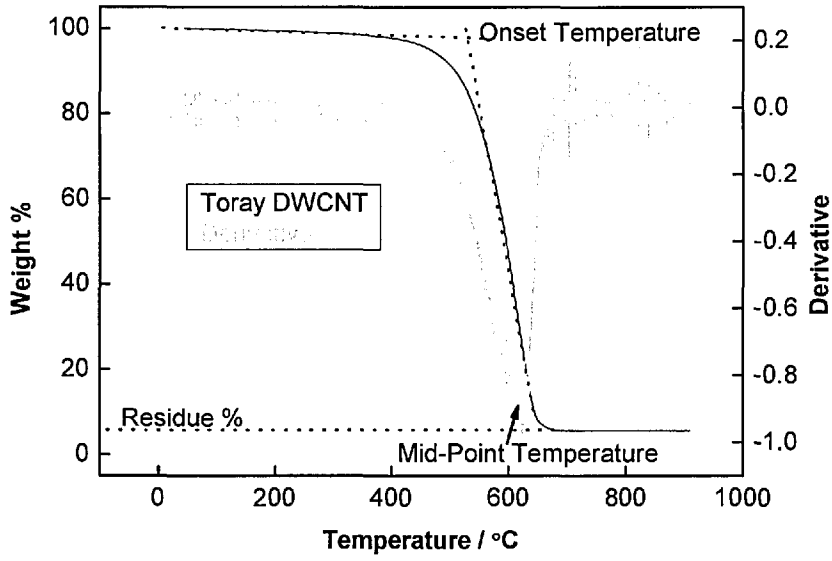

Figure 51: An example of TGA analysis of CNT

These residues relate to the metal catalysts (and supports where relevant) used during the Catalytic Vapour Deposition process used to produce the CNTs. Note that, in principle, the catalyst residue oxidises during the TGA experiment, giving a somewhat larger residue value than the original metal content.

Table 8: The residue content of CNT/CNF from TGA analysis

Supplier	Given Diameter / nm	Mean Measured Diameter / nm	Residue Content/ wt%
Heji Inc.	< 8	n/a	1.92
	8 - 15	13.4 - 21.4	1.59
	10 - 20	11.85 - 26.4	0.99
	20 - 30	14.4 - 29.2	1.24
	30 - 50	15.2 - 40.4	2.77
	20 - 40	16.7 - 47.7	4.05
	1 - 2 (SWCNT)	n/a	3.44
Toray R&D	~ 3 (DWCNT)	n/a	5.48
NanoAmor	10 - 30	17.65 - 39.6	0.67
	60 - 100	26.8 - 68.8	0.46
	100 - 200 (CNF)	68.9 - 178.9	10.45
Nanocyl	~ 10	14.9 - 30.1	8.68
Baytubes	5 - 20	9.7 - 18.1	2.38

Both MWCNTs from NanoAmor have a very small residue content compared to the CNF which has as much as 10.5 wt%. CNFs are produced under different conditions to CNTs; fundamentally, they are a kinetically favoured, rather than thermodynamically favoured product, due to the less ideal arrangement of the graphene layers. Possibly, this fact may be reflected in lower catalyst efficiency. The majority of CNTs from Heji Inc do not show any specific trend as the diameter or surface area do not seem to have an effect on the residue content; the result is not surprisingly given the similarities of the materials. For the smallest and largest diameters of Heji Inc CNTs, the metal content does increase up to 4 wt%. In the case of the Toray DWCNTs, a value of 5.5 wt% was found, and the residue was white in

colour, almost certainly reflecting the zeolite catalyst technology employed. Nanocyl MWCNTs also contain a relatively high residue content of 8.7 wt% that was grey in colour; again it is thought that a zeolite catalyst support is present. Finally, Baytubes MWCNT have a rather typical residue content of 2.8 wt%, grey in colour, reflecting the metal catalyst oxide alone, since the material is thought to be formed via a floating catalyst process, without the use of a support. Overall, there is no unambiguous trend, when comparing the residue content against either surface area or diameter.

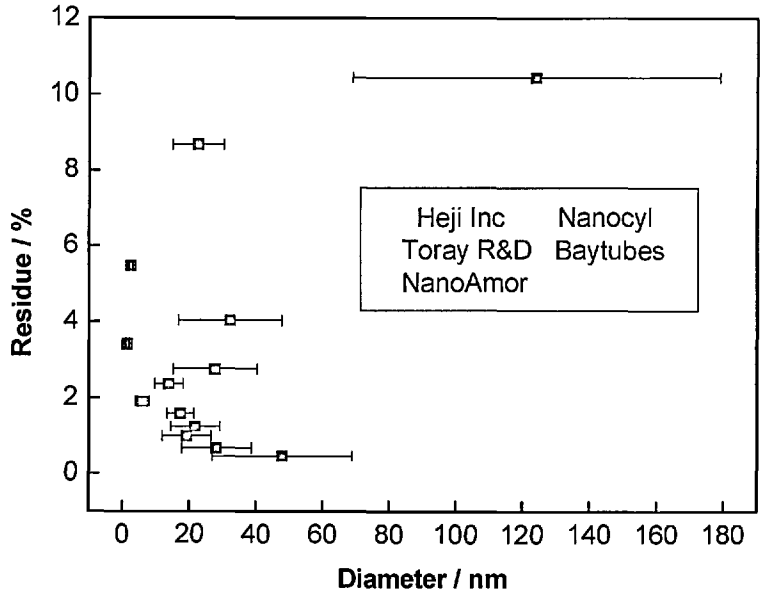

Figure 52: Relationship between residue content and CNT diameter

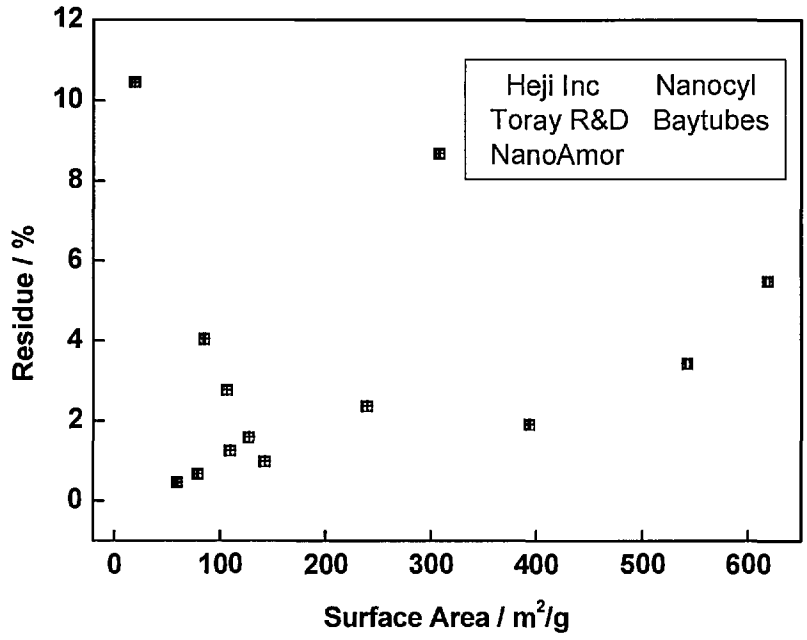

Figure 53: Relationship between residue content and the surface area of CNT

The TGA onset temperature, which corresponds to the intersection of two tangents on the curve as stated in the international standard ISO 11358 [163], is reported in Figure 54. The onset temperature is often taken as an indication of the concentration of defects within the structure, since more graphitic structures combust at higher temperatures than amorphous carbons. The mid-point temperature is the peak in the derivative of the curve (Figure 51), and is an average combustion temperature for the material. Both onset and peak temperatures are functions of TGA heating rate and oxygen partial pressure / flow rate; however, by holding these variables constant, reproducible, sample-dependent data can be obtained.

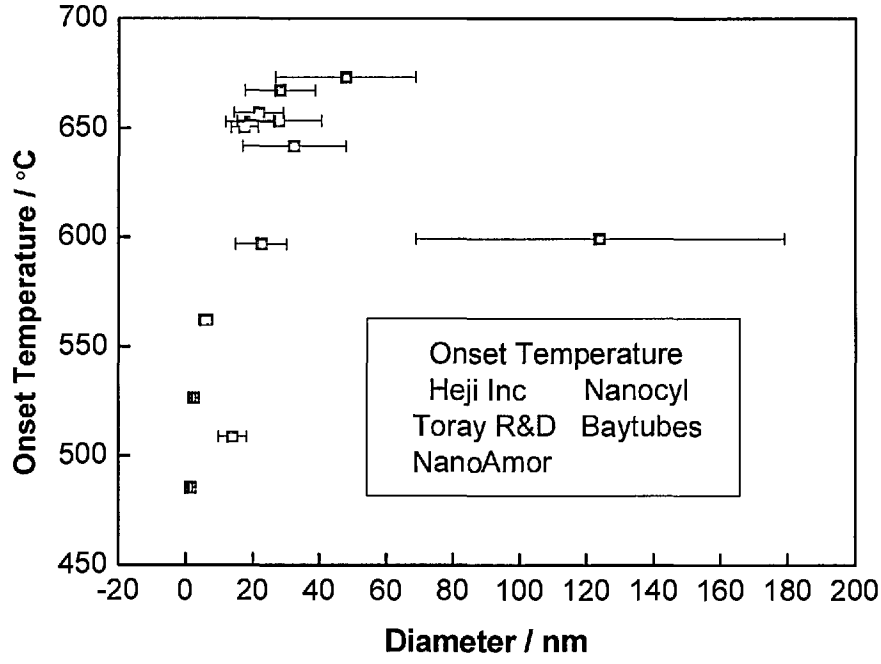

Figure 54: Relationship between the onset temperature and the diameter of CNT

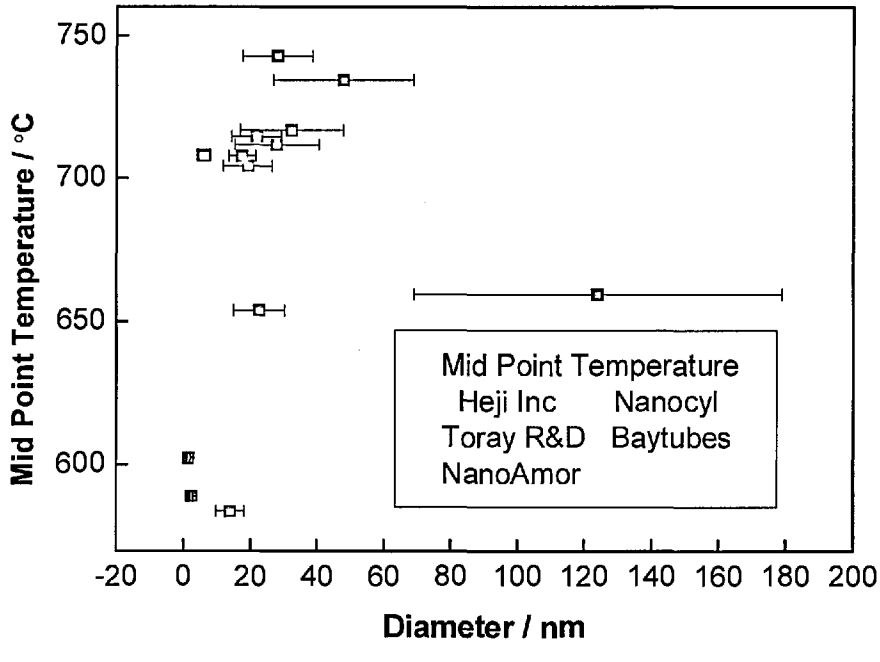

Figure 55: Relationship between the mid-point temperature and the diameter of CNT

Figure 54 and Figure 55 show the onset and mid-point decomposition temperature as a function of diameter; both variables show similar trends. Other than the large, NanoAmor CNFs which are known to have a poor crystallinity, the combustion temperatures increase reasonably consistently with diameter. One explanation might be that graphitic quality increases with diameter. However, the Raman data discussed in the next section suggests no such effect. More likely, the larger diameter structures burn more slowly due to their smaller surface area; note that the outer surface of CVD tubes often already includes oxygen-containing groups that decompose more readily.

4.1.6 Laser Raman spectroscopy

Raman spectroscopy was used as a complementary technique to study the graphitic structure of the CNTs. The ratio of the graphitic G-band (around 1580 cm^{-1}) to the defect-related D-band (around 1320 cm^{-1}) (Figure 56) is often used as an indication of sample crystallinity. It is worth noting that this relationship only works for graphitic structures with an in-plane correlation length of greater than around 2 nm; however, this condition applies to the materials in the current study. More detailed analysis can consider the ratio of the G′ band (at around 2600 cm^{-1} to the D-band, or the use of integrated areas rather than peak intensities, but qualitatively the effects are similar. A typical Raman spectrum is shown in Figure 56 below, with a summary of the G/D intensity ratio for all samples included in Figure 57. The data show a weak trend towards greater G/D (i.e. crystallinity) for decreasing diameters, with a strong increase only for SWNTs and a strong decrease for the defective CNFs. The greater apparent crystallinity of the SWNT samples may be related to an actual increase, due for example to greater selectivity for perfection during growth of these

highly strained structures, or to Raman resonance effects amplifying the signal from less defective CNTs.

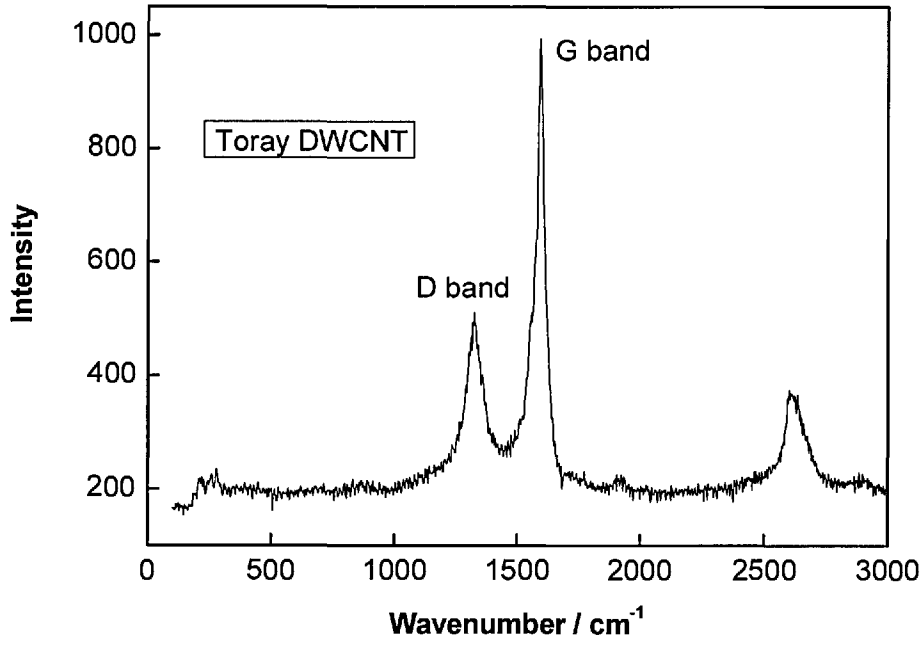

Figure 56: Raman spectra of CNT

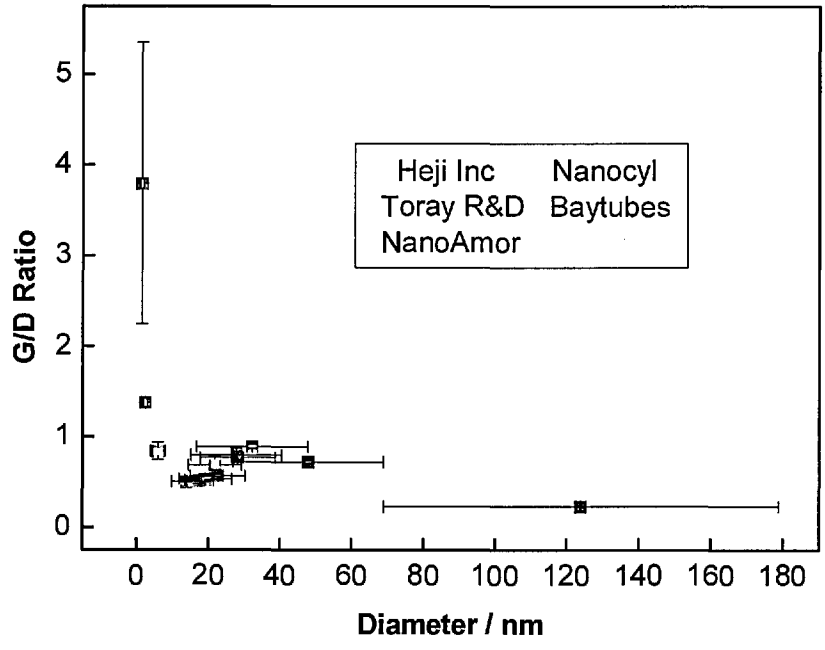

Figure 57: Relationship between G/D ratio and the diameter of CNT

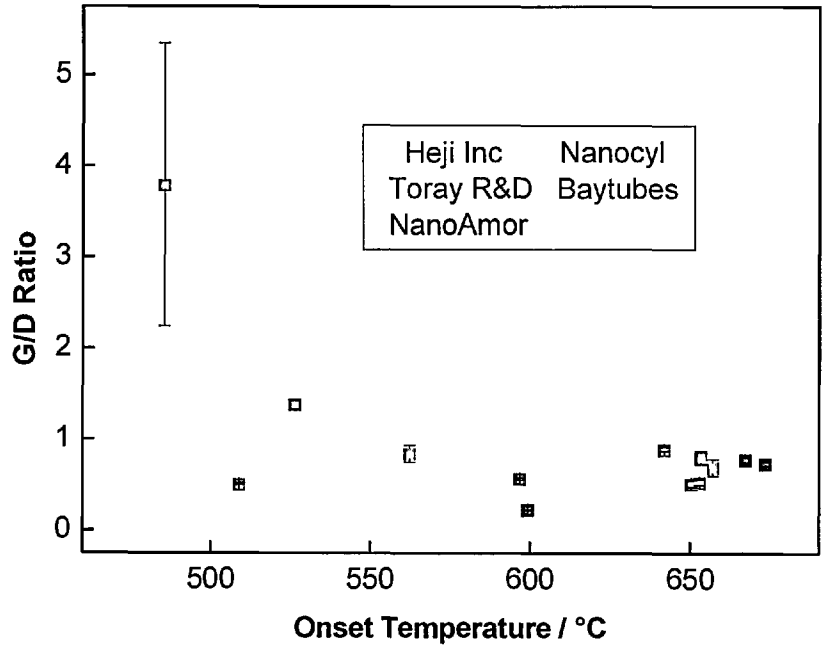

Figure 58: Relationship between the G/D ratio and the onset temperature

In Figure 58, the G/D ratio is compared to the onset temperature for combustion as determined by TGA. However, for the carbon nanomaterials investigated in this study, there is no direct correlation evident; in fact, the G/D ratio appears to be independent of onset temperature. The only outlier is the SWNT sample which behaves quite differently, probably due to the resonance effects already mentioned. The result is interesting, as the current view is that both quantities should be directly related. It seems that diameter or surface area may be the dominant factor controlling combustion. However, it may be that TGA data does provide a useful comparison of crystallinity for samples with similar dimensions, or if G/D ratios vary more dramatically; other than the SWNT sample, the G/D ratios of these as-produced CVD nanotubes samples are rather similar.

4.1.7 X-ray photoelectron spectroscopy and Boehm's titrations

The chemical composition of the CNTs was analysed at the University of York. Table 9 shows the oxygen content of the materials, as well as an estimate of the content of C-OH and C=O bonds. This analysis was performed assuming that the samples contained only carbon and oxygen, with negligible water; the residues observed in the TGA analysis have not been taken into account. However, they are relatively small, as a mass fraction, and as long as they are pure metals (or carbides) will not influence the result significantly. Of the samples studied by XPS, only the DWCNTs contain an oxide catalyst support which is likely to skew the result, since around 1 % silica is present. Nevertheless, there is a clear trend that the larger (> 8 nm) MWCNTs have similar, low oxygen contents, less than 1 at%. Whilst the smaller diameter structures, MWCNT < 8 nm and SWCNTs have significantly greater oxygen content (> 3 at%) in line with their greater surface area and more polar surface character in the wettability studies discussed above.

Table 9: XPS surface analysis of CNT

Nanomaterials	*Diameter Range*	*O 1s atomic %*	*% C=O*	*% C-OH*
Heji Inc	SWCNT 1-2 nm	3.43	1.55	1.88
	MWCNT <8 nm	3.10	1.34	1.56
	MWCNT 8-15 nm	0.49	0.07	0.42
	MWCNT 10-20 nm	0.59	0.25	0.35
	MWCNT 20-30 nm	0.93	0.19	0.75
	MWCNT 30-50 nm	0.83	0.30	0.53
	MWCNT 20-40 nm	0.42	0.20	0.23
Toray R&D	DWCNT ~3 nm	4.06	1.757	2.31

These XPS results were calibrated by Boehm's titrations on selected samples. For the larger MWCNTs which were hydrophobic in nature, reliable results were hard to obtain as the amount of material wetted by the base solution fluctuated. For most CNTs studied the amount of oxygen content which corresponds to the amount of the surface functional groups as shown with XPS analysis is very low (under 1 %) (Table 10). Considerable care was required to minimise absorption of CO_2 and to consistently use inert containers. Due to the low concentrations involved, pH equilibrium when back-titrating the solution was not always easy to observe, necessitating consideration of the full pH titration curve. Nevertheless, the overall concentration of acid surface groups was obtained reproducibly (± 5 %) for several samples. The results show a relatively high and similar oxygen-group content for the SWCNTs and MWCNTs < 8 nm, in line with the XPS data. The DWCNTs have an intermediate degree of functionality, consistent with a high surface area but a strong contribution to the XPS data from the zeolite content, as suggested above. The larger MWCNTs have a very low surface oxygen-concentration consistent with the XPS data and poor wettability in water. Note that the titration data was checked using an acid oxidised MWCNT sample, approximately 30 nm in diameter [164]. This treatment is known to give a high concentration of surface groups; the result is consistent with data in the literature.

Table 10: Boehm's titration results, in milli-equivalents of functional groups per gram of carbon

Material	*Groups neutralised by NaOH / meq/g*
SWCNT 1-2 nm	1.14
DWCNT ~3 nm	0.14
MWCNT <8 nm	1.07
MWCNT 20-40 nm	0.03
MWCNT 30nm Acid Treated	2.19

4.1.8 Summary

In summary, this section provides fundamental characterisation of the materials used in the remainder of this thesis. Both surface and bulk properties of various commercial CNTs were investigated as a function of their diameters. Detailed comparative studies of CNTs from different suppliers are relatively rare, although some examples have appeared recently [165]. The results show clearly that the purity and dimensions of the nanomaterials differ from the information provided by the original commercial supplier. As such, it is critical to carry out a detailed characterisation of any materials used, if meaningful conclusions are to be deduced later. In the current context, the similarity of the 'different' diameter Heji materials is disappointing as it limits the scope for scaling studies. It seems that many CVD MWCNTs, from different suppliers, have similar characteristics, particularly in terms of combustion behaviour and G/D ratio, despite the variations in growth processes. However, surface chemistry and surface area can vary, emphasising the importance of detailed characterisation, since these surface properties will strongly influence interactions in solution or in a polymer matrix.

4.2 Interfacial characterisation of single fibre hierarchical composites using single fibre pull-out tests: Apparent interfacial shear strength as a measure of practical adhesion

(The work presented in the following section was performed by me under the supervision of Dr. Gerhard Kalinka at the Federal Institute for Materials Research and Testing (BAM), Division V.6., in Berlin, Germany. The SEM images were captured using a SEM515, Philips, Eindhoven, The Netherlands)

The feasibility of hierarchical PEEK composites was investigated on the single fibre composite scale. The interfacial properties of these composites were studied using single fibre pull-out tests. The apparent interfacial shear strength (IFSS) between commercially available industrially oxidised sized and desized T700 (by soxhlet extraction with acetone) and unsized AS4 carbon fibres and unmodified PEEK-150 as well as CNT/PEEK-150 nanocomposites containing various loading fraction of CNTs were examined using the single fibre pull-out test. The force required to debond the interface of the single fibre model composite was determined from force-displacement curves.

A typical example of a real measured force-displacement curve is shown in Figure 59. The apparent interfacial shear strength (IFSS), as measure for the practical adhesion, of the fibre/matrix interface as well as the frictional strength after debonding of this interface of a model single fibre composite were investigated.

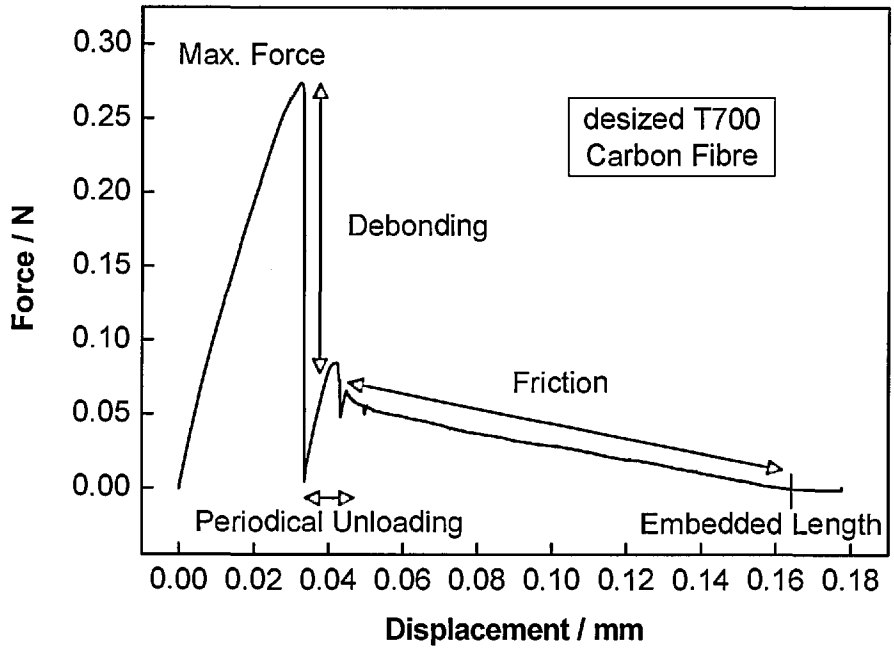

Figure 59: A typical measured pull-out force displacement curve obtained while pulling out a single desized T700 carbon fibre from PEEK, with annotations

The measured apparent interfacial shear strength as function of the embedded fibre length provides information about the fracture behaviour of the fibre/matrix interface of model single fibre composites [166] (Figure 60).

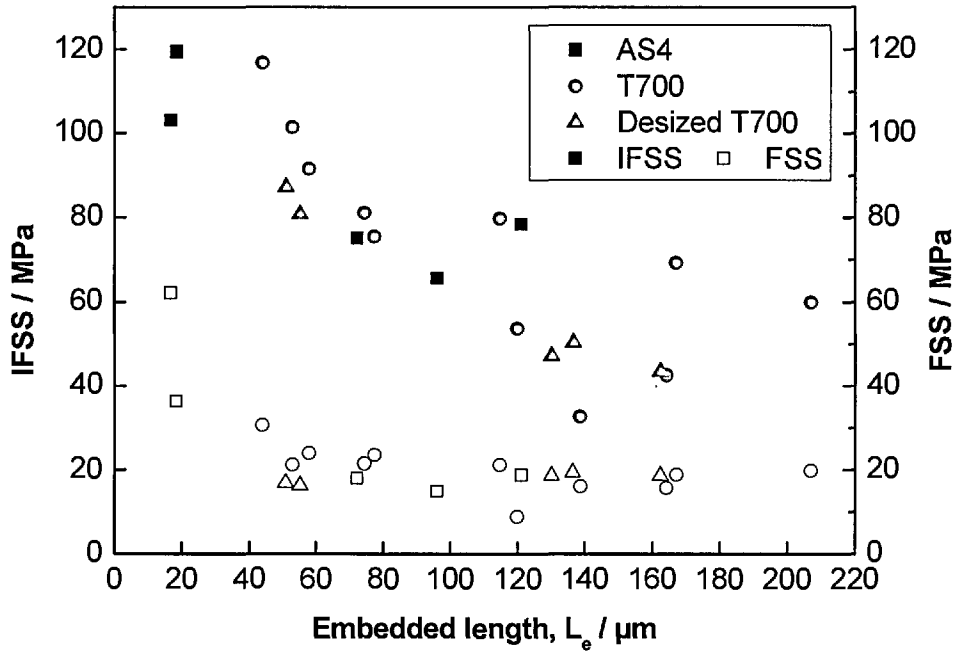

Figure 60: Apparent interfacial shear strength and frictional shear strength as function of the embedded fibre length for unsized AS4, epoxy sized T700 and desized T700 carbon fibres and PEEK-150.

The IFSS between all investigated carbon fibres and PEEK-150 decreases exponentially with increasing embedded fibre length. For example in case of the desized T700, the measured IFSS was between 80-85 MPa for an embedded fibre length of 50 µm. When the embedded fibre length was increased to 160 µm, the measured IFSS dropped to about 40 MPa. Such behaviour indicates a brittle fracture behaviour at the fibre/matrix interface of the model composites and that the interface failed at once [166].

On the other hand, the frictional shear strength of all investigated carbon fibres and PEEK-150 is virtually independent of the embedded fibre length with the exception of the unsized AS4 fibres at a very low embedded fibre length (20 µm). This is

because for such a low embedded fibre length, the weight of the single fibre filament is not properly supported by the matrix, which affects the measured data. A high frictional shear stress is recommended to counteract fibre pull-out during failure of a composite. For unsized AS4 and T700 fibres (either sized or desized), there is no difference in the mean FSS value, therefore all fibres will behave in the same manner during failure after debonding occurred.

SEM micrographs of carbon fibres after being pulled out, as well as the corresponding PEEK droplets, were taken (Figure 61) to investigate the fracture behaviour. The formation of a wetting cone, due to the partial wetting of the carbon fibres by the PEEK melt, can clearly be seen in Figure 61. This meniscus is formed when the PEEK polymer melt made contact with the fibre. Three factors determine the size and shape of the meniscus (wetting cone): 1) the contact angle between fibre and matrix which is determined by the surface tension of the PEEK melt, the fibre/PEEK melt interfacial tension and the surface (tension or) energy of the carbon fibre, 2) the droplet is flowing under the influence of gravity and thus is moving relative to the fibre and 3) the PEEK melt droplet shrinks onto the fibres during the cooling process. The top micrographs in Figure 61, show an AS4 carbon fibre, which fractured during the pull-out test as a result of a very high embedded fibre length. If the embedded fibre length is too large, the force to debond the fibre from the matrix would be larger than the tensile strength of the single fibre, so the fibre fails.

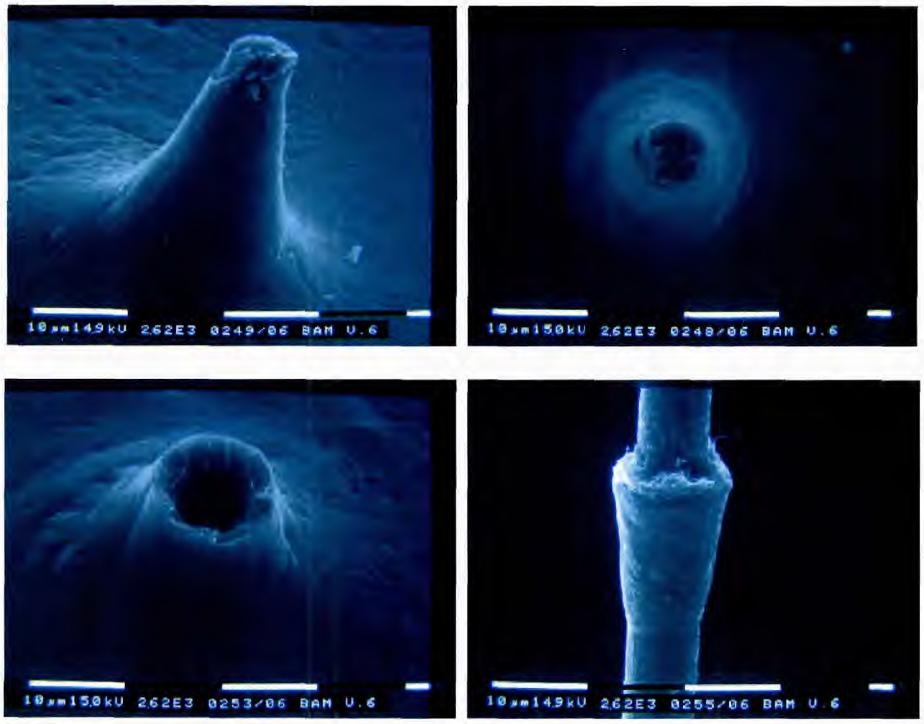

Figure 61: Representative SEM images of AS4/PEEK showing fibre breakage (top) and successful fibre pull-out (bottom) from PEEK 150 droplet

However, when the embedded fibre length was reduced the fibre could be pulled-out from the matrix (Figure 61, bottom). When pulling at the end of the embedded fibre, the weakest part of the single fibre composite failed first. Usually, the highest stresses arise in the region where the fibre was in contact with the matrix droplet. The failure of the model composite seems to have started with the fracture of the wetting cone or at the fibre/matrix interface failure inside the droplet within the wetting cone. As can be seen from the SEM micrograph (Figure 61, bottom), the energy required to fracture the matrix, separating the wetting cone from the droplet, was lower than the energy required to completely debond the fibre/matrix interface. This causes the shift of the maximum pull-out force as function of embedded fibre area away from the zero origin (see for example Figure 62). Therefore, after the single fibre was completely pulled out from the matrix droplet, a part of the meniscus remained attached to the surface of the pulled-out fibre (Figure 61, bottom). The

formation of PEEK microfibrils caused by the plastic deformation and drawing of the matrix can be seen on the fracture surfaces of the wetting cone. Moreover, parts of the PEEK matrix still stuck to the pulled out fibre indicating a strong fibre/matrix adhesion.

In order to be able to determine the average IFSS between PEEK-150 and the unsized AS4 as well as epoxy sized T700 and desized T700 carbon fibres (the same methodology was used for all other model composites), the maximum pull-out force was plotted as function of the embedded fibre area (Figure 62), which follows a linear dependency. The slope of the maximum pull-out force as function of embedded fibre area ($F_{max} = f(A_e)$) corresponds to the apparent interfacial shear strength. The steeper slope for the unsized AS4 fibres shows clearly that the AS4 adheres much better to PEEK-150 than the sized T700 fibres and even desized T700. These once more highlights that epoxy sizings are detrimental to establish a strong fibre/thermoplastic interface [167 - 169]. The epoxy sizing does not mix or dissolve into the PEEK melt, which leads to the formation of a weak boundary layer [170] between the sizing and solidified matrix. Removing the sizing, by acetone extraction, results in a significant increase of the IFSS. Figure 63 compares the IFSS between the carbon fibres used and PEEK-150. Further discussion of the impact of the epoxy sizing on fibre/matrix adhesion dominated composite properties, namely the short beam shear strength, can be found in Section 4.4.

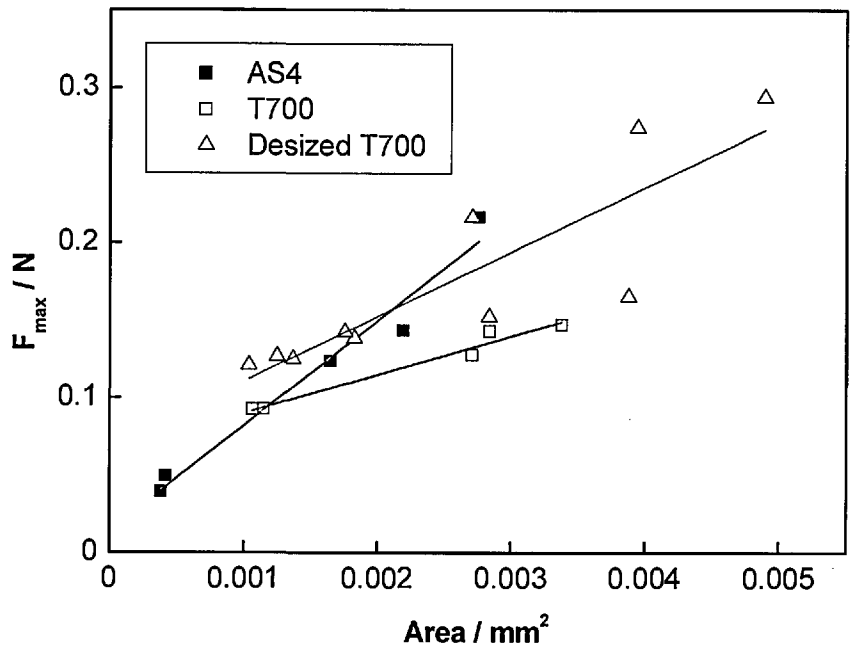

Figure 62: Maximum pull-out force as a function of the embedded area of unsized AS4, sized and desized T700 carbon fibres

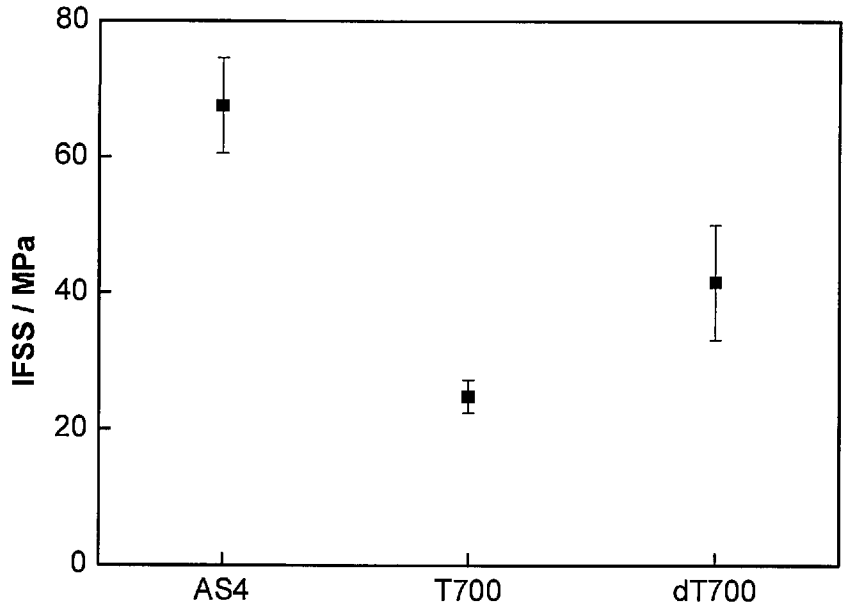

Figure 63: Comparison of the apparent interfacial shear strength between the investigated CFs and PEEK-150

Nanocyl CNTs are used throughout the rest of this study. The effect of a CNT modification of PEEK with CNT loading fractions up to 5 wt% on the apparent interfacial shear strength to desized T700 was also examined using the single fibre pull-out test. (Figure 64) Also in this case the IFSS between desized T700 and PEEK-150 containing a CNTs loading from 0 to 5 wt% is dependent on the embedded carbon fibre length. This once again indicates brittle fracture behaviour of the model composite and that the boundary layer is predominantly semi-crystalline[171]. The frictional shear strength between the debonded desized T700 carbon fibres and PEEK-150 CNT nanocomposites is again virtually independent of the embedded fibre length.

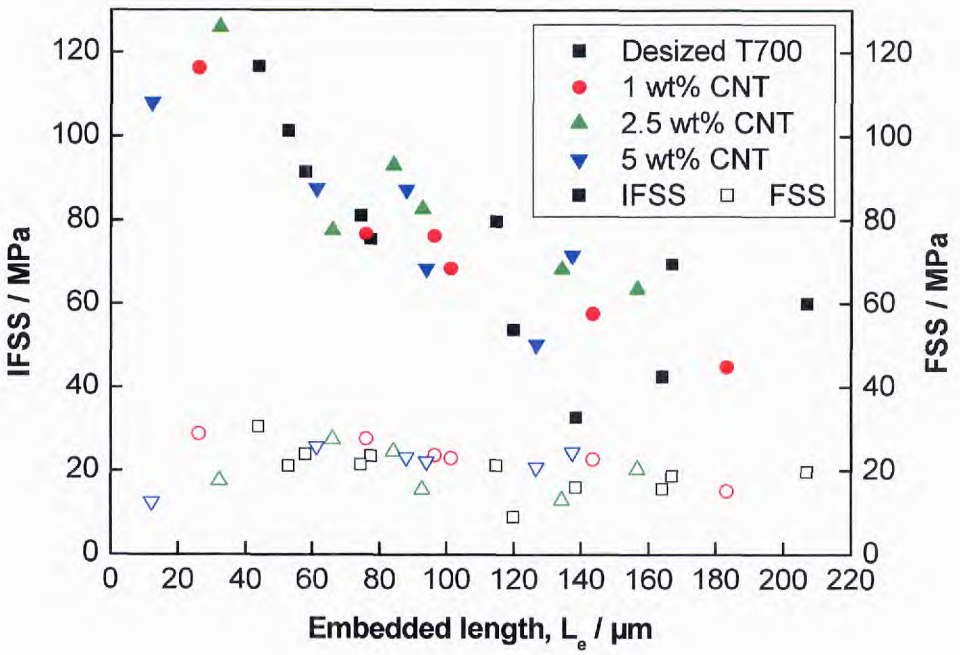

Figure 64: Apparent interfacial shear strength and frictional shear strength as function of the embedded length of investigated CFs and Nanocyl CNT-reinforced PEEK

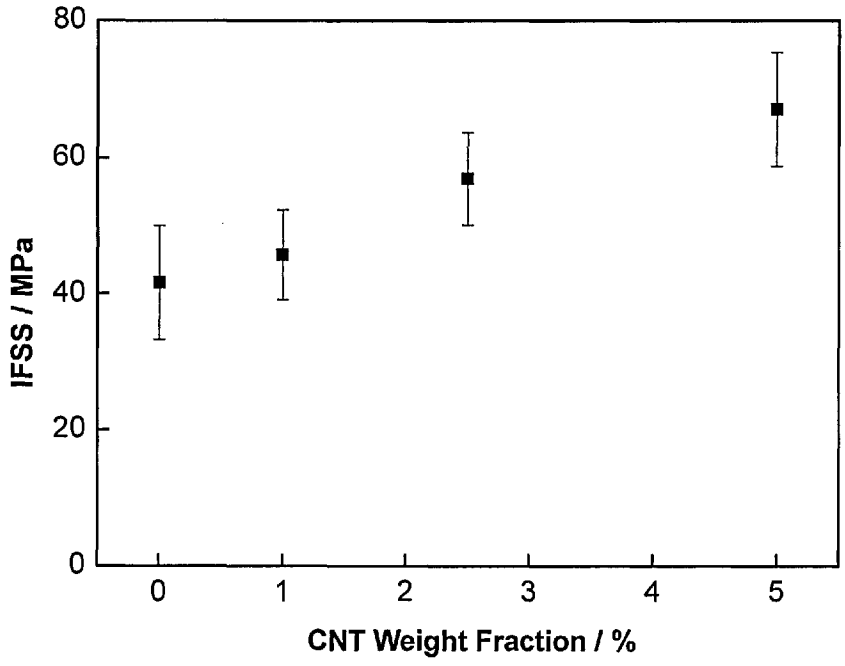

Figure 65: Apparent interfacial shear strength as a function of Nanocyl CNT loading in PEEK to desized T700 fibres

The average IFSS between desized T700 carbon fibres and PEEK-150 CNT nanocomposites was again determined by plotting the maximum pull-out force as function of embedded fibre area. The average IFSS between the desized T700 and CNT modified PEEK-150 increased steadily with increasing the CNT loading fraction to 5 wt% (Figure 65). Adding 5 wt% CNTs into the PEEK matrix increases the interfacial adhesion by 50 %. The increase in the IFSS is surprising considering that the PEEK matrix was not otherwise modified and can only be explained by the mechanical modification of the PEEK which improves stress transfer from the fibre into the matrix during the pull out test. However, one should note that the CNT reinforced PEEK matrix used for the preparation of the single fibre hierarchical composites was produced by micro-extrusion (see experimental section 3.3.2 for details) and was therefore (almost) free of DPS, in contrast to the unidirectional

continuous carbon fibre reinforced CNT/PEEK nanocomposites. Therefore, the higher measured IFSS between the desized T700 fibre and the PEEK nanocomposites is purely the result of the incorporation of CNTs into PEEK-150.

However, the literature contains a number of papers reporting significant increases by as much as 32 % of the IFSS of single glass fibre/CNT modified epoxy composites when compared to the pure epoxy matrix [172]. The authors claim the increase in IFSS is due to the increased surface tension of the CNT modified epoxy matrix [172]. Vlasveld et al. [173] characterised E-glass fibre/nano-sized exfoliated synthetic layered silicate reinforced polyamide-6. They report a significant reduction in the interfacial adhesion (i.e. an increase of the aspect ratio L/D as determined using the single fibre fragmentation test) for the nano-reinforced matrices. On the other hand, Lew et al. [174] report rather small improvements of the IFSS in carbon fibre/silica nanoparticle reinforced epoxy single fibre composites measured using the single fibre fragmentation test.

SEM micrographs of the pulled out carbon fibres and the corresponding 2.5 wt% of CNT containing PEEK nanocomposite droplets (Figure 66) were taken to illustrate the fracture behaviour of the model single fibre hierarchical composites.

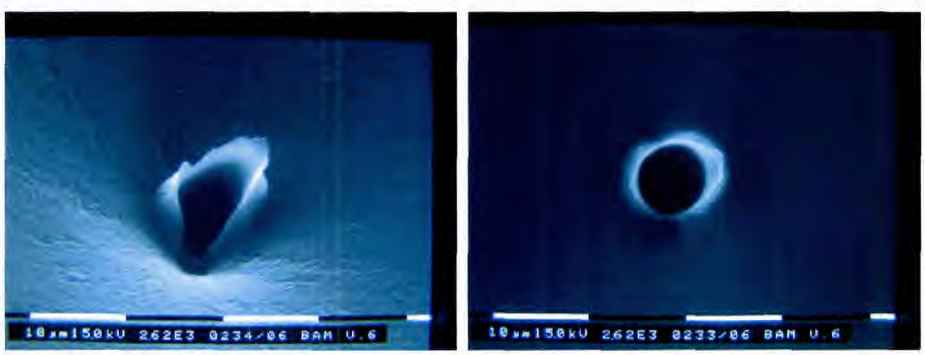

Figure 66: Representative SEM micrographs of 2.5 wt% CNT in PEEK matrix after fibre pull-out

For the CNT/PEEK nanocomposites rather than the formation of a wetting cone as seen for the pure PEEK-150 matrix (Figure 61), a concave impression formed during the embedding of the fibre into the nanocomposite melt (Figure 66). This is largely due to the massive increase of the melt viscosity of the PEEK matrix caused by the incorporation of CNTs. The melt viscosity increases from 246 Pa.s to 542 Pa.s (please see section 4.3.3.1 nanocomposites rheology). During the preparation of the single fibre hierarchical composites it was noted that with increasing CNT loading it became more and more difficult to embed the carbon fibres into the matrix, which correlates with the increased melt viscosity of the CNT nanocomposites with increasing CNT loading fraction. Nevertheless, it is interesting to note that after pull-out the fibres are still coated with the nanocomposite matrix (Figure 67a and Figure 67c), which again is an indication of the rather good adhesion between the fibres and the nanocomposite matrix.

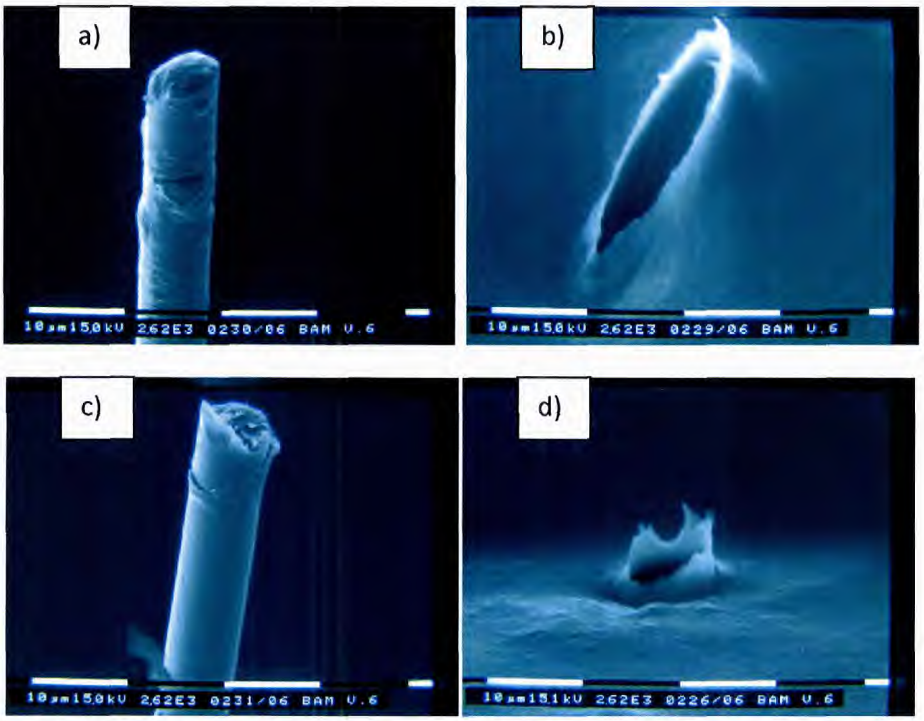

Figure 67: Representative SEM images of desized T700 carbon fibres pull-out from 5 wt% a), b) and 10 wt% c) and d) of CNT in PEEK-150 nanocomposite droplets

4.3 Production and characterisation of PEEK reinforced carbon nanotubes composites

4.3.1 Tensile testing of CNT/PEEK nanocomposite monofilaments

Nanocomposite monofilaments were produced using a twin screw micro-extruder, to provide an initial assessment on the effect of CNT diameter on the composite tensile strength and Young's modulus. All specimens were annealed prior to testing to ensure a consistent degree of crystallinity.

A basic rheological study was conducted using the twin screw micro-extruder, modelling it as a viscometer in which the viscosity (η) is given by the relationship:

$$\eta = C\frac{T}{N} \tag{26}$$

where C is the coefficient related to the extruder, T is the torque and N is the rotating speed.

The relative viscosity (η_r) is calculated as being a ratio between the composite torque (T_c) and the matrix torque (T_m) taken during the last 10 s of mixing, thus:

$$\eta_r = \frac{T_c}{T_m} \tag{27}$$

As the shear rate of the micro-extruder is unknown for the parameters used, it is only possible to present relative viscosity values. As guidance for the reader, PEEK viscosity has a value of 150 Pa.s for a shear rate of 1000 s^{-1}.

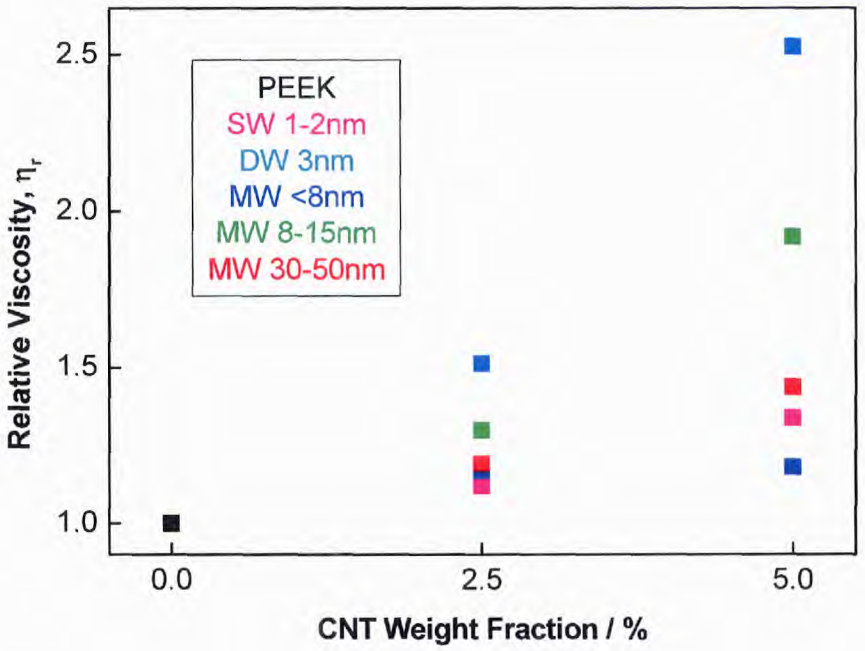

Figure 68: Relative viscosity of the polymer melt in the micro-extruder as a function of CNT loading fraction

Figure 68 shows the relative viscosity of the blended materials as a function of CNT weight fraction. As expected, the relative viscosity increases with increasing CNT weight fraction, as has been shown in more detailed, recent studies of PEEK melt rheology[175]. However, there is no clear trend relating to diameter. This conclusion is consistent with an understanding that the degree of dispersion of the CNTs and their absolute length are the main factors controlling viscosity. If well-dispersed, the length of the nanotubes controls network formation; long nanotubes occupy a large hydrodynamic volume and increase viscosity particularly at modest shear rates (before significant shear thinning). It is assumed that the length of the nanotubes in the melt depends on their original length and their tendency to break under shear, which may have a diameter dependence, though it is not immediately obvious in which direction. For a given loading fraction, smaller diameter tubes will have a

greater number of interacting structures, and hence should give a high viscosity. However, entangled or bundled nanotubes (SWCNTs) that do not disperse individually will display the opposite trend.

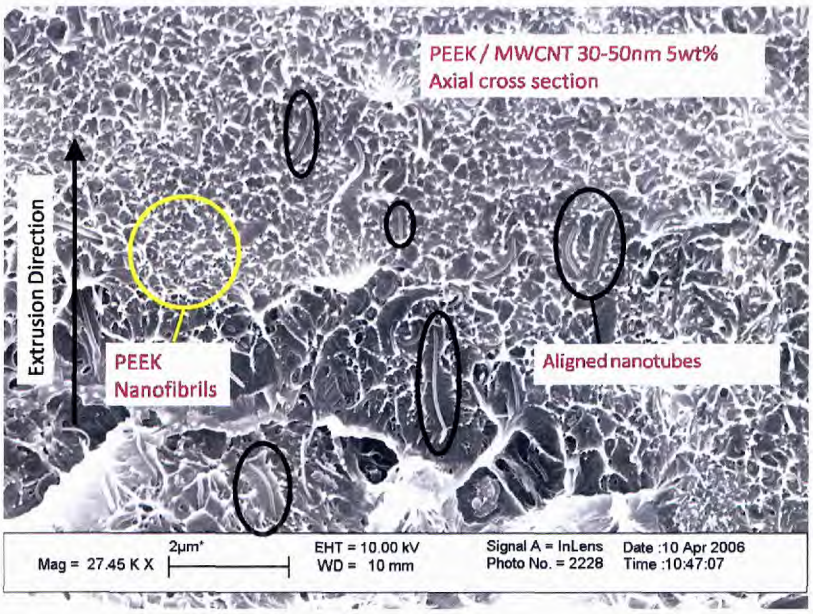

Figure 69: SEM micrograph showing the tensile fracture surface of PEEK/MWCNT (30 – 50 nm) at 5 wt% loading fraction

The SEM micrograph of the tensile fracture surface above (Figure 69) shows a region of well-dispersed MWCNTs (30-50 nm) within the matrix, and hints at a preferential alignment along the extrusion direction. In addition, PEEK nanofibrils drawn from the tensile fracture of the specimen are also visible; interestingly these fibrils do not form in the immediate vicinity of the CNTs, suggesting that the load carried by the nanotubes locally interrupt fibril formation. On the other hand, lower magnification SEM images of fracture surface indicate a tendency for local agglomeration (Figure 70 and Figure 71); most likely, these small structures are never disentangled from their as-produced state, although shear-induced agglomeration processes are also known [176].

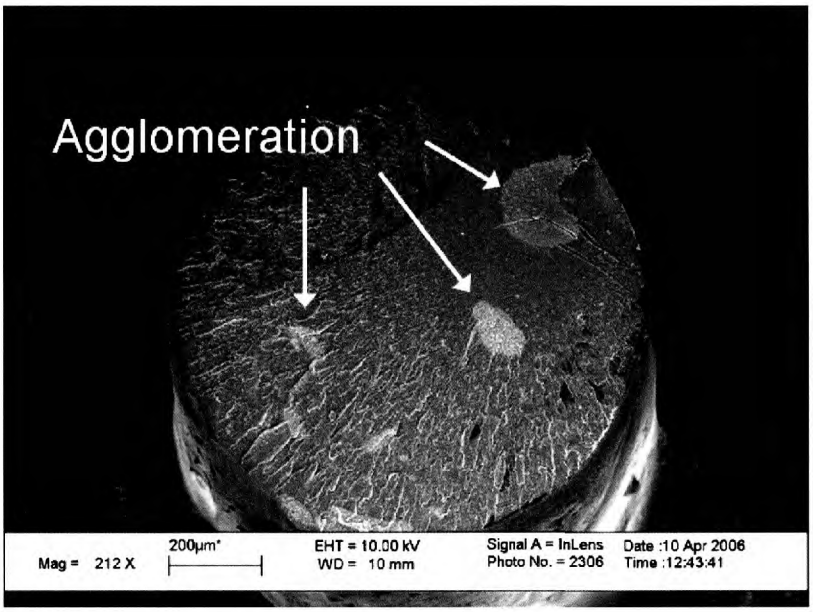

Figure 70: SEM micrograph showing the tensile fracture surface of PEEK/DWCNT (~3 nm) composites at 5 wt% loading fraction

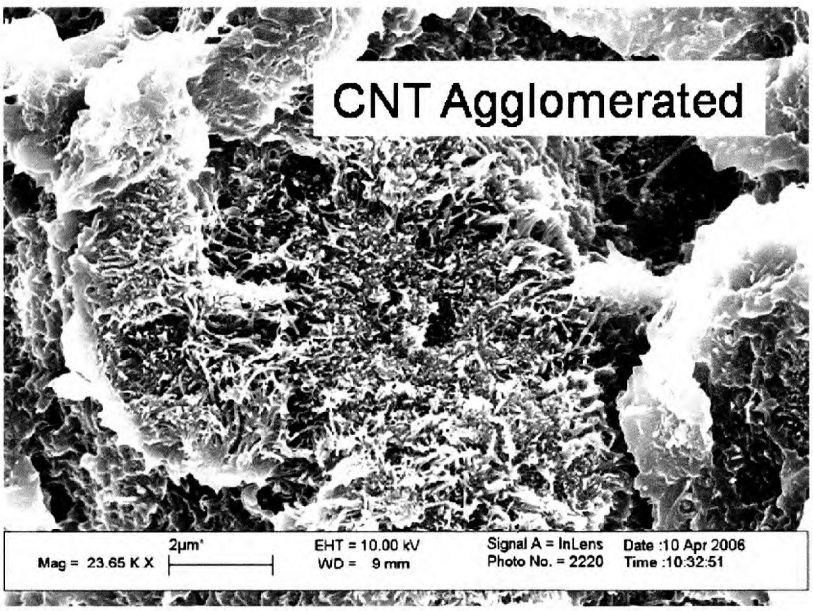

Figure 71: SEM micrograph showing the tensile fracture surface of PEEK/MWCNT (30 – 50 nm) composites at 5 wt% loading fraction

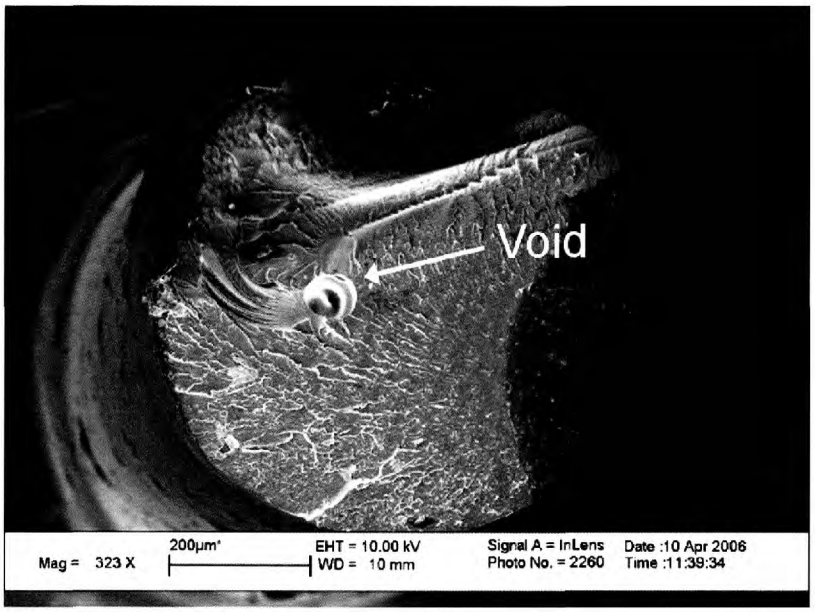

Figure 72: SEM micrograph showing the tensile fracture surface of PEEK/MWCNT (< 8 nm) at 2.5 wt% loading fraction

Voids are also present within some of the extruded monofilaments due to trapped gas (Figure 72). These features, observed in the micrographs, such as agglomerates and voids within the extruded monofilaments are expected to degrade the measured tensile properties.

Figure 73 shows the yield stress of the extruded monofilaments as a function of the CNT weight fraction. An increase in yield stress can be seen for all nanocomposites with a loading fraction of 2.5 wt% from 80 MPa for pure PEEK up to 90 MPa with no particular improvement related to the varying CNTs diameter. With a higher CNT loading within the matrix, the tensile strength decreased to around 82 MPa for most nanocomposites except for the large MWCNT 30-50 nm which had a yield stress of 94 MPa. The performance reduction is likely due to the presence of agglomerations and voids as discussed previously. Similar trends were observed for the tensile strength at break (Figure 74).

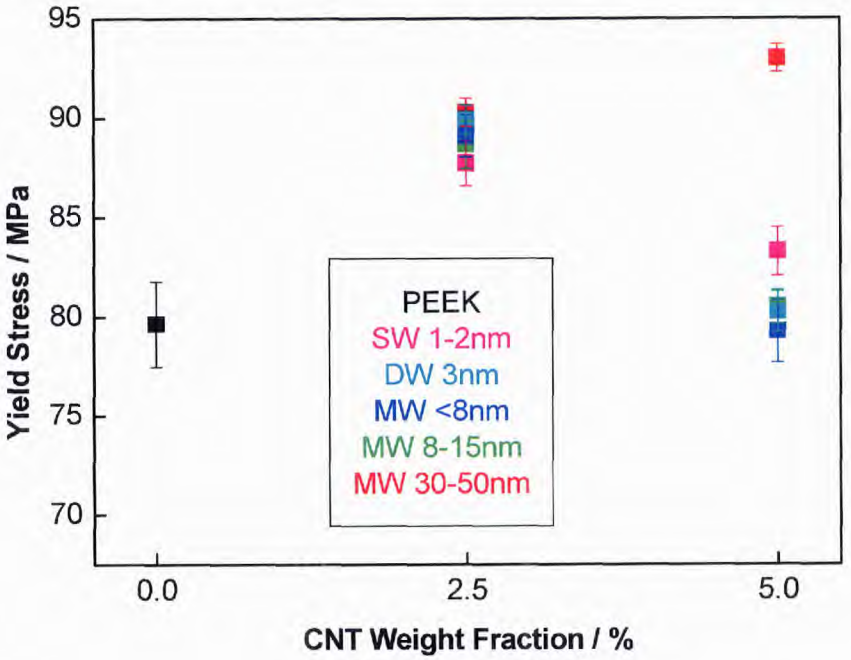

Figure 73: PEEK monofilament yield stress as a function of CNT loading fraction

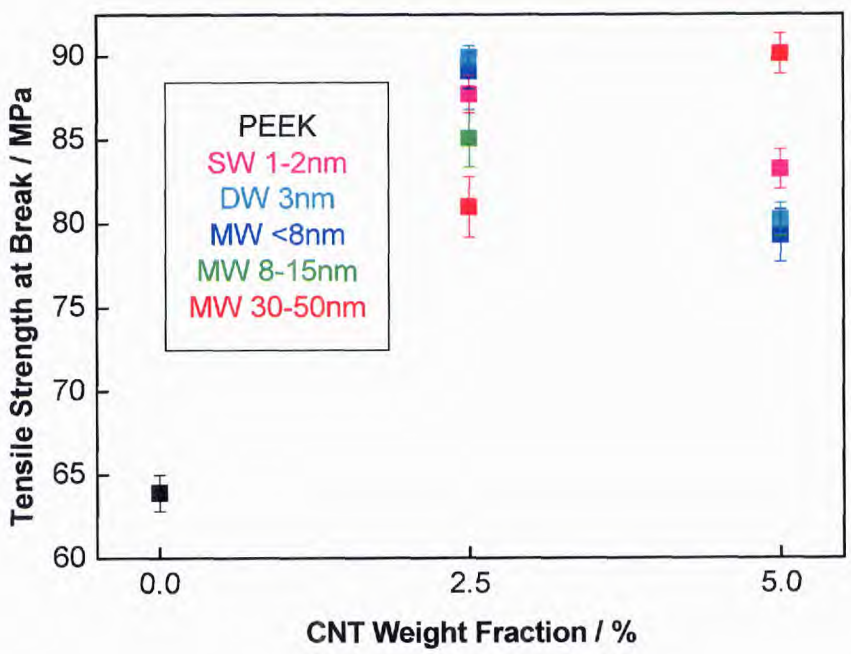

Figure 74: PEEK monofilament tensile strength at break as a function of CNT loading fraction

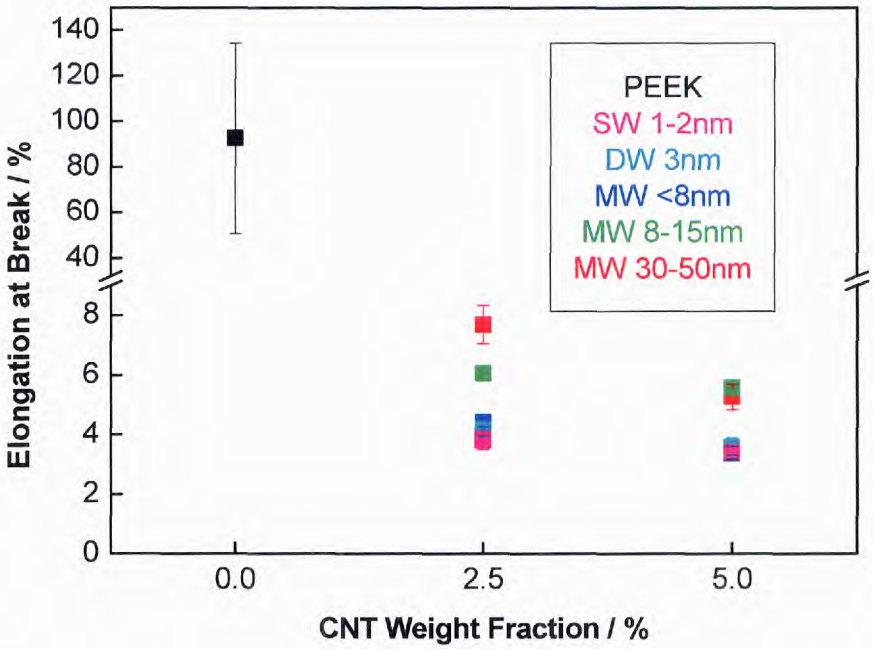

Figure 75: Monofilament elongation at break as a function of CNT loading fraction

Figure 75 shows the monofilament tensile elongation at break for the nanocomposites mixed with the micro-extruder. The elongation at break of pure PEEK monofilaments is ductile with a value of around 100 %. For all nanocomposites, the elongation at break decreased substantially down to about 5 %, as observed in other studies. Monofilament elongation at break does seem to decrease more quickly for smaller diameter fillers. The presence of CNTs presumably constrains the pure PEEK locally, which is itself very much more ductile. Smaller diameter structures may interact more effectively with the PEEK due to their higher surface area, constraining more PEEK molecules, and reducing ductility more strongly.

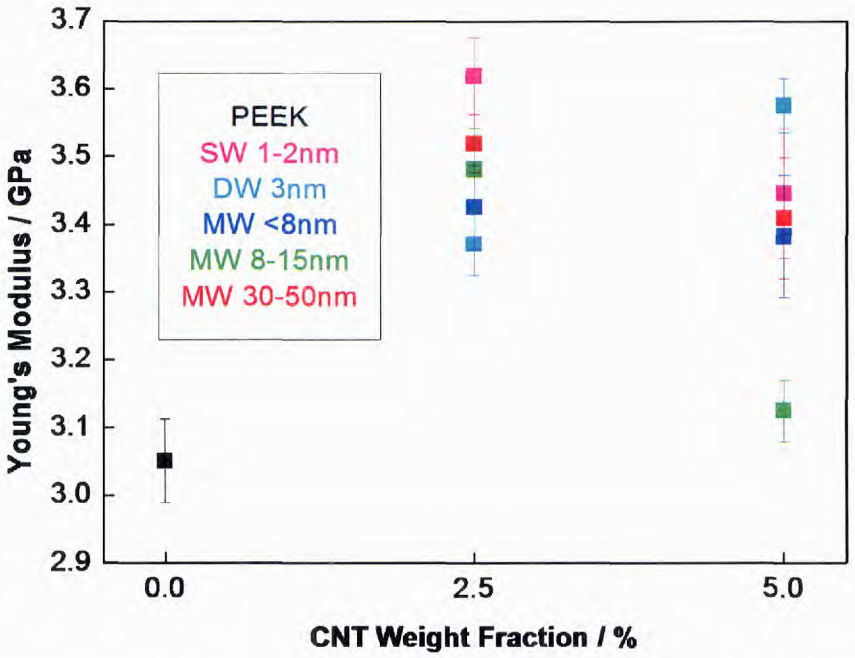

Figure 76: PEEK monofilament Young's modulus as a function of CNT loading fraction

The Young's modulus for all nanocomposites is shown on Figure 76. An increase in the Young's modulus from 3.05 GPa for PEEK up to 3.6 GPa for the SWCNT 1 - 2 nm can be seen with a loading fraction of 2.5 %. However, with higher loading fraction of CNTs, no particular trend can be seen for the Young's modulus. It can be seen that some nanocomposites showed an increase in the Young's modulus, such as for DWCNT ~3 nm, whilst other specimens exhibited a decrease in the Young's modulus, such as for MWCNT 8-15 nm. Furthermore the effect of carbon nanomaterials diameter on the Young's modulus is randomly scattered for each loading fraction used in this study. This outcome could be due to the presence of agglomerations and voids within the extruded monofilaments as discussed previously.

It was generally observed from micrographs that better dispersion can be obtained with larger diameter CNTs; smaller diameter CNTs generated large agglomerates after compounding. Tensile strength at yield and Young's modulus increased by 17 % and 18 %, respectively, as well as the tensile strength at break by 42 %, in the best case. However, a loss in matrix ductility was observed in all cases.

4.3.2 Tensile testing of CNT/PEEK nanocomposite films

Another short study was performed to examine the effect of CNT weight fraction on the mechanical properties of nanocomposites with high loading fractions. Nanocyl MWCNTs were chosen for this study, they are commercially available in industrial quantities. Blends were compounded using the twin screw micro-extruder using the parameters (see 3.3.1) but with a longer mixing time of 15 min to increase the amount of shear mixing within the melt and hence improve the breakup of agglomerates and increase the dispersion of the CNTs. Nitrogen gas was not used during mixing to avoid any trapped gas from within the extruded compounds, therefore creating voids. Loading fractions of up to 15 % by weight were achieved, and all specimens were annealed prior to testing to ensure a high degree of crystallinity.

The Young's modulus of the films was not calculated as the compliance of the equipment could not be determined in tension and individual specimens were too thin and narrow in size therefore no extensometer or strain gauges were used. The yield stress is reported below (Figure 77), this was chosen for comparison purposes as above a CNT weight fraction of 2.5 %, the specimens strength at both yield and break were equal due to the brittleness of the nanocomposites. The yield stress was

higher for both the pure PEEK and 1 % CNT weight fraction specimens than the tensile strength at break and it was of higher significance for mechanical design.

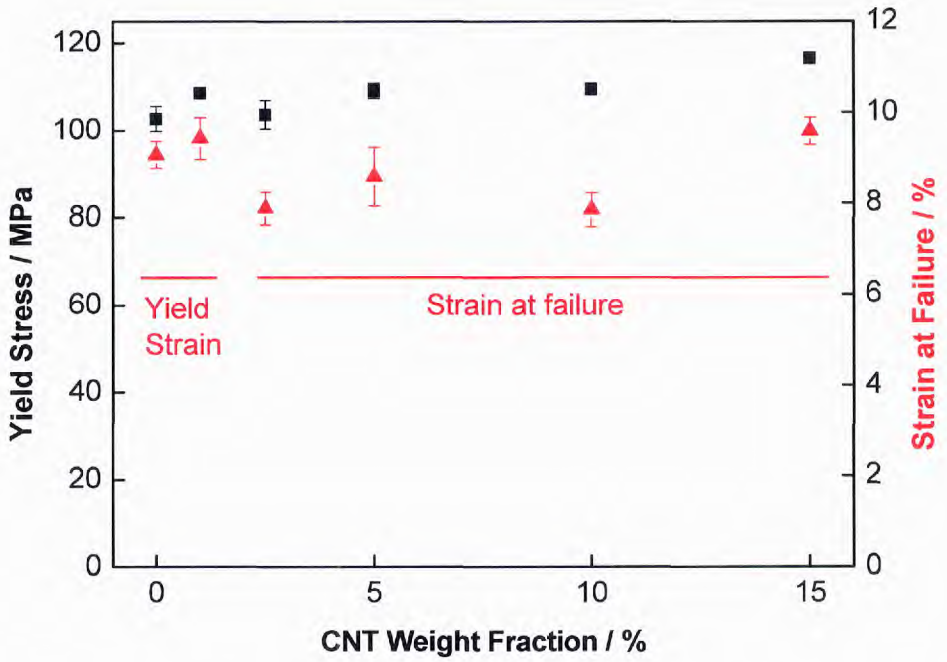

Figure 77: Yield stress of the nanocomposite films as a function of CNT loading fraction

Yield stress of the nanocomposites film showed (Figure 77) a linear increase from 103 MPa for PEEK up to 117 MPa for a CNT weight fraction of 15 %. Tensile strain decreased when the CNT weight fraction went above 2.5 %. This is because data points at yield strain were used in calculating the tensile strain rather than strain at failure for the nanocomposites with CNT weight fraction loading below 2.5 %. No further decrease in matrix ductility was observed for 2.5 % CNT weight fraction nanocomposite films onwards.

It should be noted that the increase in mixing time from 5 to 15 min within the micro-extruder was beneficial. This is because the tensile strength increased by 15 %

linearly as the CNT weight fraction increased up to 15 %, suggesting that improvements in CNT dispersion had been achieved.

4.3.3 Characterisation of CNT/PEEK nanocomposites

Initial trials were conducted as described previously with the varying diameters of CNTs study (see 4.3.1) and also the increasing CNT weight loading study (see 4.3.2). Bulk mechanical properties of nanocomposites were required in order to understand the behaviour of such composites in real world applications. To do so, large batches of nanocomposites were produced by compounding 500 g batches at a time using a continuous twin screw co-rotating extruder. Nanocyl CNTs were once again used as they are commercially available in large quantities. All specimens were annealed prior to testing to ensure a high degree of crystallinity.

4.3.3.1 Rheology of CNT/PEEK nanocomposites melt

The rheology work presented in the following section was performed by Dr Chris Crawley (Victrex Technology Centre, Thornton Cleveleys, Lancashire, UK) using a capillary rheometer with a simple shear rate sweep from $100 - 10000\ s^{-1}$ at a temperature of 380 °C using 25 g of material.

It can be seen from Figure 78 that the shear viscosity increased with increasing CNT weight fraction at all shear rates. Shear viscosity decreases with increasing shear rate due to shear thinning. A constant increase in shear stress with increasing shear rate is observed for all materials can also be seen from Figure 79. The melt strength was enhanced upon increase of shear rate with higher loadings of CNT weight fraction.

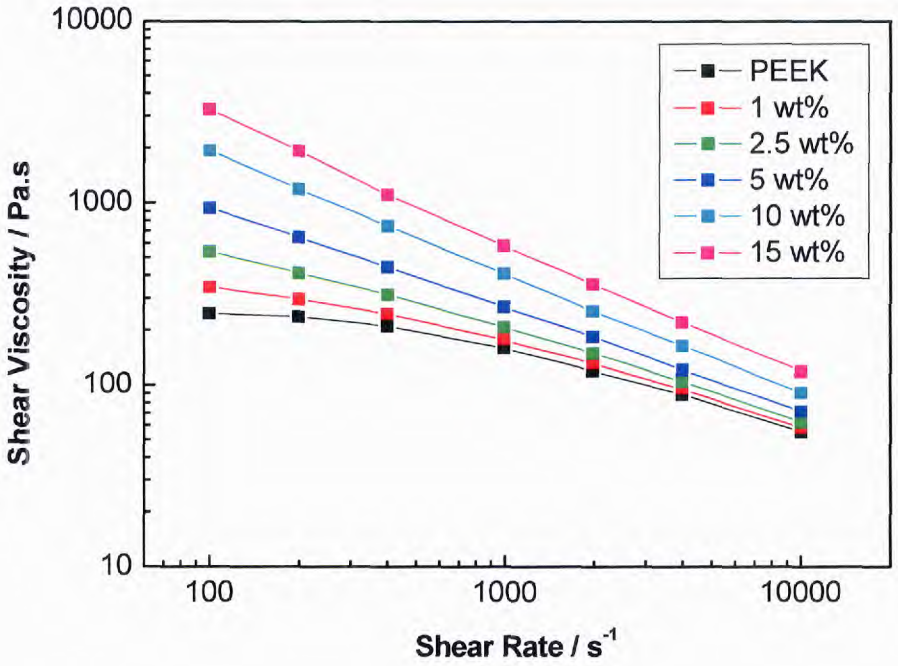

Figure 78: Shear viscosity vs shear rate at different CNT loading fractions

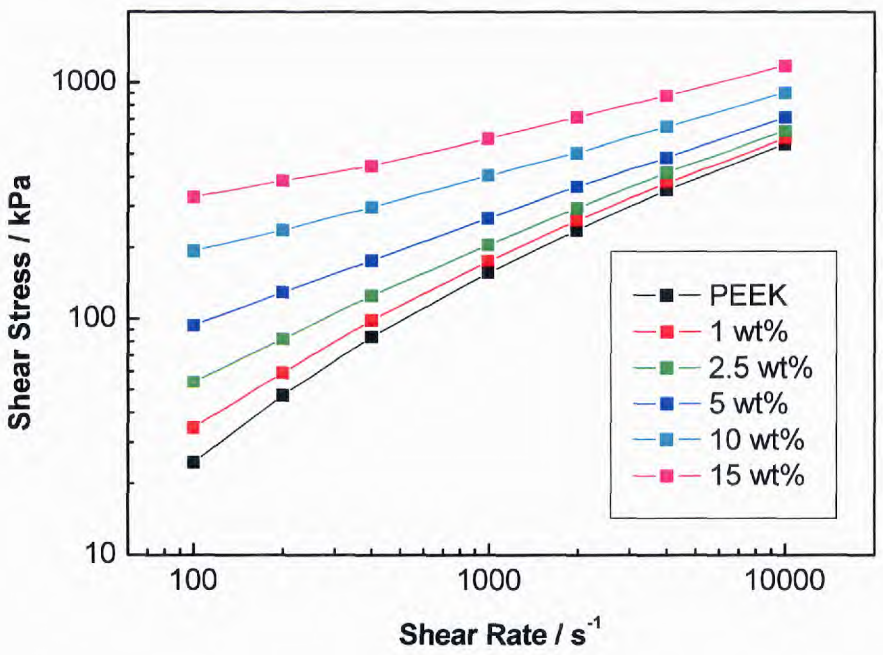

Figure 79: Shear stress vs shear rate at different CNT loading fractions

4.3.3.2 Crystallinity of CNT/PEEK nanocomposites

All specimens were annealed prior to mechanical testing to ensure a high degree of crystallinity and the formation of small crystallites. This also ensured that the mechanical properties measured was due to the reinforcement of CNTs (if any) and not to a higher degree of crystallinity in the matrix caused by the nucleating effect of CNTs.

Typical DSC curves for nanocomposites are shown below for both non-annealed and annealed materials. PEEK and 15 % CNTs were plotted to clearly see any change in thermal behaviour as they are the extremes of this study.

The DSC curve for non-annealed nanocomposite is shown below (Figure 80) for PEEK and 15 % CNT weight fraction. It can be seen that PEEK had a high but narrow melting peak at a temperature of 344 °C. For 15 wt% CNT, the melting peak had a slightly lower melting temperature at 342 °C but was broader with a shoulder starting from 310 °C. Furthermore a shallow peak can be seen for 15 % CNTs at a temperature of 252 °C which could not be seen for PEEK. The high and narrow melting peak for PEEK indicates the presence of crystallised material with a narrow spherulite size distribution. The broadness of the melting peak for 15 % CNTs relates to the presence of different spherulite sizes which have a lower melting temperature. The shallow peak at 252 °C indicated that some interaction at the molecular level took place, 250 °C being the mould temperature within the injection moulding process. It can be assumed that some crystallisation occurred during that process to a small extent due to the nucleating effect of CNT on the polymer matrix.

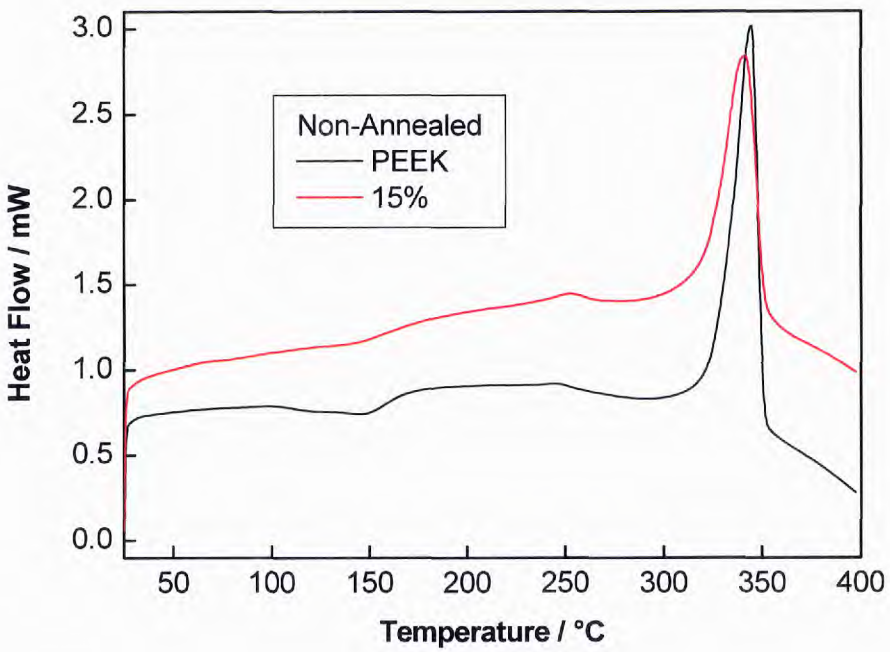

Figure 80: DSC curves of non-annealed neat and 15 wt% CNT loaded PEEK

Annealed nanocomposites are shown below (Figure 81) with PEEK and 15 % CNT weight fraction. As previously described, PEEK showed a high and narrow melting peak with a maximum at a temperature of 343 °C and 15 % CNTs has a slightly broader melting peak with a maximum at 343 °C. A more pronounced peak could be seen for both materials at a temperature of 256 °C. Compared to non-annealed nanocomposites, the main distinction that was seen was the peak present at 256 °C, this certainly was due to the annealing process through spherulite growth for all nanocomposites and will be called the annealing peak from now on.

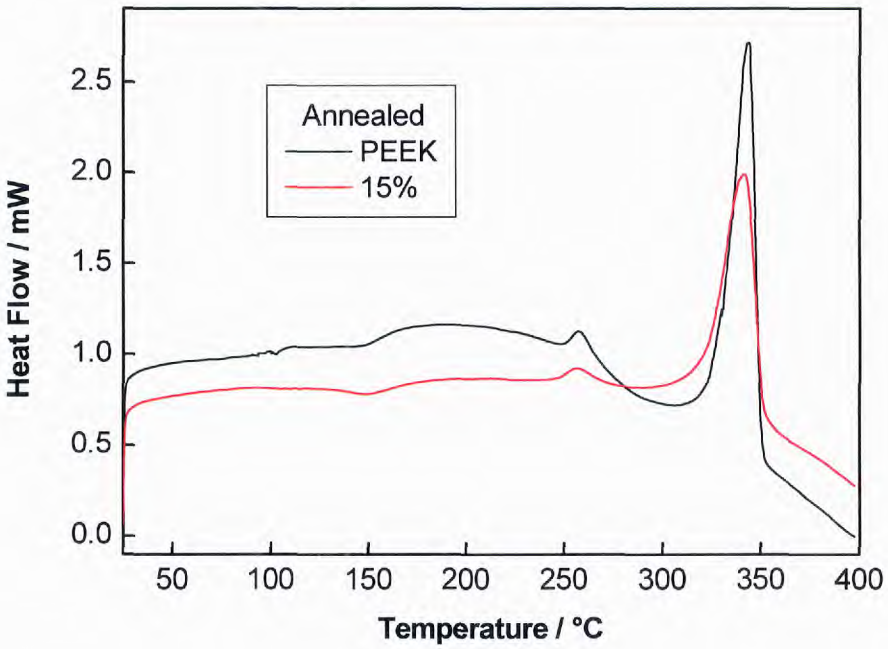

Figure 81: DSC curves of annealed neat and 15 wt% CNT loaded PEEK

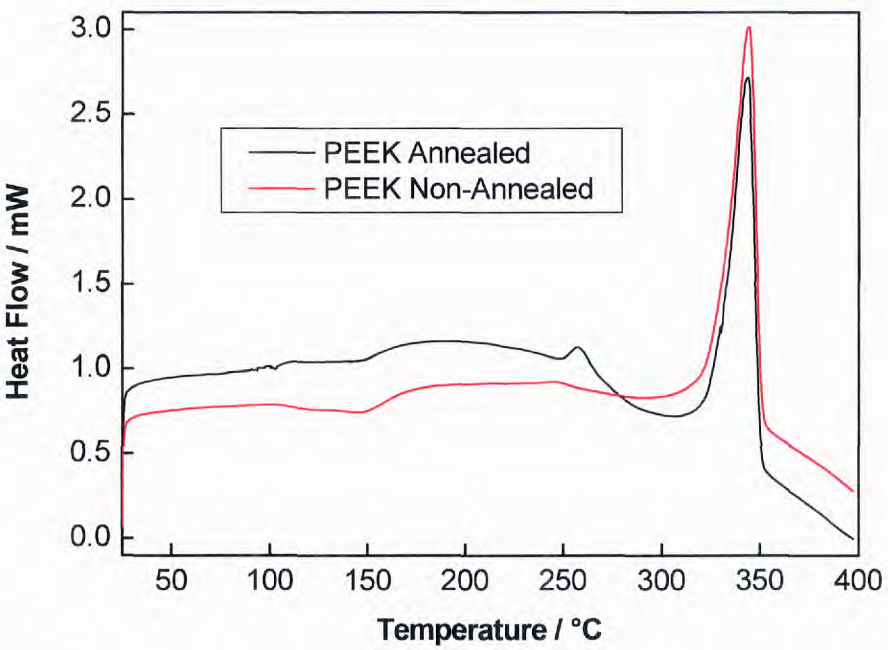

Figure 82: DSC curves of annealed and non-annealed PEEK

Figure 82 shows the DSC curves of PEEK for both non-annealed and annealed materials. It can be seen that the high and narrow shape of the melting peaks was not modified throughout the annealing process and only the presence of an additional annealing peak at a temperature of 256 °C was seen. This further supports the suggestion that the annealing of all nanocomposites enhances spherulite growth independently of the presence of CNTs within the matrix.

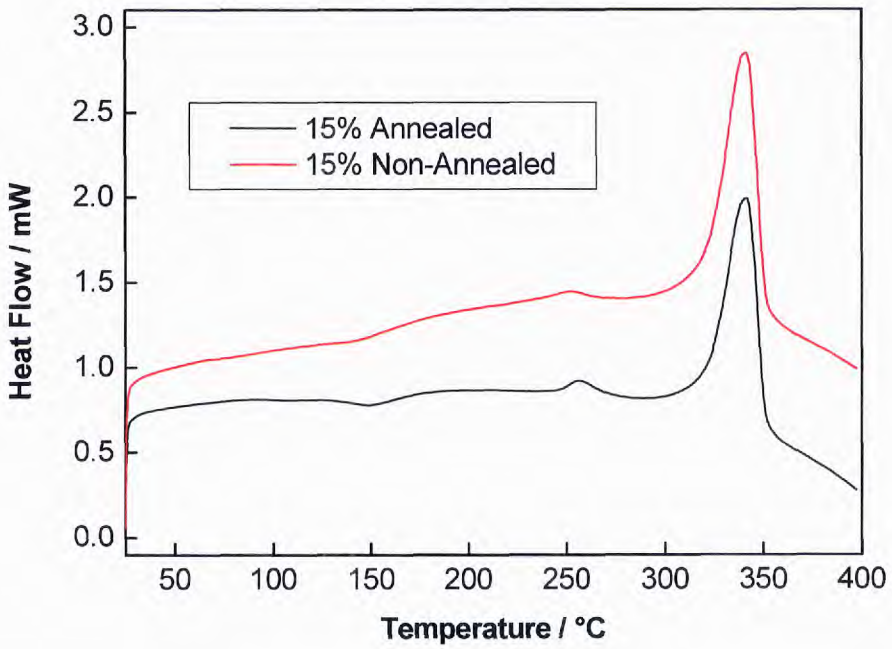

Figure 83: DSC curves of annealed and non-annealed PEEK nanocomposites with 15 wt% CNT loading fraction

DSC curves of non-annealed and annealed 15 % CNT weight fraction are shown in Figure 83. As with the PEEK DSC curves above, the shape of the melting peak for both materials was not modified upon annealing with a broad shape starting from 310 °C. Even though the annealing peak was present for both materials, it was much more pronounced for the annealed sample. This shows that the spherulite growth was not obstructed by the presence of CNTs.

The annealing process used throughout this study promoted spherulite growth within nanocomposites compared to as-produced materials made from the injection moulding process. The overall degree of crystallinity was measured by fitting each DSC curve with a baseline using the analytical software from the DSC machine and fitting all peaks including the annealing peak (Figure 84).

No evidence is shown of spherulite growth or sizes, trials were performed to do chemical etching of the nanocomposites to characterise the spherulites using microscopy but it was not possible to successfully etch the specimens.

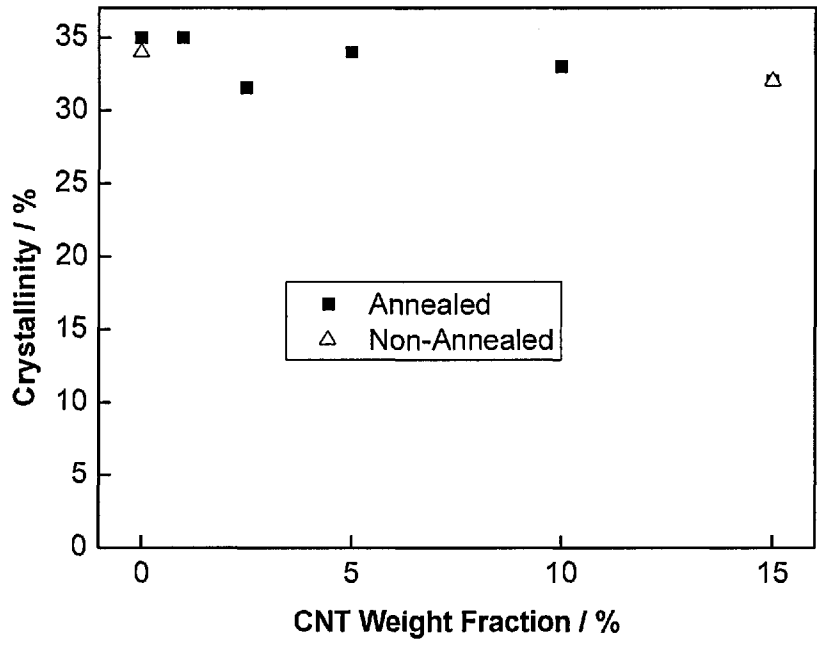

Figure 84: Degree of crystallinity of the nanocomposites as a function of CNT loading fraction

The degree of crystallinity decreased slightly with increasing CNT weight fraction for both non-annealed and annealed materials from 35 % for PEEK down to 32 % for 15 wt% CNTs. Given that the degree of crystallinity variation was minimal,

therefore, no conclusions should be drawn based on the weight fraction loading of CNTs and the crystallinity of PEEK.

The annealing process should promote mechanical properties for all nanocomposites including PEEK. Furthermore the separation of the nucleation effect of CNT on PEEK from the reinforcement effect of CNT on PEEK can be investigated further in the following sections with the evaluation of bulk mechanical properties of these nanocomposites.

4.3.3.3 Tensile properties of CNT/PEEK nanocomposites

Tensile is one of the main mechanical property investigated by the research community studying nanocomposites as it is a well established testing method. Bulk tensile properties were investigated using the ASTM D638 standard, a dog bone shape specimen for which a valid failure should occur within the specified specimen gauge length. An extensometer was also used for accurate measurements of the Young's modulus without having to take into account the machine compliance. The yield stress was determined along with the tensile strain and the Young's modulus.

Values presented throughout this section for pure PEEK (annealed and non-annealed) are for yield strain, for all other materials strain at failure is shown due to the loss of matrix ductility with the addition of CNTs.

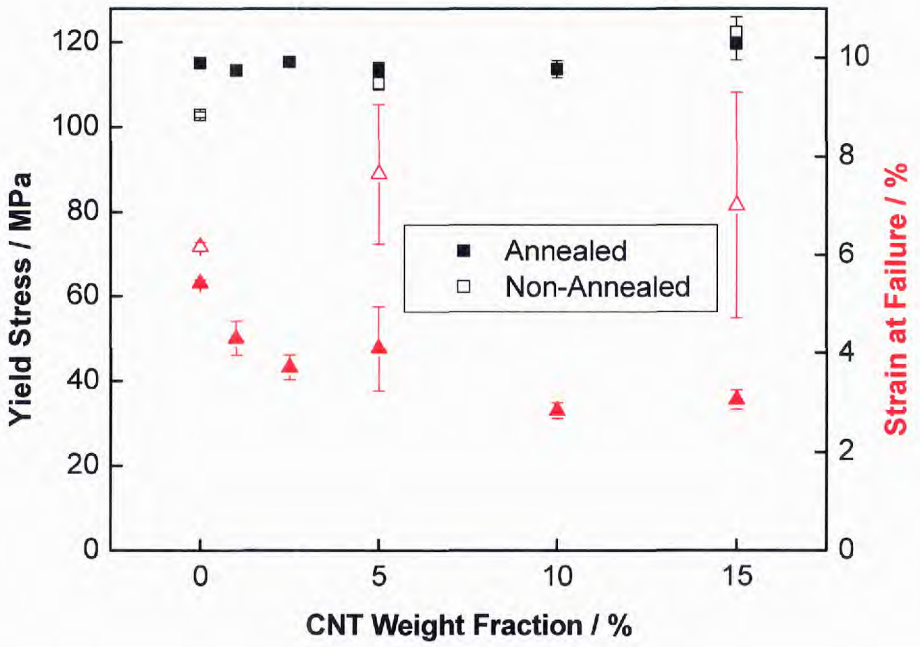

Figure 85: Yield stress and strain at failure of the nanocomposites as a function of CNT loading fraction

Nanocomposite yield stress and tensile strain are shown on Figure 85 for both annealed and non-annealed materials. Non-annealed nanocomposites 0, 5 and 15 % CNT weight fractions show an increase in yield stress with values of 103, 110 and 122 MPa respectively. This corresponded to a linear improvement in yield stress. Tensile strain at failure showed a constant value of around 6-7 % whilst higher scatter in the data was seen with increasing CNT weight fraction. The increased in scatter could indicate regions of varying crystallinity at the fracture plane as it tends to be located at the weakest site in the material and could indicate differences in the ductility of the matrix. This argument is credible because the specimens were non-annealed and variations produced from their manufacturing processes such as during extrusion or injection moulding could cause such discrepancies.

Annealed nanocomposites did not exhibit any improvement in yield stress with increasing CNT weight fraction. Yield stress for nanocomposites from 0 up to 10 % loading fraction are in the region of 113 to 115 MPa, with the exception of 15 wt% CNT having a value of 119 MPa but its scatter increased accordingly. Such small improvement should be considered as non-significant as no trend could be observed. The tensile strain of annealed specimens decreased with increasing CNT weight fraction, a sharp decrease is seen from 0 to 1% with a loss of matrix ductility. All CNTs specimens underwent a brittle fracture compared to the PEEK specimens which showed plastic deformation with necking and drawing of the polymer prior to failure.

In conclusion, the increase in tensile strength of nanocomposites based on CNTs and PEEK is due to an increase in crystallinity from the annealing process and not from any reinforcing effect of the CNTs. In this case the CNTs acted as a nucleating agent.

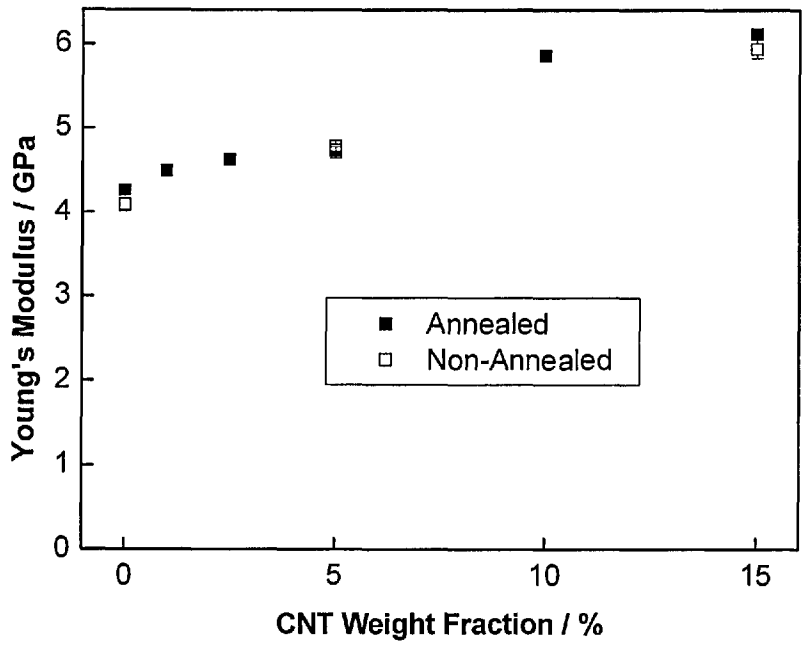

Figure 86: Young's modulus of the nanocomposites as a function of CNT loading fraction

The Young's modulus measured during tensile testing is shown above (Figure 86) for both non-annealed and annealed nanocomposites. No differences can be seen from the annealing process on the Young's modulus for all CNT weight fractions. A linear increase is shown from 4.2 GPa to 6.2 GPa, giving an improvement in Young's modulus by 48 %. This follows a rule of mixtures since it is stated when a matrix and a reinforcement are blended together to obtain a composite, then the modulus of individual components are combined together based on the loading fraction. Given the superior Young's modulus of CNTs, even a low loading fraction would compensate for the decrease in volume fraction of the PEEK matrix and hence an overall increase in the Young's modulus.

4.3.3.4 Compressive properties of CNT/PEEK nanocomposites

Compressive mechanical properties are important for the matrix of any composite materials, indeed for composite materials the matrix governs the compression and shear properties. Little information can be found on compression properties of nanocomposites as the research community has mainly focused on tensile testing. Compression testing was performed following ASTM D695 [154], an anti-buckling device was used to prevent buckling and provide support to the specimen. It is worth noting that the specimen was only supported across its thickness and not its width. Compressive strength at break could not be determined as all the specimens did not fracture but buckled across the width of individual specimen as it was not supported in this direction within the jig. Instead the compressive offset yield stress at 0.2 % was used for evaluation purposes of the compressive properties of the nanocomposite materials. The Young's modulus was determined taking into account the compliance of the machine.

Nanocomposite compressive offset yield stress at 0.2 % is shown in Figure 87 for non-annealed and annealed specimens. It can be seen that the compressive strength for non-annealed materials exhibited a decrease from 90 MPa to 83 MPa for PEEK and 15 wt% CNT respectively. For annealed nanocomposite materials, the compressive strength linearly decreased with increasing CNT weight fraction from 108 MPa down to 93 MPa for PEEK and 15 wt% respectively. Although the crystallinity of the matrix was enhanced by annealing the samples, the compressive yield properties were not governed by the matrix brittleness as seen in tensile properties. This is because compressive yield is not comparable to compression strength as compressive yield also takes into account ongoing plastic deformation. Therefore one could assume that the results shown reflect on a decrease in plastic deformation of the nanocomposites.

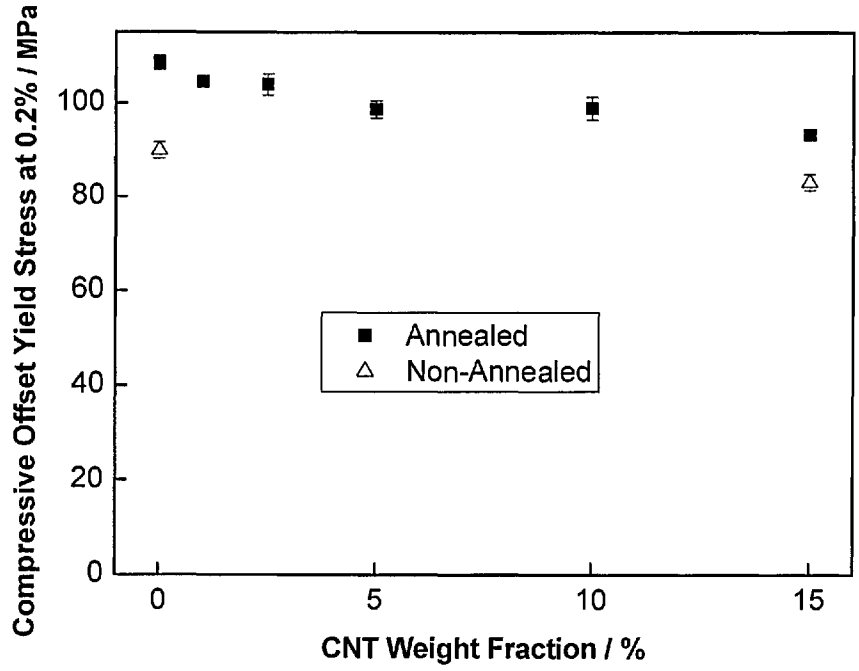

Figure 87: Compressive offset yield stress at 0.2 % of the nanocomposites as a function of CNT loading fraction

Nanocomposites Young's modulus as determined by compressive testing is shown on Figure 88 for both non-annealed and annealed materials. The Young's modulus for non-annealed nanocomposites increased with increasing CNT weight fraction with values of 2.85 GPa and 4.07 GPa for PEEK and 15 wt% CNT respectively. The large scatter represented possible variation in the crystalline regions within the specimens. Nanocomposite Young's modulii for annealed CNT weight fraction showed an increase with increasing CNT weight fraction with values of 3.06 GPa to 4.82 GPa, giving an improvement in Young's modulus by 58 %. These results indicate that the increase in compression modulus is highly governed by the degree of crystallinity within the composite, as highlighted in this annealing study. The enhancement in compressive modulus by the incorporation of CNTs (at 15 wt% loading) into the matrix is only secondary.

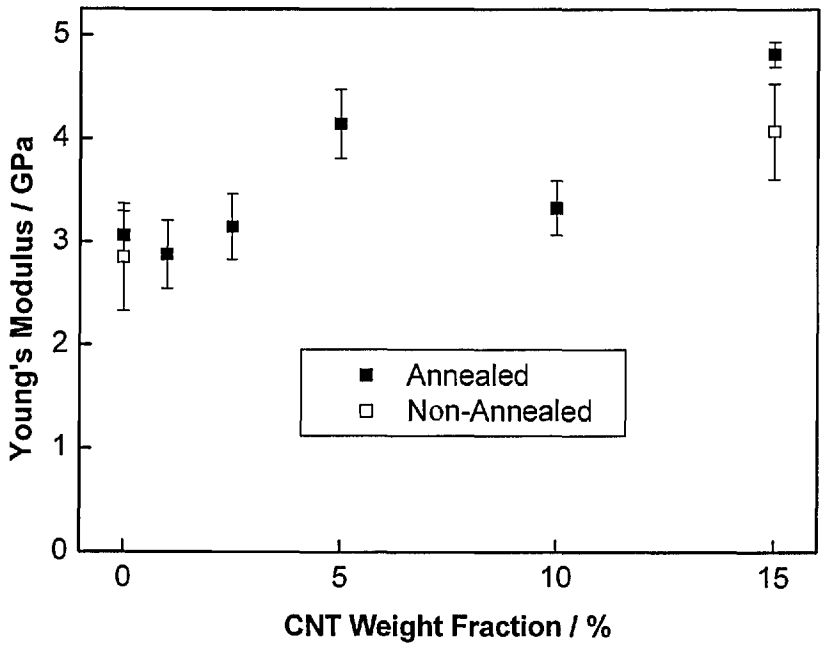

Figure 88: Compression modulus of the nanocomposites as a function of CNT loading fraction

4.3.3.5 Flexural properties of CNT/PEEK nanocomposites

Flexural testing is of importance for mechanical design purposes in industry as it shows the bending characteristics of materials, which is a common loading condition associated with components and structures. As mentioned for compressive testing, flexural properties of nanocomposites are not commonly measured within the research community. Flexural properties were determined according to ASTM D790 in 3 point bending with a span to thickness ratio of 16. Flexural strength was measured, it is stated in the standard that it is only valid for strains up to 5 %, all CNTs containing materials showed a brittle failure before 5 % strain was obtained, PEEK showed plastic deformation during testing, hence the strength value measured at 5 % strain was used. The flexural modulus was also determined for the interval 0.05-0.25 % flexural strain.

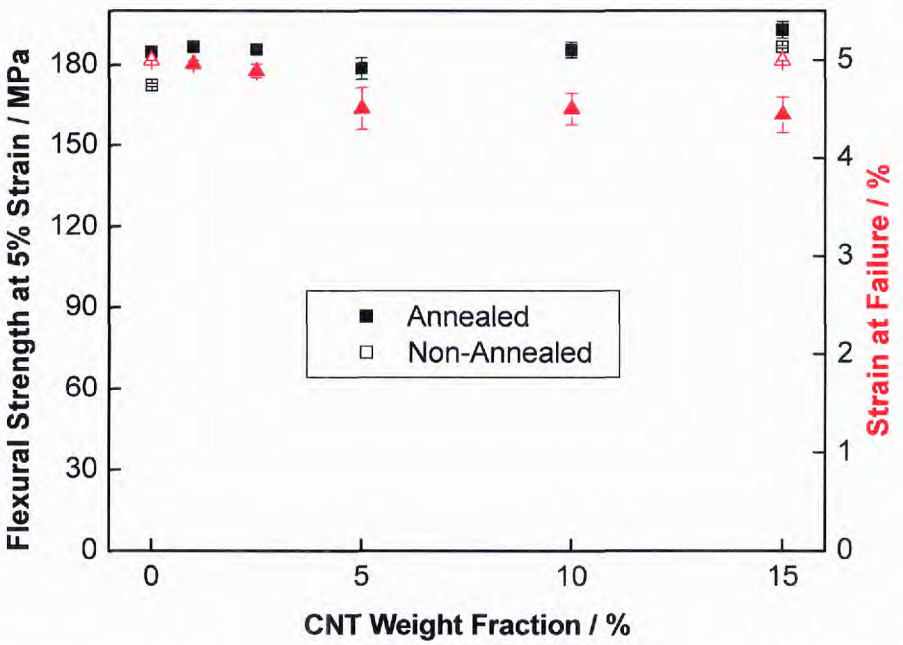

Figure 89: Flexural strength and strain at failure of the nanocomposites as a function of CNT loading fraction

Failure within 5 % strain was not observed for non-annealed materials and annealed PEEK, as stated in the standard, therefore the test was stopped when 5 % strain was reached for these materials. Flexural strength at 5 % strain and flexural elongation are shown in Figure 89 for both non-annealed and annealed nanocomposites. Non-annealed nanocomposites show an increase in flexural strength from PEEK to 15 wt% CNT with values of 172 MPa and 187 MPa respectively. Annealed nanocomposites show a very slight increase in flexural strength with increasing CNT weight fraction from 185 MPa up to 193 MPa for PEEK and 15 wt% CNT respectively, with the exception of 5 wt% CNT. The flexural strain for nanocomposites failing before 5 % strain was reached, shows a decrease in strain to failure with increasing CNT weight fraction from 4.96 % down to 4.45 % exhibiting a loss in matrix ductility. The findings from the flexural testing show that the increase in flexural strength is governed by the annealing process and most probably by the spherulite sizes. The enhancement in flexural strength by the incorporation of CNTs (at 15 % weight fraction loading) into the matrix is once again only secondary.

The nanocomposite flexural modulus results are shown on Figure 90 for both non-annealed and annealed materials. No differences can be seen among non-annealed and annealed nanocomposites with increasing CNT weight fraction. The flexural modulus shows an increase by 38% with the addition of 15wt% CNT compared to PEEK with an increase from 3.95 GPa up to 5.45 GPa. Therefore in this case the increase in flexural modulus is only governed by the incorporation of CNTs and not the degree of crystallinity within the specimens.

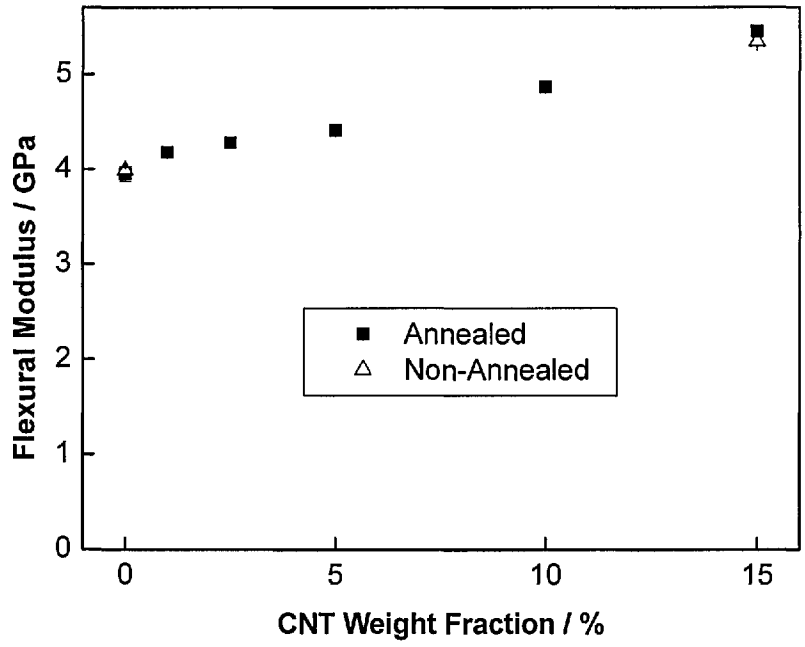

Figure 90: Flexural modulus of the nanocomposites as a function of CNT loading fraction

4.3.3.6 In-Plane shear properties of CNT/PEEK nanocomposites

In-plane shear mechanical testing of plastics is used in this work to evaluate the adhesion between the reinforcement and the matrix of the composite as well as for example new sizing technology for the composite industry. In-plane shear testing was determined following the ASTM D3846[156] standard for reinforced plastic materials which uses a double-notch rectangular bar that generates shear within the plane of the two notches located halfway through the specimen thickness on opposite sides (Figure 34). The specimens were loaded in compression within the same anti-buckling device used for compression testing.

Nanocomposites exhibited plastic deformation and no failure occurred in shear during the testing, therefore the shear strength (offset yield 0.2 %) was used to evaluate the in-plane shear strength for all materials. In-plane shear testing was not

performed on non-annealed materials as the amount of available compounded materials was limited, therefore only annealed materials were examined.

The shear strength data (Figure 91) shows an initial value of 44 MPa for PEEK. The in-plane shear strength increases to 48 MPa with 1 wt% CNT and subsequently decreases with increasing CNT weight fraction up to 15 wt%, where the value has dropped to 45 MPa. A minor improvement by 9 % of the in-plane shear strength was observed with the addition of 1 wt% CNT but this receded with increasing CNT weight fraction down to 2 %.

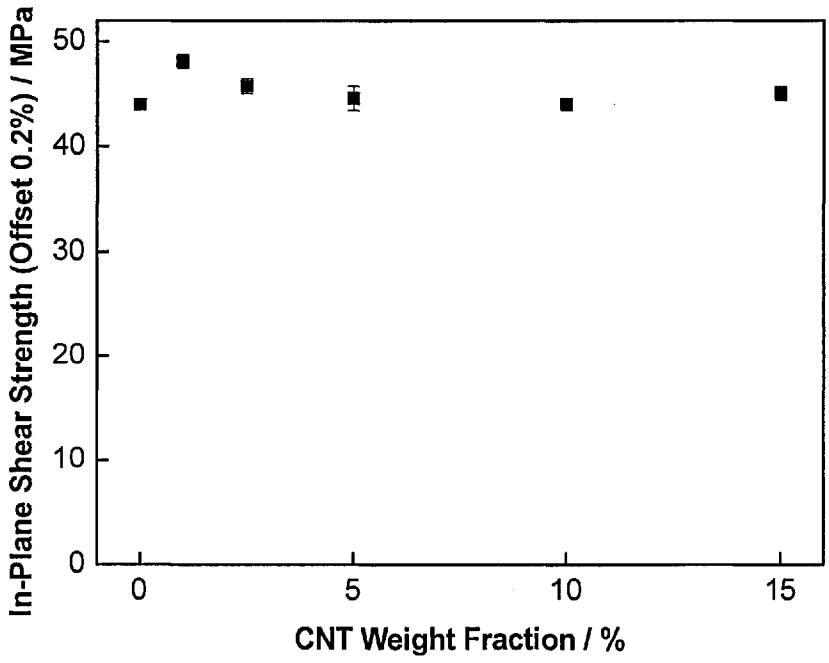

Figure 91: In-plane shear strength of the nanocomposites as a function of CNT loading fraction

Even though the ASTM standard is specified for reinforced plastics, the specimens did not undergo any fracture in shear along the opposite notches but instead only excessive plastic deformation was observed. It is believed that the standard refers to

reinforced thermoset composites and not thermoplastic reinforced composites. Therefore it is challenging to measure the in-plane shear properties for thermoplastics as plastic deformation will almost certainly be the major failure mechanism and, therefore, puts the validation of this test into doubt. Nevertheless, the influence of low % of CNTs loading into PEEK led to enhanced in-plane shear strength (offset 0.2 %) and may well be beneficial for design consideration purposes.

4.4 Validation of the continuous aqueous powder slurry based thermoplastic composite production line

4.4.1 Influence of powder impregnation bath concentration on composite tape quality

The polymer powder (as received PEEK) concentration in the impregnation bath needed to be optimised to manufacture unidirectional carbon fibre reinforced PEEK composite tapes with consistent fibre volume content of 60 %. Figure 92 shows the fibre volume content of as produced carbon fibre reinforced PEEK composite tapes, using the commercial Vicote 804 PEEK suspension, as a function of bath concentration. The required bath concentration to produce a consistent CF/PEEK tape with a V_f of 60 % over 2 h of manufacturing time was identified to be 8 wt%. However, it is worth noting that this bath concentration was determined using the as received commercially available grade PEEK suspension whose particle size d50 was 10 μm, whereas the CNT/PEEK nanocomposite powder had a particle size d50 of ~50 μm.

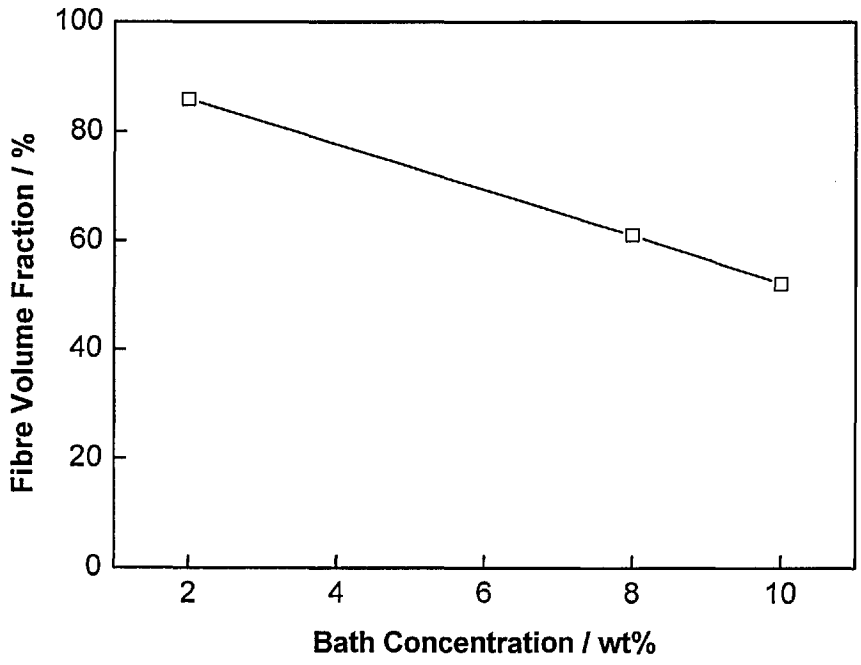

Figure 92: Fibre volume content of the produced CF/PEEK tape as a function of PEEK Vicote 804 concentration in the impregnation bath

The particle size distributions of the PEEK powder are shown in Figure 93. The average particle size of the PEEK-150 was slightly larger than that of the Vicote 804 and the average particle size of the CNT/PEEK nanocomposite powder can be found in Section 4.5. The mass balance calculation (see Experimental Section) showed that the required PEEK powder concentration in the impregnation bath should be maintained at 8 wt% for a PEEK powder with a d_{50} of 10 μm. However, the bath concentration for the larger PEEK powders should be much lower.

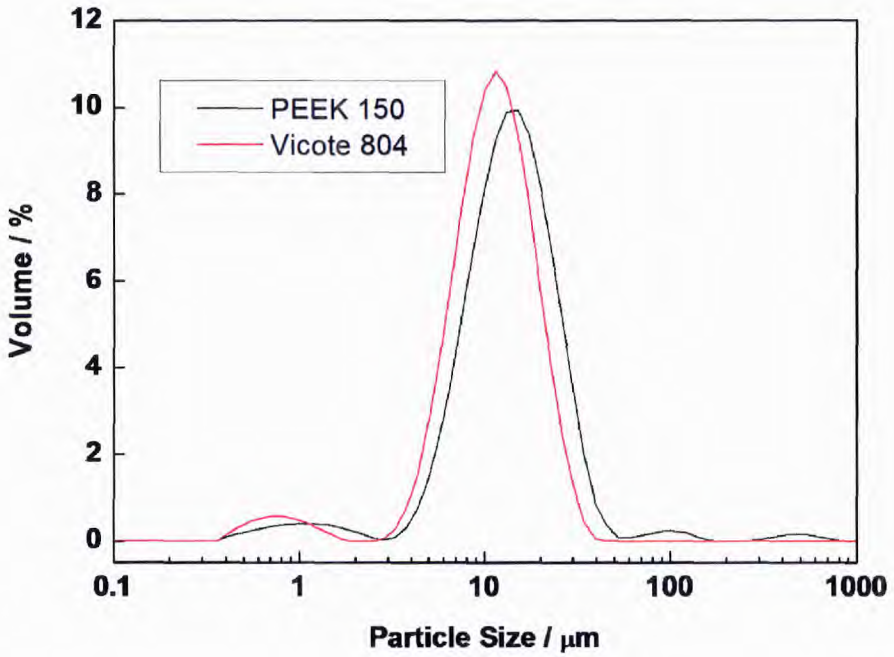

Figure 93: Particle size distribution of as-received PEEK 150 powder and PEEK powder suspended in Vicote 804

4.4.2 Mechanical properties of carbon fibre/PEEK composites

The bond strength between reinforcing fibres and the surrounding PEEK matrix was inferred from macromechanical tests [177]. The aim of this particular study was to compare the quality of the in-house manufactured CF/PEEK composites made from two different forms of PEEK with commercially available CF/PEEK APC-2 tapes. The following PEEK grades and CF/PEEK composites were studied:

a) PEEK in powder form (PEEK-150)

b) PEEK in a pre-dispersed solution already containing surfactant and defoamer (Vicote 804)

c) Commercially available APC-2

4.4.3 Influence of the fibres/matrix type on flexural properties of carbon fibre reinforced PEEK

Flexural testing is one of the simplest tests to perform, to determine the flexural modulus and flexural strength and is mainly governed by the fibre/matrix properties. Generally, these tests are used for qualitative assessment during the material selection process rather than for determination of absolute engineering values. This is mainly because of the simplicity of this test, which means that there is a wide range of standard methods in use throughout the industry. Most test methods available apply to homogenous solids but a few tests have been developed to test high performance fibre reinforced composites. Of the methods that fall into the latter category, the ASTM standard D7264-07 [158] for flexural properties of polymer matrix composite materials was strictly followed during this study using a span to thickness ratio of 32.

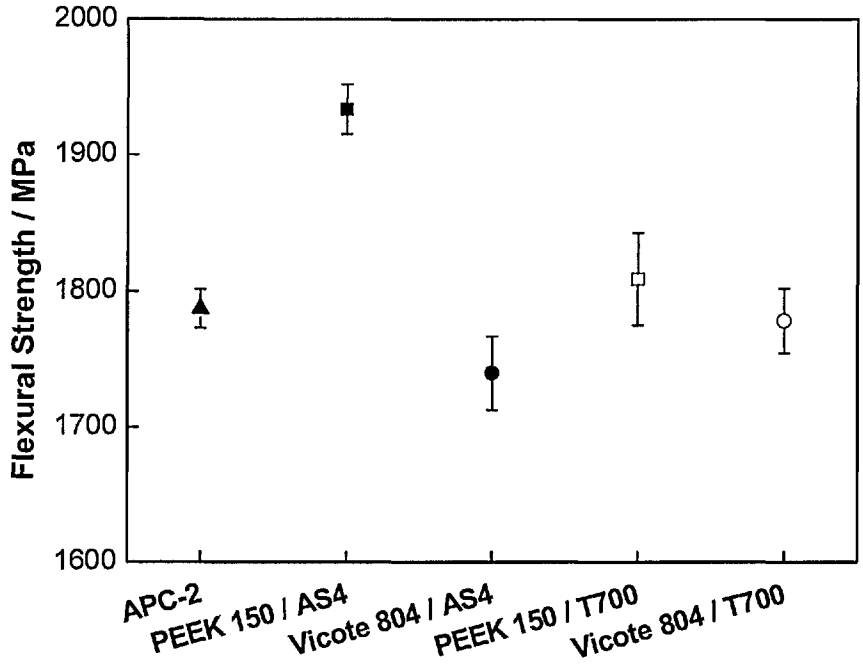

Figure 94: Flexural strength of the laminated CF/PEEK composites manufactured using various PEEK grades and carbon fibres

The flexural strength of the commercially available APC-2 PEEK composites which contain AS4 carbon fibres was 1780 MPa (Figure 94). The flexural strength of the in-house manufactured CF/PEEK composites also containing AS4 carbon fibres was about 10 % higher. The reason for the higher flexural strength of the in-house CF/PEEK is probably the fact that APC-2 still contains appreciable amounts of DPS [59] (which have been quantified by Bismarck et al. [178]). The Cytec process is a melt impregnation process; PEEK is melted in DPS, which is a good solvent for PEEK but also acts as plasticizer for PEEK. One can therefore expect that the presence of DPS impacts upon the mechanical properties of CF/PEEK. Moreover, the PEEK grade used to manufacture APC-2 is a well-guarded secret of the manufacturer Cytec, but it can be assumed that it is a low melt viscosity grade. The fibre (mis)alignment of the laminated CF/PEEK tapes, caused by the different melt viscosity of the matrix during compression moulding at conditions optimised for the in-house CF/PEEK tape, is also a factor influencing the mechanical properties of the final composites.

The in-house manufactured CF/PEEK-150 composites containing T700 carbon fibres have a flexural strength of 1800 MPa, which is lower than that of the PEEK-150/AS4 composites (Figure 94). The lower flexural strength could be caused by a lower bond strength between the T700 fibres and the matrix. These results suggested that the bond strength between AS4 fibres and PEEK-150 is higher than that of T700 fibres and PEEK-150. The surface chemistry of the two carbon fibres is very different; AS4 carbon fibres have a surface oxygen content, as determined by XPS, of 7 at.% [179] whereas T700 carbon fibres contain 18 at.% surface oxygen [180]. Also, please note that T700 is commercially only available with an epoxy sizing. This however, could be

partially degraded during the production of composite tape as PEEK is processed at 390 °C. The (partially) degraded epoxy sizing on the carbon fibres could possibly act as weak boundary layer [181] at the fibre/matrix interface. Moreover, the different interaction between the different carbon fibres and the PEEK-150 matrix cannot be explained by mechanical interlocking as both fibres have relatively similar BET surface areas of around 0.35 m^2/g [180, 182].

The flexural strength of AS4/Vicote 804 and T700/Vicote 804 composites remained constant at around 1770 MPa (Figure 94). The reason for this is that the Vicote 804 PEEK suspension already contained the defoamer, which is ethanol, and a surfactant. Ethanol is not only a very efficient defoamer but at the same time it also helps to, at least, partially desize the fibres [183]. Therefore the amount of sizing of the T700 carbon fibres impregnated with PEEK from Vicote 804 is expected to be lower than that of the T700 carbon fibres impregnated directly with a PEEK-150 suspension. Therefore, using Vicote 804 PEEK suspension for the impregnation of carbon fibres reduces the impact of the epoxy sizing on the fibre matrix interface. In general the composite manufactured using the Vicote 804 PEEK matrix has a lower flexural strength, but the differences are marginal.

A representative SEM micrograph of a Vicote 804 PEEK/T700 composite (Figure 95) demonstrated that the CF/PEEK composites generally failed in compression on the upper surface of the test specimen.

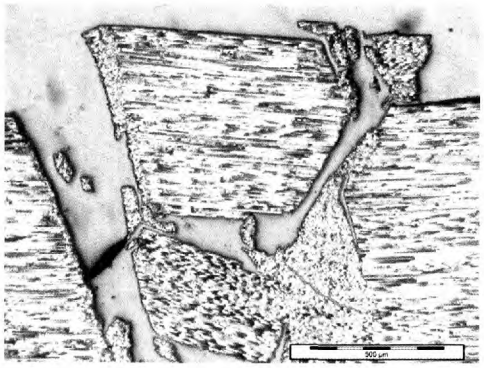

Figure 95: Fractured upper surface (below loading pin) of Vicote 804/T700 flexural test specimen

The flexural modulus of all investigated CF/PEEK composite tape laminates was the same (Figure 96). Flexural modulus is not dominated by the interface properties. Given that the matrices of the CF/PEEK composites were not modified (except for maybe the higher amount of DPS in APC-2), i.e. reinforced by CNTs which will be discussed later on in the thesis, the results obtained are those one would expect.

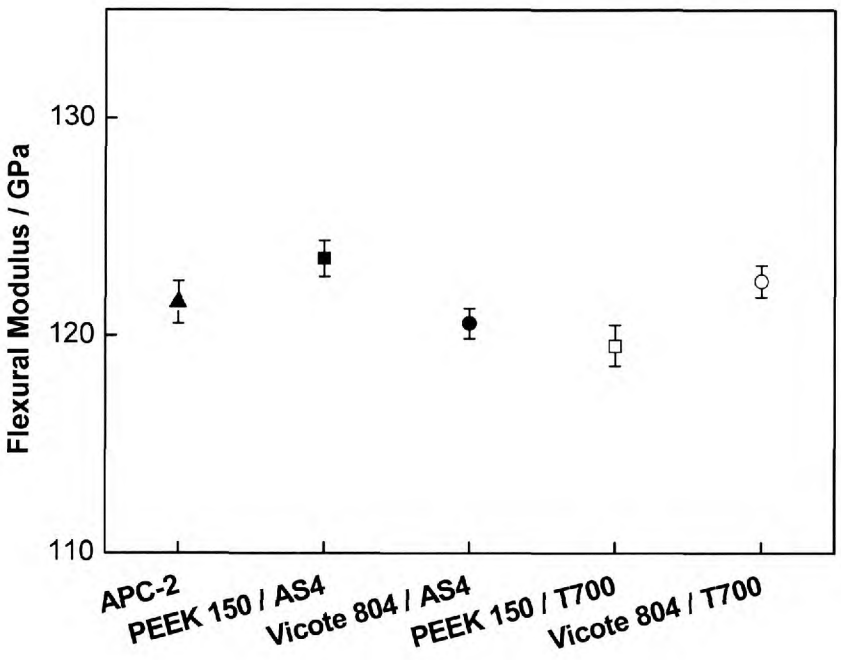

Figure 96: Flexural modulus of the laminated CF/PEEK composite tapes manufactured using various PEEK grades and carbon fibres

4.4.4 Influence of PEEK grade on the short beam shear properties of carbon fibre reinforced PEEK

The short beam shear test is a 3-point bending test with a small span-to-thickness ratio to induce shear. The specimen geometry is designed to reduce tensile and compression flexural stresses and to maximise and induce through-thickness shear stresses in the test specimen. The short beam test is not an ideal shear strength test; the stresses induced are not pure shear because it is not possible to eliminate flexural stresses completely. This has been reflected in the most recent edition for the ASTM testing standard D2344[159], in which the test method was renamed the 'Short Beam Strength test' replacing the previous title 'Short Beam Shear test'. In regions away from the loading and support points, the shear stress induced in the specimen theoretically varies parabolically from zero on the specimen top and bottom surfaces, to a maximum value in the specimen mid-plane. Correspondingly, the flexural tensile and compressive stresses are at a maximum on the specimen top and bottom surface, varying linearly to zero at the mid-plane. Therefore, the undesired stress fields reduce to zero where the desired shear stress field is a maximum. However, this is an ideal picture and because the test specimen is so short, the entire stress field throughout the test piece is significantly affected by the local forces acting at the loading and support points. With these aforementioned points in mind, it is still true that a region of high shear stress exists along the mid-plane of the test piece and it is this stress which results in the failure of the tested specimens.

A typical force-displacement curve obtained during short beam shear testing of a unidirectional carbon fibre reinforced PEEK composite is shown below (Figure 97).

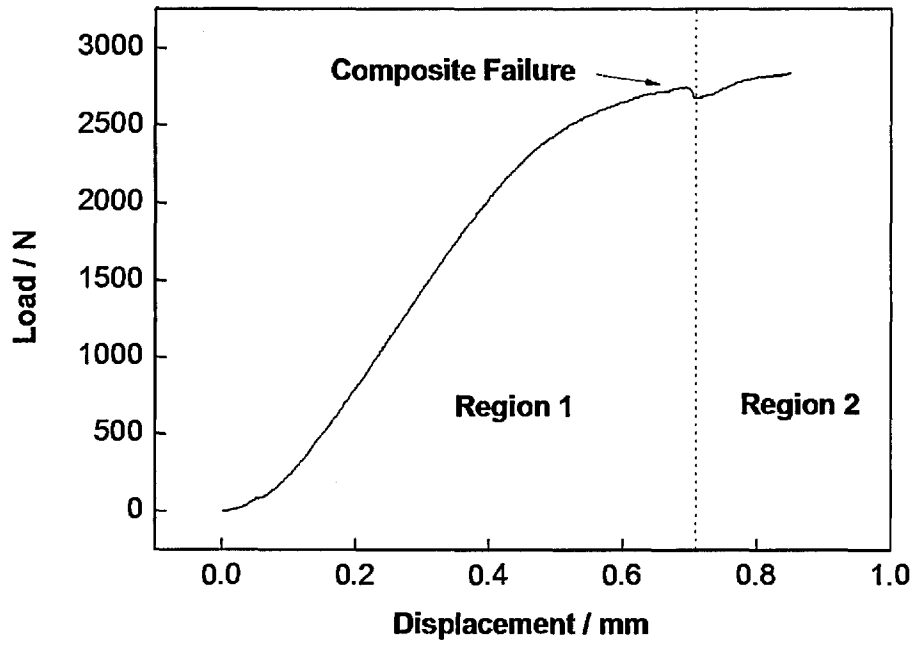

Figure 97: Typical load-displacement curve obtained from a short beam shear of a CF/PEEK composite

In Region 1 of the force-displacement curve the three point bending load increases as a function of displacement until compressive failure of the upper surface occurs under the loading pin (as shown in Figure 97). In accordance with the standard, the load before failure was used for the calculations of the short beam shear strength. When the specimen was subjected to a steady state load, the load is transferred from the matrix to the fibres via the interface and is in this case directly related to the shear stress causing interfacial failure. The force as function of displacement further increases in Region 2. In this region the composite undergoes plastic deformation while the crosshead is crushing the test piece inside the test jig.

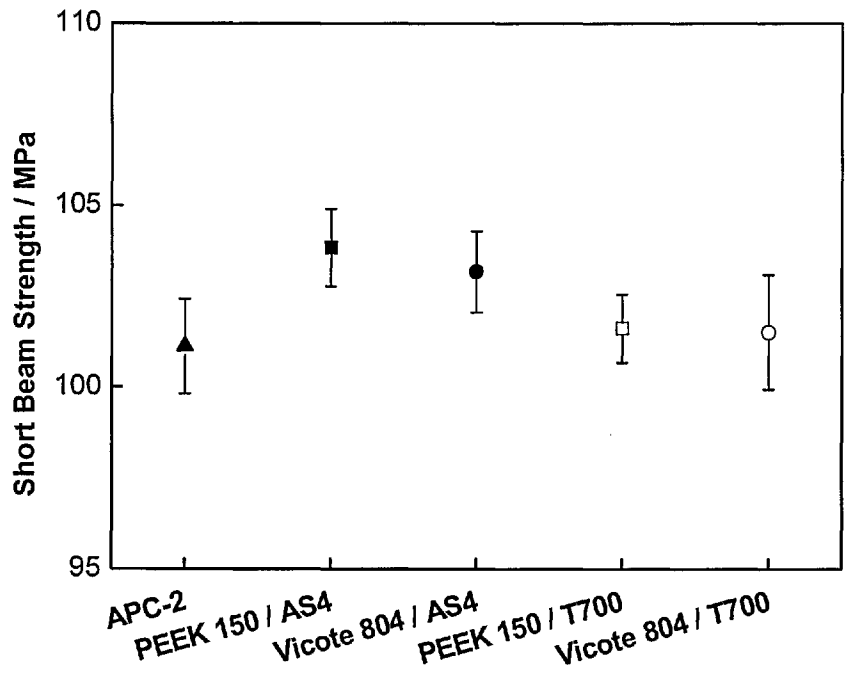

Figure 98: Apparent short beam shear strength of the laminated CF/PEEK tape composites manufactured from various PEEK grades and CFs

The T700/PEEK composites (independent of the PEEK grade used) have about the same SBS strength than the commercially available APC-2 composites but both have a significantly lower SBS strength than the AS4/PEEK composites (Figure 98). The interface dominated short beam shear strength, measured by the SBS test, showed once more (Section 4.2) that the AS4/PEEK composites (irrespectively of the PEEK grade used) have a slightly enhanced fibre/matrix interface as compared to the T700/PEEK and APC-2 composite laminates. Again this should be largely due to the fact that the T700 fibres were industrially epoxy sized and APC-2 still contains some DPS plasticiser. In conclusion it can be said that the quality of the composites produced using out home-build modular laboratory scale composite production line is comparable if not superior to commercial grade (APC-2) composites.

Comparing micromechanical properties (single fibre pull-out test results) from Section 4.2 to macromechanical properties obtained from flexural and SBS test, the results complement well with each other (Figure 99). The T700 CF/ PEEK-150 model composites exhibited a low IFSS (25 MPa), the measured flexural and SBS strengths are also much lower than of the AS4 CF/ PEEK-150 composites. The AS4 CF/ PEEK-150 model composites with a corresponding IFSS of 70 MPa had a flexural and SBS strength of 1940 MPa and 104 MPa, respectively. It can be seen that the orders of magnitude differences in IFSS between the unsized AS4 and the sized T700 fibres are much higher in a single fibre composite model compared to the macroscale composites. The explanation for this is once again due to the sizing surface finish by the manufacturer on the parent fibres. Flexural and SBS test specimens that were continuously processed and compression moulded (see sections 3.3.5 and 3.3.8), the time at which the fibres were subjected to a temperature environment during processing is much longer than preparation of single fibre pull-out test specimens (see section 3.2.7). Given that both processing temperatures were 390 °C, above the degradation temperature of the epoxy sizing, the sizing burn off rate would be much higher in the macro-composites and resulted in more defective sites at the fibre/ matrix interface. It can be concluded that sizing on fibres influences interfacial adhesion between CFs and PEEK-150. In fact T700 carbon fibres have higher mechanical properties than AS4 carbon fibres (see Section 3.1), therefore, one would expect the mechanical properties of composites consisting of T700 fibres to be higher than that of AS4 fibres. Since the Hexcel AS4 fibres were available in unsized form whereas the Torayca T700 fibres were only available with an applied sizing, it is difficult to further consolidate such statement by studying fibres from the same manufacturer. Given that sizing is commonly designed to give better compatibility to

epoxy matrices, it is not surprising that sizing inhibits the interaction with PEEK-150 because the processing temperature of PEEK-150 is above most epoxy resins.

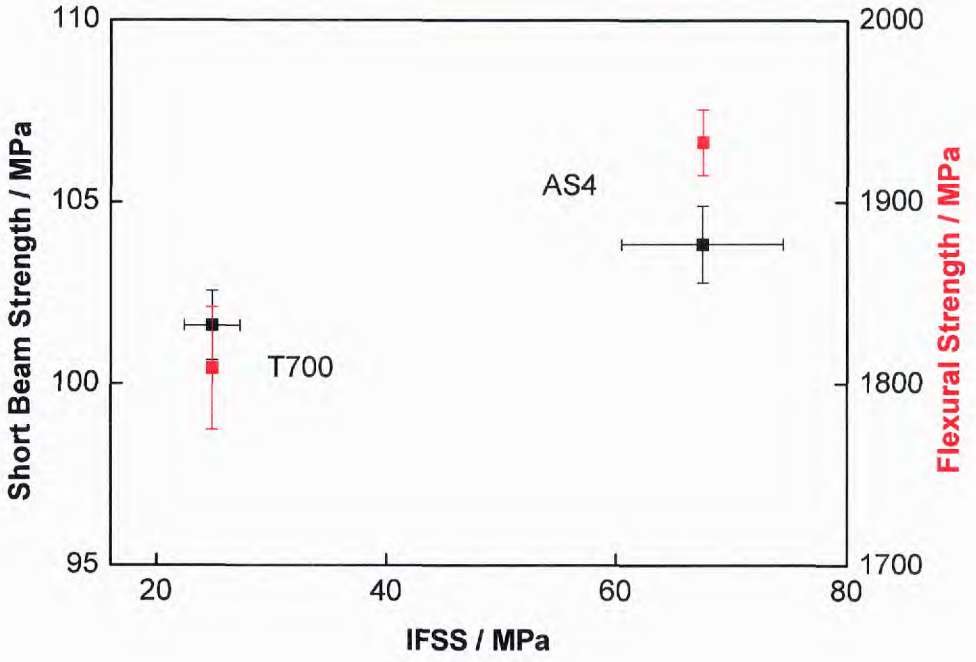

Figure 99: Short beam and flexural strength as a function of apparent interfacial shear strength

4.5 Characterisation of hierarchical fibre reinforced PEEK nanocomposites

An important feature of the powder material in the aqueous powder impregnation process during production of unidirectional carbon fibre, hierarchically-reinforced PEEK is the average and homogeneity of the particle sizes. If the particles are too small, they would drop out of the spread carbon fibre tow after exiting the impregnation bath. On the other hand if the powder is too large, it is difficult for the powder to be impregnated into the carbon fibre tow uniformly. This would then lead to powders being filtered out of the carbon fibre tow and result in some resin/ fibre rich regions.

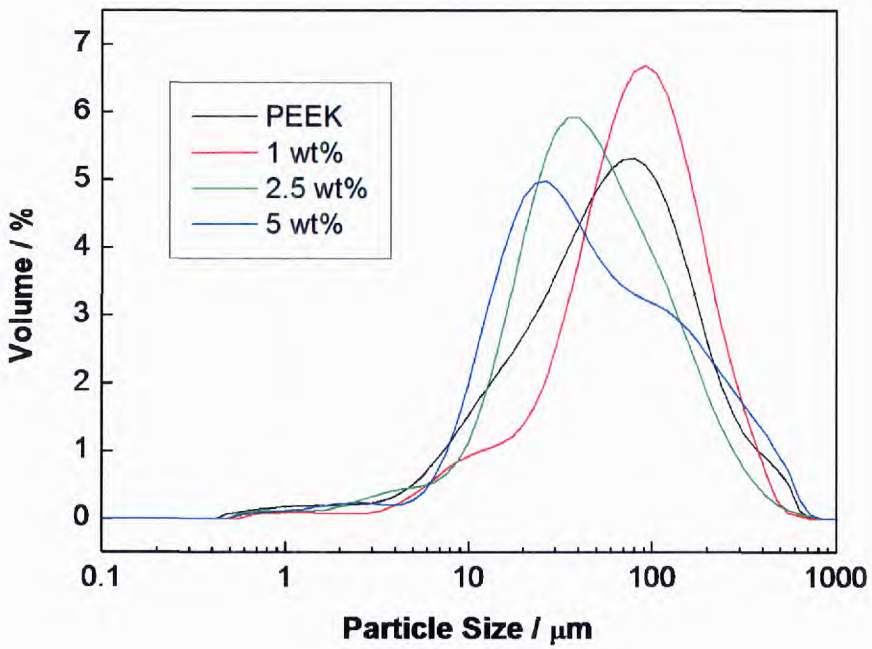

Figure 100: Particle size distribution of pure PEEK powder and CNT-reinforced PEEK powder processed using the "powder" route

The influence of different CNT loadings on the particle size distribution (PSD) of CNT reinforced PEEK powder produced using the 'powder' route (see Section 3.3.4) is presented in Figure 100: at 1 % CNT loading, the CNT reinforced PEEK powder has a d_{50} of 74.5 μm. As the CNT loading increased to 2.5%, the d_{50} decreased to 40.6 μm. The d_{50} decreased further to 38.2 μm when the CNT loading increased to 5 %. Comparing to the baseline of which the pure PEEK powder processing using the same 'powder' route, the d_{50} was 55.5 μm. What can be seen is that the PSD of the processed PEEK powder and the processed CNT reinforced PEEK powder has larger particle sizes than commercially available PEEK powder (see Section 4.4.1) where the average d_{50} is 10 μm. It is critical that if the experimental parameters as well as the results of the composites manufactured using PEEK-150 (Section 4.5) are to be compared, then the d_{50} between these starting materials should be as close as

possible. As cryogenic grinding of extruded CNT/PEEK nanocomposites to 10 μm is not possible at a laboratory scale (see Section 3.3.4), the 'powder' route would therefore be the most applicable approach at a research scale.

A series of SEM micrographs were taken to examine the morphology of the PEEK powder processed using the 'powder' route (example shown in Figure 101). No agglomeration could be observed from the images which is encouraging. The same powder morphology can be observed in Figure 102 (left) with 5 % CNTs loading in PEEK powder. Furthermore, at high magnification (Figure 102, right) it can be seen that the CNTs are not condensed on the surface of the matrix but evenly distributed into the bulk of the matrix.

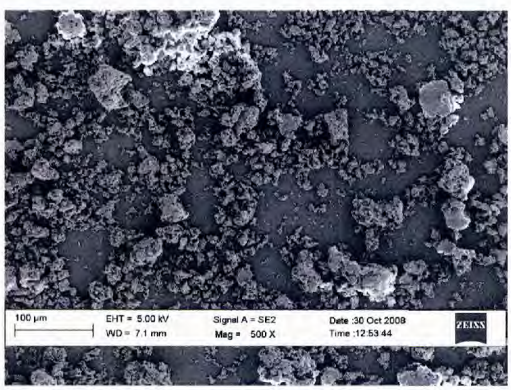

Figure 101: Representative SEM micrograph of pure PEEK powder processed via the "powder" route

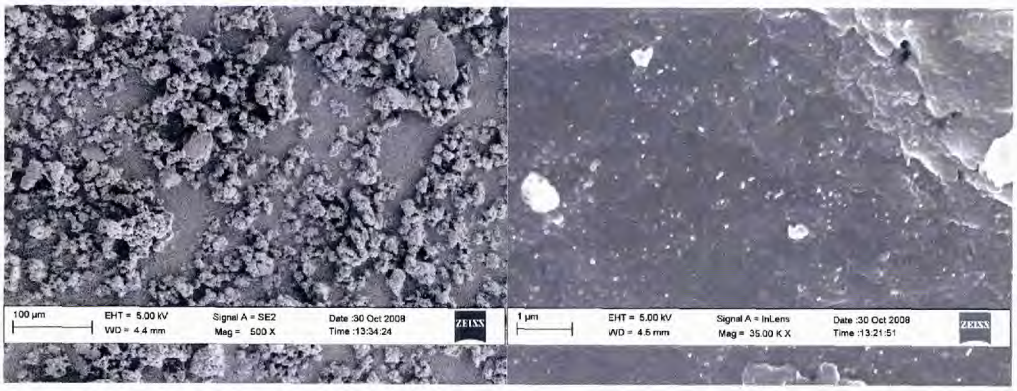

Figure 102: Representative SEM micrograph 5 % CNT loading in PEEK powder at low (left) and high magnification (right). CNTs can be seen on the right image (small white dots)

4.5.1 Influence of CNT loading on the flexural properties of the unidirectional carbon fibre, hierarchically-reinforced PEEK

As shown in Figure 103, an eight percent lower flexural strength was recorded for the in-house manufactured T700 carbon fibre reinforced PEEK as compared to commercially available APC-2.

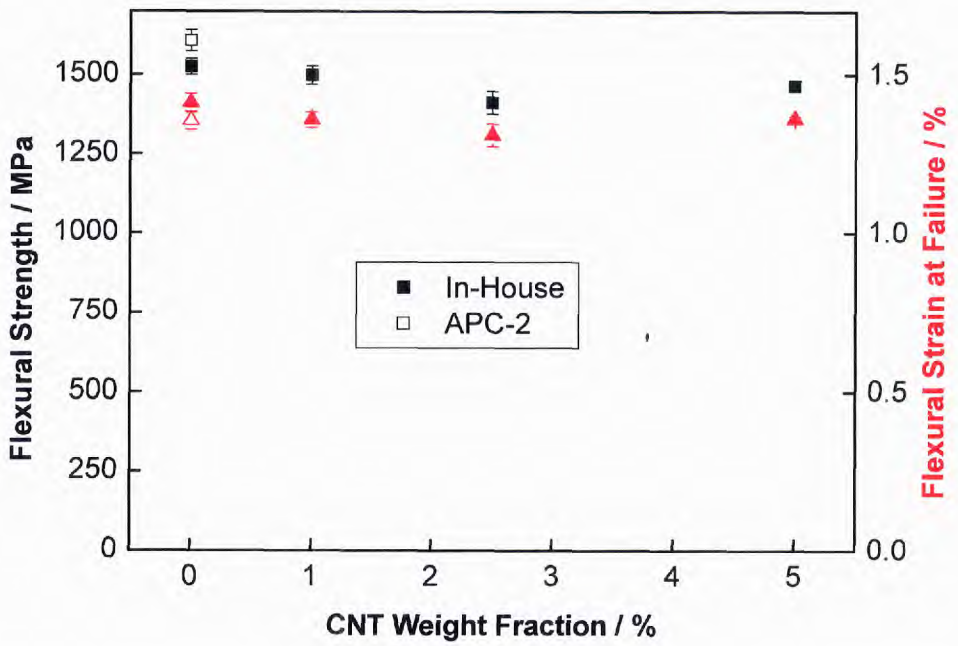

Figure 103: Flexural strength and strain at failure of APC-2 and in-house composites as a function of CNT loading fraction

Despite the consistency in sample preparation via compression moulding; the thickness of APC-2 (0.2 mm) was in fact double the thickness of the composite tape manufactured. This would mean that in order to achieve the same specimen thickness (span to thickness ratio: 32:1), as specified in the standard, the amount of manufactured composite tapes required is twice the amount of the hand cut APC-2 strips, i.e. the experimental error was higher. Certainly the grade of PEEK variations in the two samples remained. When the CNT loading in the unidirectional carbon fibre hierarchically-reinforced PEEK increased, no improvements in the interface dominated property, flexural strength, were observed. The flexural strain at failure of the set of data also exhibits the same trend, which implied that the brittleness of the tested specimens increases due to the presence of CNTs. This is a common observation and is consistent with the rheology data in section 4.3.3.1.

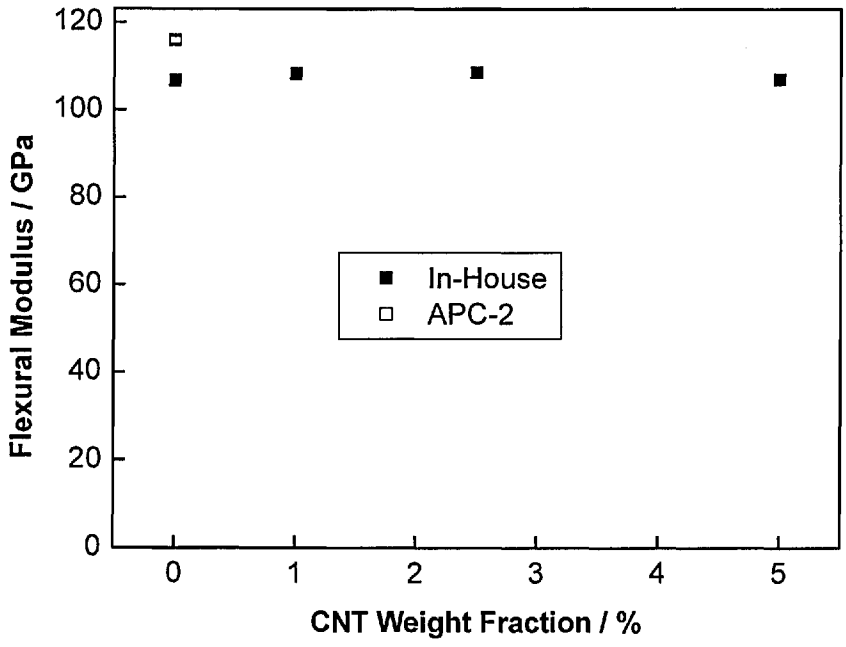

Figure 104: Flexural modulus as a function of CNT loading fraction

The measured flexural modulus of the in-house T700 carbon fibre reinforced PEEK composite tape manufactured revealed an 8 % drop as compared to the APC-2 specimens (Figure 104). The factors previously discussed regarding the amount of material required as well as the grade of PEEK polymer employed are still valid. Furthermore, the fibre volume fraction was different between the two samples. A fibre volume fraction of 60 % is present in APC-2, however the in-house manufactured T700/PEEK composite only has a fibre volume fraction of 55 %. This was targeted for a particular reason. One should not forget the aim of this research work is to modify the matrix within a fibre reinforced composite system by the incorporation of CNTs. If the matrix content in such system increases, then the effectiveness of matrix modification on the overall mechanical properties of the composite should be enlarged accordingly. Nevertheless a probable explanation for the decrease in flexural properties of the hierarchical composites is due to higher matrix viscosity as well as the wide powder size distribution which could create voids.

4.5.2 Influence of CNTs loading on the Short Beam Shear properties of the unidirectional carbon fibre, hierarchically-reinforced PEEK

The apparent short beam shear (SBS) strength test is a common analytical technique used for quality control, for example it is used in epoxy systems to examine the degree of curing.

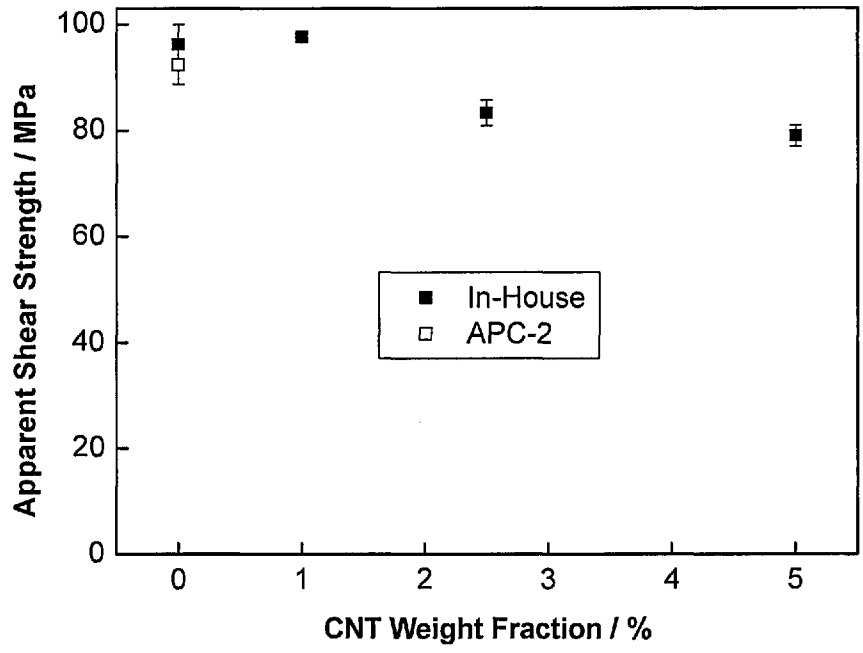

Figure 105: Short beam shear strength as a function of CNT loading fraction

It can be seen that (Figure 105) the in-house manufactured T700/PEEK composite specimens had a higher SBS strength compared to APC-2. This is because of the higher resin content in the in-house manufactured specimens. Therefore, the mid shear plane region of which the composite is subjected under load is larger and can carry more load as compared to the APC-2 specimens which have a lower resin content.

Interestingly as the CNTs loading increased, the SBS strength remained stable up to 1.25 % of CNTs loading, after which a 20 % drop in the SBS strength was observed when the CNTs loading increased to 2.5 % and 5 %. This finding would suggest that perhaps at very low CNTs loading, interface dominated properties of a hierarchical composite could be improved, but as the CNTs loading increased further then the enhancement would diminish. This should be due to a few traditional issues involved

when processing CNTs, i.e. alignment of the CNTs, arrangement of the CNTs and voids due to the higher matrix viscosity to name a few.

4.6 Summary

Characterisation results of carbon nanomaterials and mechanical properties of composite materials were analysed and discussed. Carbon nanomaterials were characterised for both their bulk and surface properties to assess their quality and potential as reinforcement for composite materials. Single fibre pull-out tests were conducted on model single carbon fibre pure PEEK matrix as well as CNT-reinforced matrices. Nanocomposites were mechanically tested for both micro- and macro-scale using conventional testing methods such as tensile, compressive, flexure and in-plane shear tests. The continuous thermoplastic composite production line was validated by comparing in-house made carbon fibre reinforced PEEK with commercially available APC-2 PEEK composites using flexural and short beam shear tests. Finally, mechanical properties of hierarchical thermoplastic composites were conducted and discussed.

Chapter 5 - Conclusions

New advanced high performance composite materials with enhanced mechanical properties have been developed during the course of this research. This was achieved by first using CNTs to reinforce a PEEK matrix, then using conventional carbon fibres to further reinforce the nano-reinforced matrix to form what we call hierarchical composites. Challenges such as selecting a suitable CNT reinforcement, achieving a good dispersion of these CNTs within the matrix, producing micrometre scale nanocomposite powders and impregnating 12k carbon fibre rovings with an extremely high viscosity nanocomposite melt were overcome.

The first step was to analyse the surface and bulk properties of 13 different carbon nanomaterials, ranging from SWCNT to CNF. Based on the results obtained, three different studies on the mechanical properties of nanocomposites were conducted. Monofilaments of CNT (with varying diameters) reinforced PEEK nanocomposites were produced using a small-scale batch process micro-extruder. The tensile strength and the Young's modulus of the monofilament CNT/PEEK nanocomposites increased by 42 % and 18 %, respectively, with 5 wt% CNTs loading. However, the elongation at break reduced by 95 %. Based on the CNT and nanocomposite characterisation, Nanocyl MWCNTs were selected as the CNT material to be used for the rest of the study as they are one of the few industrially available and affordable materials. At high loading fractions, Nanocyl MWCNTs were compounded for an extended period of time, extruded, pelletised and compression moulded into nanocomposite films. Tensile properties showed a linear increase of up to 15 % in strength with a CNT loading fraction of 15 wt%. Afterwards, it was decided to produce larger batches of nanocomposites in order to fully characterise

the bulk mechanical properties of these CNT/PEEK nanocomposites. It was found that, as expected, the melt viscosity of the PEEK increased with increasing CNT loading fraction.

The influence of annealing of nanocomposites on the mechanical properties of PEEK nanocomposites was studied. In case of the non-annealed PEEK nanocomposites the tensile strength increased by 20 % with CNT loading fraction of 15 wt%, whilst for annealed samples the CNT incorporation resulted on in an improvement of 8 %. Furthermore, flexural tests were performed and the flexural strength increased by 9 % and 4 % for non-annealed and annealed nanocomposites with 15 wt% CNT loading, respectively. However, the flexural modulus improved independently of the annealing process by 38 % upon CNT incorporation. Hence the incorporation of CNT into PEEK allows for a modest improvement of the mechanical properties of PEEK. It should also be noted that not only are the diameter, quality, loading and dispersion of the CNTs important but also the control of the PEEK matrix crystallinity.

Secondly, a modular lab-scale aqueous powder slurry impregnation line for the production of thin, flexible continuous unidirectional fibre reinforced thermoplastic polymer tapes was successfully designed, constructed (in cooperation with Dr K.K.C. Ho and Dr M.Q.B. Tran) and validated. In order to validate this piece of home-built apparatus, unsized AS4 and sized T700 carbon fibre reinforced PEEK-150 tapes with a fibre volume fraction of $V_f = 60$ % were manufactured and were compared against a commercially available CF/PEEK composite prepreg (APC-2). This was done by preparing macromechanical test specimens using compression

moulding. Results from flexural and short beam shear tests showed that the CF/PEEK composite laminates produced had slightly better properties than APC-2, both composites contained AS4 carbon fibres. It was also found that the AS4/PEEK-150 composite exhibited higher flexural strength than the sized T700/PEEK-150 composite despite the higher mechanical properties of the T700 fibres, which was due to the fact that the T700 fibres were epoxy sized, which most probably led to the formation of a weak boundary layer. These findings agree with measured apparent interfacial shear strength of single AS4 and T700 fibre/PEEK-150 composites.

The next step was to assess the feasibility of hierarchical PEEK composites on the single fibre composite scale. The interfacial properties of these composites were studied (at the BAM Berlin) using the single fibre pull-out tests. The force required to debond a fibre from a solidified droplet of annealed nano-reinforced PEEK matrix was measured and the apparent interfacial shear strength, as measure of the practical adhesion, was determined. As much as 50 % improvement in the apparent interfacial shear strength was recorded as a result of the incorporation of 5 wt% CNTs into PEEK, showing that the incorporation of CNTs into the PEEK matrix enhanced the interfacial properties. Potentially high performance hierarchical composite materials with good mechanical properties could thus be developed. To achieve this aim, a CNT reinforced PEEK powder with a particle size preferably smaller than 100 μm had to be made in order to manufacture carbon fibre reinforced CNT reinforced PEEK nanocomposites using the powder impregnation route. A temperature induced solution precipitation method was developed to produce a nanocomposite powder with a d_{50} of around 50 μm. SEM micrographs showed that CNTs were well dispersed throughout and uniformly embedded within the nanocomposite powder.

Finally, the CNT/PEEK nanocomposite powder was used to manufacture unidirectional, continuous carbon fibre hierarchical PEEK composites. Various CNTs loading were investigated and flexural and short beam shear (SBS) properties were measured. Preliminary findings showed a decrease of 4% in flexural strength with no difference in flexural modulus and 15 % decrease in the SBS strength. This is probably due to the inclusion of voids caused by the high viscosity of the nanocomposite matrix and the wide powder size distribution. However, the results show that potentially high quality hierarchical carbon fibre reinforced thermoplastic composites with high CNT loading fractions could be manufactured even at an industrial scale and, therefore, the full benefit of CNTs incorporation in to fibre reinforced composites could become reality provided that high quality CNTs with suitable surface properties for the desired matrix become available at an industrial scale.

Chapter 6 – Suggestions for future work

The concept of fibre reinforced carbon nanotube composites, we call them hierarchical composites and the Composite Materials Group (around Prof I. Verpoest) in Leuven call them nano-engineered fibre reinforced polymer composites, was when I started my PhD still an entirely new approach to composite engineering. However, in recent years many more papers dealing with this subject matter reporting in a few cases extraordinary improvements of composite properties or focus on multifunctional (mainly sensing aspects) properties that can be added to composites by adding low loading fractions of CNTs to conventional composite matrices. Nevertheless, from my work I identified a few areas of research and engineering that seem worth pursuing in the future not only on hierarchical composites themselves:

Anticipated Future Improvement in Thermoplastic Hierarchical Composites

This study highlighted the potential of additional nanoscale reinforcements in composite matrices but showed also that a simple annealing of a semi-crystalline thermoplastic matrix, such as PEEK, negates all anticipated matrix dominated property improvements, simply because the crystalline regions of the polymer act as self-reinforcing phase. The potential of an additional CNT reinforcement might actually be realised only in amorphous matrices, such as polyethersulfone (PES), polysulfone (PSU), polycarbonate (PC) or polyimide (PI). The production of such composites presents its own challenges, such as the intrinsically higher melt viscosity of amorphous polymers. However, using such matrices might offer huge potential for the production of composites with high impact resistance and toughness.

Optimisation of the home-built modular laboratory scale composite production line

During the course of my PhD research, I identified aspects of our composite tape production line which could or need to be improved:

Infrared radiation (IR) sensors

The heaters have the capability to be controlled by various different input parameters. The initial mode of operation relied on a feedback control system using thermocouples located inside the ovens as sensors, but it would be desirable for the control strategy to account for factors that affect the amount of heat required to dry the tape or melt the polymer powder on the tape. If this would be possible the heating could be set to power rather than to set fixed temperatures. This not only will allow better control of tape drying and polymer melting but also in the long term, this will help conserve energy. The composite line was fitted with infra-red sensors to measure the temperature of the tape when exiting the drying and the melting ovens. It was attempted to provide information on when the temperature of ovens was needed to be increased or/and lowered. However this proved to be unreliable when a single carbon fibre roving was used to produce a composite tape because of the slight misalignment of the tow whenever a twist on the fibres passed below the IR sensor. Perhaps, such infra-red sensors are more suitable for industrial scale manufacturing where up to 60 carbon fibres rovings are processed at the same time and therefore the fibre misalignment caused by twists is minimised. As a result, an upgraded controller unit had been installed after my experimental research period finished; this unit allows the heating rate to be controlled in a more precise manner because the heating

rate is lower. This should be beneficial for future researchers using the composite production line.

Consolidation

The temperature of the heated pins was controlled by a thermocouple positioned inside the cartridge heater, however very large temperature gradients arose due to the open air design and a temperature difference of up to 50 °C was observed between the surface of the heated pins and the temperature sensor. Additional thermocouples should be attached to the heated pins which should allow for accurate control of the temperature of the tape surface. Furthermore, top and bottom cover brackets should be fitted to reduce heat lost from the consolidation area.

Automatisation of the composite line: control of the polymer suspension concentration in powder impregnation to control the fibre volume content of the produced composite tape

The fibre volume content of the produced thermoplastic composites is controlled by two factors: mainly the powder concentration of the polymer suspension in the impregnation bath and the line speed. When manufacturing of (hierarchical) thermoplastic composite tapes, I (and so do my colleagues) needed to increase the powder concentration of the impregnation bath in order to maintain the fibre volume fraction of the composite tape, which was done by frequently adding concentrated suspension and/or removing dilute suspension from the bath. Hence the running of the composite line alone is difficult and could be avoided only if an automatic dosing system could be incorporated into the existing composite manufacturing line. This requires a measuring system that could determine the powder concentration in the

suspension which should be however insensitive to the many broken carbon fibres that end up in the bath. The measured output would then be used as input to control the feed of the concentrated suspension to the impregnation bath. The suspension could be added to the bath by opening/closing a valve of a container containing the concentrated suspension or by using a peristaltic pump. The diameter of tubing, length of tubing, pump rate would need to be balanced to ensure no sedimentation of powder during delivery to void blocking the system as well as a constant stirring of the concentrate is required. The potential advantage of such a system is a better quality and more constant quality of the produced composites.

Different approaches to manufacturing unidirectional carbon fibre reinforced PEEK composites

Integrated spreading pins located within the infra-red melting oven would preserve the power required to heat up the triple heating cartridges. In addition the heat lost from the open oven set up that was previously discussed could also be overcome. A better tape quality would occur because the heat provided for spreading the polymer melt into the fibre tow would come from all around the impregnated rovings rather than only the contact points between the fibre tow and the cartridge heaters.

Twist control or removal to enable proper spreading of the fibre rovings would allow the production of very thin composite tapes, which are more flexible and could therefore be easier processed, for instance by weaving. This would allow new designs for thermoplastic composites to be explored and might open up new application areas.

I showed that standard epoxy sizings negatively affect the carbon fibre/PEEK (and more generally thermoplastic polymer) adhesion, which will directly impact on the composite properties. Unfortunately, only Hexcel AS4 and IM7 fibres are commercially available in an unsized form. It would therefore be desirable to develop a continuous desizing procedure for sized carbon fibres to utilise other carbon fibres as reinforcement. This might in fact be possible using our in-line atmospheric plasma unit by simply sputtering or oxidising the sizing away in an inert (such as nitrogen) or air or oxygen plasma. In a preliminary study on the impact of an atmospheric air plasma treatment on the carbon fibre/PEEK adhesion it will be possible to show that such a treatment does allow to increase the fibre/matrix adhesion considerably, which should prove beneficial for the overall composite performance, especially on interface dominated properties, such as interlaminar and off-axis properties and fracture toughness. In a separate study we [184] showed that an atmospheric oxygen plasma treatment increases the carbon fibre/polyamide 12 adhesion by 100 % without negatively affecting the fibre bulk (including mechanical) properties.

Appendix

Determination of the diameters of carbon nanomaterials

SEM micrographs of carbon nanomaterials have been investigated and taken at set magnification (i.e. 30, 100, 150 or 200 kx) depending on the diameter of the material looked at. Random images were taken (at least 6 per sample) and saved in a TIFF format.

ImageJ [185] software was used to extract the diameters from individual SEM micrographs. The 'measure_and_label' plugin is necessary and can be found in the plugin section on ImageJ website [185]. Install the plugin within ImageJ using a known shortcut to automate the process, go in 'Plugins/Shortcuts/Install Plugin...', select the 'Measure_and_Label' plugin, type in a command (i.e. Meas-Label) and L as shortcut (in capital letter).

Open a SEM micrograph, magnify the image to 200 %, it is necessary to adjust the scale of the micrograph first. For this, draw a straight line across the SEM scale bar, go in 'Analyse/Set Scale...', input in 'known distance' the value on the micrograph scale bar and input in 'unit of length' as nm or μm depending on the scale, press Ok.

Keeping a magnification of 200%, using the straight line drawing tool, draw a line across each individual CNT/CNF normal to their length (i.e. 90° angle) and activate the shortcut created (i.e. here L by pressing Shift+l). Select another CNT/CNF and continue the process around the whole micrograph. Do not measure the diameter of

the same CNT/CNF twice. A list will be created with the length measured (i.e. the diameter in our case). The error in measurement is expected to ± 0.5 nm.

Apply the same procedure on other SEM micrographs from the same sample.

OriginPro 8 software was used for the analysis of the diameters. Extract the list within Origin and create a frequency count of the diameters. Create a histogram from that frequency count showing counts vs diameters. Fit the histogram with a Gaussian curve. It will list the mean diameter, standard deviation value is determined as half the width of the Gaussian curve.

Apply the same procedure for the rest of the materials.

References

1 A. Oberlin, M. Endo and T. Koyama, J. Cryst. Growth 32 (1976) 335.

2 P.M. Ajayan, Chem. Rev. 99 (1999) 1787.

3 P. Harris, Intern. Mater. Rev. 49 (2004) 31.

4 M. Terrones, Inter. Mater. Rev. 49 (2004) 325.

5 M. Shaffer and J. Sandler, Carbon Nanotube/Nanofibre Polymer Composites. In: S.G. Advani, ed. Processing and Properties of Nanocomposites: New Jersey, NJ: World Scientific 2007:1-59.

6 J.N. Coleman, U. Khan, W.J. Blau and Y.K. Gun'ko, Carbon 44 (2006) 1624.

7 M.S.P. Shaffer, J.K.W. Sandler, S. Pegel, A.H. Windle, F. Gojny, K. Schulte, M. Cadek, W.J. Blau, J. Lohmar and M. van Es, Mater. Res. Soc. Symposium Proceedings 791 (2004) 347.

8 E. Kostakova, L. Meszaros and J. Gregr, Mater. Lett. 63 (2009) 2419.

9 P. Werner, R. Verdejo, F. Wollecke, V. Alstädt, J.K.W. Sandler and M.S.P. Shaffer, Adv. Mater. 17 (2005) 2864.

10 G. Jell, R. Verdejo, L. Safinia, M.S.P. Shaffer, M.M. Stevens and A. Bismarck, J. Mater. Chem. 18 (2008) 1865.

11 R. Verdejo, G. Jell, L. Safinia, A. Bismarck, M.M. Stevens and M.S.P. Shaffer, J. Biomed. Mater. Res. A 88A (2009) 65.

12 R. Verdejo, R. Stämpfli, M. Alvarez-Lainez, S. Mourad, M.A. Rodriguez-Perez, P.A. Brühwiler and M. Shaffer, Comp. Sci. Tech. 69 (2009) 1564.

13 W.B. Downs and R.T.K. Baker, Carbon 29 (1991) 1173.

14 E.T. Thostenson, W.Z. Li, D.Z. Wang, Z.F. Ren and T.W. Cho, J. Appl. Phys. 91 (2002) 6034.

15 L.T. Drzal, Tough Composite Materials: Recent Develoments, Noyes Publication, New Jersey (1985).

16 B.T. Åström, Manufacturing of Composites, 1st Ed. Chapman & Hall, London (1997).

17 A.R. Bunsell and J. Renard, Fundamentals of Fibre Reinforced Composite Materials, Institute of Physics Publishing, UK (2005).

18 Directive 2000/53/EC of The European Parliament and of The Council of 18 September 2000 on end-of-life vehicles, European Commision.

19 P.K. Mallick, Composite Engineering Handbook, Marcel Dekker, Inc.: New York (1997).

20 W.K. Chin and S.W. Yang, J. Polym. Res. 2 (1995) 31.

21 S. Oken, Graphite thermoplastic YC-14 outboard elevator, 12th National Society for the Advancement of Materials and Process Engineering (SAMPE) Conference, SAMPE, Seattle (1980) 461.

22 B. Strong, Fundamentals of composites manufacturing: materials, methods and applications, 2nd Edition, Society of Manufacturing Engineers USA (2007).

23 A.A. Collyer and D.W. Clegg, In An Introduction to Fibre Reinforced Thermoplastics, D.W. Clegg and A.A. Collyer, Eds., Mechanical Properties of Reinforced Thermopastics. London: Elsevier (1986).

24 R. Vipond and C.J. Daniels, Composites 16 (1985) 14.

25 J. Njuguna and K. Pielichowski, Adv. Eng. Mater. 6 (2004) 193.

26 J. Njuguna and K. Pielichowski, Adv. Eng. Mater. 6 (2004) 204.

27 J. Njuguna and K. Pielichowski, Adv. Eng. Mater. 6 (2004) 769.

28 Anonymous. Europe gets tough on end-of-life composites, Reinforced Plastics, 47-8 (2003) 34.

29 Anonymous. Technology update: Prepregs, Reinforced Plastics, 47-6 (2003) 20.

30 R. Brooks, Manufacturing of thermoplastics composites, MSc Composites module, Imperial College London, 2007.

31 E. Mäder, K. Grundke, H.-J. Jacobasch and G. Wachinger, Composites 25 (1994) 739.

32 N. Svensson, R. Shishoo and M. Gilchrist, J. Thermoplastic Composite Mater. 11 (1998) 22.

33 S. Thomas, C. Bongiovanni and S.R. Nutt, Comp. Sci. Tech. 68 (2008) 3093.

34 A.H. Miller, N. Dodds, J.M. Hale and A.G. Gibson, Composites A 29 (1998) 773.

35 R. Bernet, V. Michaud, P.E. Bourban and J.A.E. Manson, J. Comp. Mater 33 (1999) 751.

36 F. Ko, P. Fang and H. Chiu, 33rd International SAMPE Symposium (1998), 899.

37 T.J. Whitney and T.W. Chou, Proceedings of the American Society for Composites, 3rd Technical Conference (1988), 427.

38 F. Ko, H. Chu and E. Ying, Proceedings of the 2nd Conference on Advanced Composites (1986).

39 C.T. Hua and F.K. Ko, 21st International SAMPE Technical Conference (1989) 688.

40 L. Laberge-Lebel and S.V. Hoa, J. Comp. Mater. 41 (2007) 1101.

41 B.C. Kang, K.H. Min, Y.H. Lee, B.B. Hwang and C.N. Herath, Mater. Sci. Forum 539-543 (2007) 992.

42 A.C. Long, Composite Forming Technologies, Woodhead Publishing, Cambridge, (2007).

43 M. Piggott, Load Bearing Fibre Composites, Springer US (2007).

44 Anonymous. Airbus and Tencate continue partnershi, Reinforced Plastics, 53-4 (2009) 9.

45 A.M. Vodermayer, K.J.C. Kärger and G. Hinrichsen, Comp. Tech. 4 (1993) 123.

46 J. Kärger and A. Vodermayer, Sulzer Techn. Rev. 2 (1999) 4

47 L. Tang, L. Li, X. Yi, Z. Pan, Polym. Composites 18 (1997) 223.

48 A.M. Vodermayer, J.C. Kärger, W.F.W. Auersch, M. Hofmeier, C. Bellusci and C. Mayer, US Patent 2002/0071,907.

49 R.M. Matthew, R.J. Friedman, H. Del Schutte Jr and R.A. Latour Jr., J. Biomed. Mater. Res. 28 (1994) 1221.

50 C.C.M. Ma, C.L. Lee and N.H. Tai, Polym. Composites 13 (1992) 435.

51 Z. P. Lu and K. Friedrich, Wear 181-183 (1995) 624.

52 J. Flöck, K. Friedrich and Q. Yua, Wear 225-229 (1999) 304.

53 APC-2 Thermoplastic polymer, Cytec Engineered Materials, Technical Datasheet.

54 Victrex PEEK properties guide, www.victrex.com/en/victrex-library/datasheets/datasheets.php (last accessed on 29/11/09).

55 J. Li and X.H. Sheng, Mater. Sci. Tech. 25 (2009) 1051.

56 J. Li, Surf. Int. Analys. 41 (2009) 310.

57 Q. Yuan, S.A. Bateman and K. Friedrich, J. Therm. Comp. Mater. 21 (2008) 323.

58 G.C. McGrath, D.W. Clegg and A.A. Collyer, Composites 19 (1988) 211.

59 F.N. Cogswell, Thermoplastic aromatic polymer composites, Butterworth-Heinmann Ltd, UK (1992).

60 Y. Lee and R.S. Porter, Poly. Eng. Sci. 26 (1986) 633.

61 J.-K. Kim, in Proceedings of 2nd International Bhurban conference on Applied Sciences and Technology, Bhurban, 2003.

62 S.L. Gao and J.K. Kim, Composites A 31 (2001) 517.

63 E. Stober, J Seferis and J Keenan, Polymer 25 (1984) 1845.

64 B.H. Stuart and D.R. Williams, Polymer 35 (1994) 1326.

65 C.J. Wolf and M.A. Grayson, Polymer 34 (1993) 746.

66 H. Dillon, Investigation into welding of thermoplastic composites, MSc thesis 2004, Imperial College London.

67 D. Patel, Impact on composite laminates, MSc thesis 2005, Imperial College London.

68 H. Miyagawa, M. Misra and A.K. Mohanty, J. Nanosci. and Tech. 5 (2005) 1593.

69 P.J.F. Harris, Carbon Nanotubes and Related Structures, Cambridge University Press: Cambridge, (1999).

70 E.T. Thostenson, Z.F. Ren and T.W. Chou, Comp. Sci. Tech. 61 (2001) 1899.

71 B. Miller, Plastics World, 1993.

72 J. Sandler, M.S.P. Shaffer, T. Prasse, W. Bauhofer, K. Schulte and A.H. Windle, Polymer 40 (1999) 5967.

73 J.K.W. Sandler, J.E. Kirk, I.A. Kinloch, M.S.P. Shaffer and A.H. Windle, Polymer 44 (2003) 5893.

74 E.T. Thostenson, C. Li and T.-W. Chou, Comp. Sci. Tech. 65 (2005) 491.

75 O. Breuer and U Sundararaj, Poly. Comp. 25 (2004) 630.

76 P.M. Ajayan, P. Redlich and M. Rühle, J. Microscop. 185 (1997) 275.

77 A.M. Diez-Pascual, M. Naffakh, M.A. Gomez, C. Marco, G. Ellis, M.T. Martinez, A. Anson, J.M. Gonzalez-Dominguez, Y. Martinez-Rubi and B. Simard, Carbon 47 (2009) 3079.

78 L. Song, H. Zhang, Z. Zhang and S.S. Xie, Composites A 38 (2007) 388.

79 J. Sandler, P. Werner, M.S.P. Shaffer, V. Demchuk, V. Altstädt and A.H. Windle, Composites A 33 (2002) 1033.

80 R. Verdejo, P. Werner, J. Sandler, V. Altstädt and M.S.P. Shaffer, J. Mater. Sci. 44 (2009) 1427.

81 S.L. Gao and J.K. Kim, Composites A 31 (2001) 517.

82 S.L. Gao and J.K. Kim, Composites A 32 (2001) 763.

83 S.L. Gao and J.K. Kim, Composites A 32 (2001) 775.

84 N. Coleman, U. Khan and Y. K. Gun'ko, Adv. Mat. 18 (2006) 689.

85 D.J. Blundell, J.M. Chalmers, M.W. Mackenzie and W.F. Gaskin, SAMPE Quart. 16 (1985) 1985.

86 G.M.K. Ostberg and J.C. Seferis, J. Appl. Polym. Sci. 33 (1987) 29.

87 J. Denault and T. Vukhanh, Polym. Composites 13 (1992) 361.

88 B.S. Hsiao, I.Y. Chang and B.B. Sauer, Polymer 32 (1991) 2799.

89 H.M. Lin, R.F. Lee, C.H. Liu, J.S. Wu and C.S. Huang, Comp. Sci. Tech. 52 (1994) 407.

90 A. Tregub, H. Harel and G. Marom, J. Mater. Sci. Lett. 13 (1994) 329.

91 A.A. Mehmetalkan and J.N. Hay, Polymer 34 (1993) 3529.

92 B.D. Hachmi and T. VuKhanh, J. Thermoplastic Composite Mater. 10 (1997) 488.

93 M. Chen and C.T. Chung, Polym. Composites 19 (1998) 689.

94 P.Y. Jar, W.J. Cantwell and H.H. Kausch, Comp. Sci. Tech. 43 (1992) 299.

95 P. Cebe, J. Mat. Sci. 23 (1988) 3721.

96 H. Zeng, Z. Zhang, W. Peng and T. Pu, Eur. Polym. J, 30 (1994) 235.

97 W. Wang, Z. Qi and G. Jeronimidis, J. Mat. Sci. Lett. 26 (1991) 5915.

98 Z.H. Fan, M.H. Santare and S.G. Advani, Composites A 39 (2008) 540.

99 Y.X. Zhou, F. Pervin, L. Lewis and S. Jeelani, Mater. Sci. Eng. A 475 (2008) 157.

100 K.J. Green, D.R. Dean, U.K. Vaidya and E. Nyairo, Composites A 40 (2009) 1470.

101 M. Kim, Y.B. Park, O.I. Okoli and C. Zhang, Comp. Sci. Tech. 69 (2009) 335.

102 P. Karapappas, S. Tsantzalis, E. Fiamegou, A. Vavouliotis, K. Dassios and V. Kostopoulos, Adv. Composite Lett. 17 (2008) 103.

103 F.H. Zhang, R.G. Wang, X.D. He, C. Wang and L.N. Ren, J. Mater. Sci.44 (2009) 3574.

104 R.J. Sager, P.J. Klein, D.C. Lagoudas, Q. Zhang, J. Liu, L. Dai, et al., Comp. Sci. Tech. 69 (2009) 898.

105 L.J. Ci, Z.G. Zhao and J.B. Bai. Carbon 43 (2005) 883.

106 A.Y. Cao, V.P. Veedu, X.S. Li, Z.L. Yao, M.N. Ghasemi-Nejhad and P.M. Ajayan, Nature Mater. 4 (2005) 540.

107 V.P. Veedu, A.Y. Cao, X.S. Li, K.G. Ma, C. Soldano, S. Kar, et al. Nature Mater. 5 (2006) 457.

108 Q. Zhang, W.Z. Qian, R. Xiang, Z. Yang, G.H. Luo, Y. Wang, et al., Mater. Chem. Phys. 107 (2008) 317.

109 H. Qian, A. Bismarck, E.S. Greenhalgh and M.S.P. Shaffer, Carbon 48 (2010) 277.

110 H. Qian, A. Bismarck, E.S. Greenhalgh and M.S.P. Shaffer. Comp. Sci. Tech. 70 (2009) 393.

111 B.O. Boskovic, V.B. Golovko, M. Cantoro, B. Kleinsorge, A.T.H. Chuang, C. Ducati, et al., Carbon 43 (2005) 2643.

112 J.O. Zhao, L. Liu, Q.G. Guo, J.L. Shi, G.T. Zhai, J.R. Song, et al. Carbon 46 (2008) 380.

113 X.D. He, F.H. Zhang, R.G. Wang and W.B. Liu, Carbon 45 (2007) 2559.

114 T. Susi, A.G. Nasibulin, H. Jiang and E.I. Kauppinen, J. Nanomaterials (2008) article number: 425195.

115 H. Qian, A. Bismarck, E.S. Greenhalgh, G. Kalinka and M.S.P. Shaffer, Chem. Mater. 20 (2008) 1862.

116 Q.H. Zhang, J.W. Liu, R. Sager, L.M. Dai and J. Baur, Comp. Sci. Tech. 69 (2009) 594.

117 I. O'Connor, H. Hayden, S. O'Connor, J.N. Coleman and Y.K. Gun'ko, J. Phys. Chem. C 113 (2009) 20184.

118 E. Bekyarova, E.T. Thostenson, A. Yu, H. Kim, J. Gao, J. Tang, et al., Langmuir 23 (2007) 3970.

119 N.A. Siddiqui, M.L. Sham, B.Z. Tang, A. Munir and J.K. Kim, Composites A 40 (2009) 1606.

120 H. Qian, Carbon Nanotube Grafted Fibres: A Route to Advanced Hierarchical Composites, PhD Thesis, Imperial College London (2009).

121 T. Yokozeki, Y. Iwahori, S. Ishiwata and K. Enomoto, Composites A 38 (2007) 2121.

122 R. Sadeghian, S. Gangireddy, B. Minale and K.-T. Hsiao, Composites A 37 (2006) 1787.

123 J. Juntaro, M. Pommet, G. Kalinka, A. Mantalaris, M.S.P. Shaffer and A. Bismarck, Adv. Mater. 16 (2008) 3122.

124 M. Pommet, J. Juntaro, J.Y.Y. Heng, A. Mantalaris, A.F. Lee, K. Wilson, G. Kalinka, M.S.P. Shaffer and A. Bismarck, Biomacromolecules 9 (2008) 1643.

125 J. Juntaro, M. Pommet, A. Mantalaris, M.S.P. Shaffer and A. Bismarck, Composite Interfaces 14 (2007) 753.

126 K.-T. Hsiao, Processing and Mechanical Properties Characterization of Hybrid Thermoset Polymer Composites with Micro-Fiber and Carbon Nano-Fiber Reinforcements, Processing and Properties of Nanocomposites, S.G. Advani, Processing and Properties of Nanocomposites, World Scientific, New Jersey (2007).

127 P. Dubois and M. Alexandre, Adv. Eng. Mater., 8 (2006) 147.

128 M.Q. Tran, M.S.P. Shaffer and A. Bismarck, Macromol. Mater. Eng. 292 (2008) 188.

129 Y. Iwahori, S. Ishiwata, T. Sumisawa and T. Ishikawa, Composites A 36 (2005) 1430.

130 F.H. Gojny, M.H.G. Wichmann, B. Fidler, W. Bauhofer and K. Schulte, Composites A 36 (2005) 1525.

131 E.T. Thostenson, J.J. Gangloff, C.Y. Li and J.-H. Byun, Appl. Phys. Lett. 95 (2009) article no.: 073111.

132 F. Pervin, Y.X. Zhou, V.K. Rangari and S Jeelani, Mater. Sci. Eng. A 405 (2005) 246.

133 P.A. Song, L.H. Xu, Z.H. Guo, Y. Zhang and Z.P. Fang, J. Mater. Chem. 18 (2008) 5083.

134 R. Menzel, A. Lee, A. Bismarck, M.S.P. Shaffer, Langmuir 25 (2009) 8340

135 Nanostructured & Amorphous Materials Inc, www.nanoamor.com/carbon_nanotubes___nanofibers (last accessed on 29/11/09).

136 Nanocyl s.a., www.nanocyl.com/en/Products-Solutions/Products/Research-Grades/Single-Wall-Carbon-Nanotubes (last accessed on 29/11/09).

137 Heji Inc, www.nanotubeseu.com/nano/products.html (last accessed on 29/11/09).

138 Baytubes Materials Science, www.baytubes.com/product_production/product.html (last accessed on 29/11/09).

139 Personal correspondence with Toray Research and Development, 2004.

140 Hexcel, HexTow AS4 carbon fibres, www.hexcel.com/NR/rdonlyres/5659C134-6C31-463F-B86B-4B62DA0930EB/0/HexTow_AS4.pdf (last accessed on 29/11/09).

141 Toray, Quality of Torayca carbon fibres, commercial documentation – N°AQ.866 – 9. Sept 2003.

142 F.L. Mathews, R.D. Rawlings, Composite materials: Engineering and Science, Woodhead Publishing Ltd and CRC Press LLC, Boca Raton (2006).

143 ISO 9277, Determination of the specific surface area of solids by gas adsorption using the BET method, 1995.

144 D.A. Skoog, F.J. Holler and T.A. Nieman, Principles of Instrumental Analysis, 5th Edition, Thomas Learning, USA (1997).

145 F. Tuinstra and J. L. Koenig, J. Chem. Phys., 53 (1970) 1126.

146 A. Hampe, I. Boro and K. Schumacher, Forschung Aktuell der TU Berlin, 7 (1990) 21.

147 S. Meretz, T. Linke, E Schulz, A Hampe and M Hentschel, J. Mater. Sci. Lett., 11 (1992) 1471.

148 C. DiFrancia, T.C. Ward and R.O. Claus, Composites A 27a (1996) 597.

149 ISO 527-2, Determination of tensile properties - Part 2: Test conditions for moulding and extrusion plastics, 1993.

150 ASTM D638-08-V, Standard test method for tensile properties of plastics, 2008.

151 R.V. Price, US Patent (1973), 3742106.

152 H. Krueger, US Patent (1992), 5085928.

153 ASTM D3822-07, Standard test method for tensile properties of single textile fibre, 2007.

154 ASTM D695-08, Standard test method for compressive properties of rigid plastics, 2008.

155 Wyoming Test Fixtures, www.wyomingtestfixtures.com/Pictures/B-2-1%20Left.jpg (last accessed on 01/05/10).

156 ASTM D3846-08, Standard test method for in-plane shear strength of reinforced plastics, 2008.

157 ASTM D790-03, Standard test method for flexural properties of unreinforced and reinforced plastics and electrical insulating materials, 2003.

158 ASTM D7264-07, Standard test method for flexural properties of polymer matrix composite materials, 2007.

159 ASTM D2344-00, Standard test method for short beam strength of polymer matrix composite materials and their laminates, 2006.

160 E. Flahaut, R. Bacsa, A. Peigney, C. Laurent, Chem. Comm. (2003) 1442.

161 M.Q. Tran, C. Tridech, A. Alfry, A. Bismarck, M.S.P. Shaffer, Carbon 45 (2007) 2341.

162 M.B. Bryning, D.E. Milkie, M.F. Islam, L.A. Hough, J.M. Kikkawa, A.G. Yodh, Adv. Mater. 19 (2007) 661.

163 ISO 11358, Thermogravimetry (TG) of polymers – General Principles, 1997.

164 R. Verdejo, S. Lamoriniere, B. Cottam, A.Bismarck, M. Shaffer, ChemComm (2007) 513.

165 J-P. Tessonnier, D. Rosenthal, T.W. Hansen, C. Hess, M.E. Schuster, R. Blume. F. Girgsdies, N. Pfander, O. Timpe, D.S. Su, R. Schlogl, Carbon 47 (2009) 1779.

166 T. Ramanathan, A. Bismarck, E. Schulz, K. Subramanian, Comp. Sci. Tech. 61 (2001) 1703.

167 Y-T. Liao and I-C. Tung, J. Mater. Sci. Lett. 10 (1991) 272.

168 A. Bismarck, Influence of fiber desizing on mechanical properties of CF/PA12 composites, Gurit Suprem Report, GS_TB2002_006, 2002.

169 A. Bismarck and M. Hofmeier, Effect of thermal desizing of T1000GB fibers on the mechanical properties of carbon fiber/poly (ether ether ketone) (PEEK) composite tapes, Gurit Suprem Report, GS_TB2002_010, 2005.

170 A.V. Pocius, Adhesion and Adhesives Technology An Introduction, 2nd Ed., Hanser Publishers, München (2002).

171 S. Meretz, W. Auersch, C. Marotzke, E. Schulz and A. Hampe, Comp. Sci. Tech. 48 (1993) 285.

172 J.-M. Park, Z.-J. Wang, J.-H. Jang, J.R.N. Gnida Koung, W. Lee, J.-K. Park and K.L. DeVries, Composites A 40 (2009) 1722.

173 D.P.N. Vlasveld, P.P. Parlevliet, H.E.N. Bersee and S.J. Picken, Composites A 36 (2005) 1.

174 C. Lew, F. Chowdhury, M.V. Hosur and A.N. Netravali, J. Adhesion Sci. Technol. 21 (2007) 1407.

175 D.S. Bangarusampath, H. Ruckdaschel, V. Altstadt, J.K.W. Sandler, D. Garry, M.S.P. Shaffer, Polymer 50 (2009), 5803.

176 S. Pegel, P. Potschke, G. Petzold, I. Alig, S.M. Dudkin, D. Lellinger, Polymer 49 (2008) 974.

177 F.R. Jones, Handbook of Polymer Fibre Composites, Longman Scientific and Technical, Essex (1994).

178 A. Bismarck, M. Hofmeier, G. Jannerfeldt and C. Mayer, NAMAS project 2001 final report, Sulzer Composite Report, SCO_TB2002_001, 2005.

179 K.K.C. Ho, A.F. Lee, S. Lamoriniere and A. Bismarck, Composites A 39 (2008) 364.

180 K.K.C. Ho, A.F. Lee and A. Bismarck, Carbon 45 (2007) 775.

181 S. Wu, Polymer Interface and Adhesion, Marcel Dekker, New York, 1980.

182 K.K.C. Ho, G. Kalinka, M.Q. Tran, N.V. Polyakova and A. Bismarck, Comp. Sci. Tech. 13 (2007) 2699.

183 M.Q.B. Tran, Ultra-inert hierarchical fibre-reinforced nanocomposites, PhD-Thesis, Imperial College London (2007).

184 S. Erden, K.K.C. Ho, S. Lamoriniere, A.F. Lee, H. Yildiz and A. Bismarck, Plasma Chem. Plasma Proc. (2009) in press.

185 ImageJ, http://rsbweb.nih.gov/ij/